MONTHLY NOTICES

OF THE

ROYAL ASTRONOMICAL SOCIETY

Volume 122 No. 4 1961

MONTHLY NOTICES

OF THE

ROYAL ASTRONOMICAL SOCIETY

Vol. 122 No. 4

SOME ATTEMPTS TO DETECT LINEAR POLARIZATION OF GALACTIC RADIO EMISSION FROM THE SPUR AT $l^{II}=30°$

I. I. K. Pauliny-Toth, J. E. Baldwin and J. R. Shakeshaft

(Received 1960 November 7)

Summary

Experiments have been carried out in an attempt to detect linearly polarized radiation from the galactic spur at $l^{II}=30°$. Five observational methods are discussed and the results of experiments using these methods are given. The frequencies used were 160, 178 and 408 Mc/s and the region of observation covered the more intense parts of the spur. All the experiments agree in fixing a low upper limit of a few per cent on linearly polarized radiation from the spur.

1. *Introduction.*—It has been suggested by Tunmer (**1**) that the spur-shaped feature of radio emission extending from the galactic plane at $l^{II}=30°$ and following almost a great circle across the sky is due to the spiral motion of relativistic electrons in the magnetic field along the local arm of the Galaxy. Such radiation is emitted with the electric vector in the instantaneous orbital plane of the electrons and Tunmer shows that if these electrons originate in the inner parts of the Galaxy and travel outwards along the arms, most of the radiation from the spur will be due to electrons with orbits which are nearly perpendicular to the magnetic field. Under these conditions, the radiation from the spur may be partially plane polarized and this paper is an account of some efforts to detect such polarization.

Thomson (**2**), working at a frequency of 160 Mc/s using a 15° beam, has already reported an upper limit of 1 per cent for polarization in this region. The observations described have the advantages resulting from the use of a smaller beam and a higher frequency.

2. *Experimental design considerations*

(i) *Faraday rotation.*—Several mechanisms associated with the Faraday effect increase the difficulty of observing polarization (**3**). For example, any disorder of the magnetic field gives components of the field along the line of sight, so that the plane of polarization is rotated by the Faraday effect. If the emitting regions in the line of sight are at different distances, there may be enough differential rotation of the vectors representing the contributions to the emission of the nearest and farthest regions to reduce considerably the observed polarization. It is to this mechanism that Tunmer attributes the low result of Thomson, because by taking values of $0{\cdot}1\ \mathrm{cm}^{-3}$ for the electron density and 10^{-7} gauss for the longitudinal component of the field, she finds the rotation to be 0·03 radians per parsec at 160 Mc/s. If the emitting region extends over 100–150 parsecs the rotation of the

plane of polarization across it may be 3–4 radians and the observed polarization will be small.

Another mechanism which reduces the observed polarization is the differential rotation over the pass-band of the receiver. Both of these effects are reduced by observing at a higher frequency and the second by using a smaller bandwidth, but in both cases the sensitivity of the experiment is reduced.

(ii) *Spurious responses.*—Aerial systems designed to detect plane polarized radiation may respond to unpolarized sources off the axis of symmetry as though these were polarized. It is necessary to take account of this effect, especially for paraboloidal reflectors of small focal ratio.

(iii) *Resolving power.*—A narrow beam is desirable, first to avoid dilution of any polarized radiation from the spur (the width of which is some 5°) by unpolarized radiation from nearby regions and secondly to avoid the presence in the beam of regions with different planes of polarization.

3. *Observational methods.*

(i) *Ionospheric rotation method.*—The procedure here is to obtain drift curves of the total power received by an aerial with a small beamwidth over a period of several weeks, at a time of the year when the spur is in the beam at local dawn or dusk. The progressive displacement of sidereal time with respect to solar time causes the plane of polarization of any polarized radiation at the aerial to rotate as the electron density in the ionosphere changes. If a linearly polarized array is used, this rotation will change the total power received from day to day.

At frequencies below about 200 Mc/s the method is useful since the change of rotation of the plane of polarization between day and night is large; at 160 Mc/s for instance, near the zenith, it is 7–8 radians. At higher frequencies the method is less satisfactory, the change of rotation at 400 Mc/s being only 1–1½ radians.

(ii) '*Comb filter*' *method.*—To investigate the possibility of an appreciable rotation of the plane of polarization across the pass-band of the receiver a filter method can be used.

In this method, the output of the aerial is split by a hybrid network into two parts which are fed into a phase-switching receiver through two cables. If the lengths of these are the same and the plane of the polarized signal does show several rotations across the pass-band, the output may be nearly zero. If the cables differ in length, the interference of the two parts of the signal produces a response which varies with frequency f as $\cos^2(\pi d/c)f$ across the pass-band where d is the difference in the electrical lengths of the cables and c is the velocity of light. The phase-switching action of the receiver interchanges the maxima and minima of this pattern at the switching frequency. If the maxima of the frequency response and those produced by Faraday rotation of a polarized signal coincide, an output will be observed.

The procedure is to observe with a given path difference, then with an additional quarter wavelength of path. This is repeated with other path differences, in steps of c/B where B is the bandwidth of the receiver. The useful range of path differences is limited at the lower end by the finite width and sharp edges of the I.F. response, but polarized radiation with a Faraday rotation across the pass-band smaller than this would be detected directly by method (i).

(iii) *The frequency-switching method.*—This method is also designed to detect plane polarized radiation subject to appreciable Faraday rotation across the pass-band of a receiver as used in method (i). The aerial output is fed into a mixer,

in which the local oscillator frequency is switched at about 270 c/s by altering the potential across a 'varactor' diode in the resonant circuit, then through a narrow band filter into an I.F. amplifier, a switch frequency amplifier and a synchronous detector. If there is a Faraday rotation of any polarized component between the two narrow frequency bands accepted in this way, an output will be observed. A change in output will also be observed if there is a change of the spectral index of the radiation as different regions pass through the beam.

(iv) *Power difference method using crossed dipoles.*—The procedure is to measure the difference in the aerial temperature of crossed dipoles, for example at the focus of a paraboloidal reflector. A source of linearly polarized radiation will, in general, give an output at the receiver. If drift curves are obtained from the region under examination, with the dipoles in some arbitrary position and the observations are then repeated with the dipoles rotated through 45°, the magnitude and direction of the apparent polarization may then be calculated. An unpolarized source off the axis of the dish will also give an output because the polar diagrams of the dipoles in the *E* and *H* planes are different. The spurious effects may be calculated by determining the polar diagram of the system for unpolarized radiation, using the Sun, and convolving this with a map of the brightness distribution over the sky. Subtraction then gives any polarized radiation that may be present.

(v) *Correlation method using crossed dipoles.*—Correlation of the voltages induced in crossed dipoles at the focus of a paraboloid may be measured using a phase-switching receiver. As in (iv) an output is obtained both from linearly polarized sources and from unpolarized sources off the axis, although the spurious effects in the two methods are different and arise in different ways. Here, they are due to the cross-polarization terms of the polar diagrams of the dipoles (4). The procedure of observation and calculation of spurious effects is the same as that in method (iv).

Alternatively, the ionosphere may be used to provide variations in the rotation of any polarized component of the radiation and the dipoles may be continuously rotated, so that all the information required is obtained during one run—this was the method used by Thomson.

4. *Observations and results*

In this section, the terms 'polarization temperature' and 'degree of polarization' are used. By the former is meant the difference in the aerial temperatures of two dipoles, one of which receives all the polarized radiation and the other none, and by the latter is meant this difference divided by the sum of the aerial temperatures. These definitions conform to normal usage.

(i) *Ionospheric rotation method.*—Observations were carried out in 1958, March–April using a cylindrical parabolic aerial, at a frequency of 160 Mc/s. The beamwidth was 1°·2 in R.A. and 7°·7 in Dec., the bandwidth 2·5 Mc/s, and the region covered extended from R.A. 13^h to 22^h at Dec. + 17°. The upper limit of 5 per cent on the degree of polarization was imposed by variations in receiver sensitivity.

A similar experiment at 178 Mc/s was carried out in 1959 June, the bandwidth being 4 Mc/s, the beamwidth 13'·6 in R.A. and 4°·6 in Dec., and the region covered extending from R.A. 12^h to 03^h at Dec. + 19°. An upper limit of 5 °K was put on the polarization temperature, corresponding to upper limits of the

degree of polarization between 0·6 per cent and 1·5 per cent over the different regions observed.

(ii) *The 'comb filter' method.*—Observations were made in 1958 March at 160 Mc/s with the same aerial constants as those given above and covered the region R.A. 10^h to 21^h at Dec. $+17°$. The cable lengths used corresponded to all possible Faraday rotations between 1 turn and 4 turns across the pass-band. Drifts of the zero level limited the accuracy of the experiment which gave an upper limit of about 5 per cent to linear polarization with the Faraday rotations indicated above.

(iii) *The frequency-switching method.*—An experiment was carried out in 1960 April, mainly as a test of the method, at a frequency of 178 Mc/s using the aerial of method (i). The switching took place between two bands of width 250 kc/s separated by 3 Mc/s. The region observed was at R.A. 00^h to 24^h, Dec. $+19°$. Drifts of zero level limited the accuracy, but an upper limit of 5 per cent could again be placed on any linear polarization of the spur which rotates appreciably in the frequency interval given. Drifts due to variations in spectral index across the regions observed would be expected to be small compared with those observed.

(iv) *The power difference method.*—Observations using a 7·5 m paraboloid at a frequency of 408 Mc/s were carried out during 1959 September. The beamwidth was 8°. The aerial was directed at the North Pole, then at the region R.A. 17^h, Dec. $+17°$, which was allowed to drift through the beam, and finally at the North Pole again. Four runs were obtained with the same orientation of the dipoles; then the procedure was repeated for orientations at 45°, 90° and 135° to the original. The spurious effects were calculated and gave a polarization temperature of about 0·5 °K. The actual polarization temperature measured was 1 °K ± 1 °K, giving a degree of polarization in this region of less than 2 per cent.

(v) *The correlation method.*—In 1959 October, the region of sky centred at R.A. 17^h, Dec. $+20°$ was followed with the same paraboloid as in the previous experiment for three hours after sunset. During this time, the orientation of the sky with respect to the dipoles changed by only 4°, so that spurious effects would remain nearly constant, whereas a rotation of about 60° was expected for any polarized component as the electron content of the ionosphere and the line of sight through it altered. An upper limit of 2 °K could be put on the polarization temperature, or about 2 per cent on the degree of polarization of the radiation from this region.

TABLE I

Method	Frequency	Bandwidth	Beamwidth		Region		Per cent polarization
			α	δ	α	δ	less than
(i)	159 Mc/s	2·5 Mc/s	1°·2	7°·7	13^h–22^h,	+17°	5
(i)	178	4	13′·6	4°·6	12^h–03^h,	+19°	1
(ii)	159	0·3–1·25	1°·2	7°·7	10^h–21^h,	+17°	5
(iii)	178	0·25 3 Mc/s apart	13′·6	4°·6	0^h–24^h,	+19°	5
(iv)	408	1	8°		17^h	+17°	2
(v)	160	4	15°		17^h–18^h,	+22°	1 (J. Thomson)
(v)	408	1	8°		17^h	+20°	2
(v)	404	4	8°		13^h–17^h,	+17°	4 to 2

In 1960 April–May drift curves were obtained of the region of sky R.A. 13^h–17^h, Dec. $+17°$, with the same paraboloid, at a frequency of 404 Mc/s, using two orientations of the dipoles. The spurious responses fixed the limit of detection of polarized radiation at 2 °K over the region as a whole (or a degree of polarization of 4 per cent near R.A. 13^h to 2 per cent near R.A. 17^h). No significant polarized radiation was detected.

All these results are summarized in Table I, together with those of Thomson (**2**).

5. *Conclusions.*—The experiments have shown that the degree of polarization in the bright region of the spur, at the lower frequencies of 160 and 178 Mc/s and at the higher frequency of 408 Mc/s, is very small and that depolarization across the bandwidth does not occur at the lower frequencies.

It is possible to account for Thomson's null result at 160 Mc/s on the basis of Tunmer's mechanism if the usual values of the interstellar magnetic field and electron density are assumed, but it is difficult to explain the low results at 178 Mc/s, in view of the smaller beamwidth used, and those at 408 Mc/s, in view of the smaller interstellar Faraday rotation. Some alternative explanation of this galactic feature should therefore be sought.

The theoretical implications of the observations will be discussed in more detail in a further paper.

Mullard Radio Astronomy Observatory,
Cavendish Laboratory,
Cambridge:
1960 *November* 4.

References

(1) H. Tunmer, *Phil. Mag.*, **3**, 28, 370, 1958.
(2) J. H. Thomson, *Nature* (*Lond.*), **180**, 495, 1957.
(3) V. A. Razin, *Astr. J., U.S.S.R.*, **35**, 241, 1958.
(4) S. Silver, *Microwave Antenna Theory and Design*, Ch. 12, McGraw-Hill, 1949.

VEILED ABSORPTION LINES

F. M. Hawkins

(Communicated by the Director, University Observatory, Oxford)

(Received 1960 November 28)*

Summary

It has been suggested that some apparently faint Fraunhofer lines may not be faint in the theoretical sense, but may be formed in low photospheric layers and ' veiled ' by a higher emitting atmosphere.

This paper contains a theoretical investigation of this hypothesis. An exact solution is found for the residual intensity subject to certain standard though rather restrictive conditions. In the concluding section line profiles are drawn for veiled lines and for lines without veiling to show the effect of veiling on a line profile.

---

1. *Introduction.*—In a letter to *The Observatory* C. de Jager and L. Neven (**9**) wrote: "It is well known to many workers in the field of stellar spectroscopy that some faint Fraunhofer lines need not necessarily be 'faint' in the theoretical sense, which means that they should not necessarily be situated on the 45° part of the curve of growth. There are lines that are caused by strong absorption in deep layers of a stellar atmosphere and which are veiled by the radiation from the non-selectively absorbing higher layers. Such lines may apparently be weak, but nevertheless behave as a strong or medium strong line, and show saturation effects since they are caused by strong absorption in the relevant parts of the stellar photosphere, where the line is principally formed."

In view of this suggestion, it seems desirable to use a model in which the star is surrounded by a continuously absorbing region, which will be called the atmosphere, and to compare the exact solution with the corresponding solution in the *standard case* in which there is no such atmosphere. This comparison is effected by computing the profiles of veiled lines at various points of the disk in the two cases. More information about the centre to limb variation of the profiles of weak lines, thought to be veiled, will be required before adequate comparison with observation will be possible.

The model used (see Fig. 1) is that of a plane parallel atmosphere of thickness x_1, lying above a plane parallel photosphere of infinite extent. Throughout both the atmosphere and the photosphere there is continuous emission according to a linear Planck function. Absorption lines are formed in the photosphere and the atmosphere is non-scattering. There is no radiation falling on the upper surface of the atmosphere. It is required to find the emergent intensity at any point of the line profile considered.

In the first section of this paper an exact solution is found for the emergent intensity subject to certain standard conditions which will be enumerated later. The method used is one, developed by I. W. Busbridge, which was originally given by Ambartsumian for semi-infinite atmospheres. With this method it is

* Received in original form 1960 August 3.

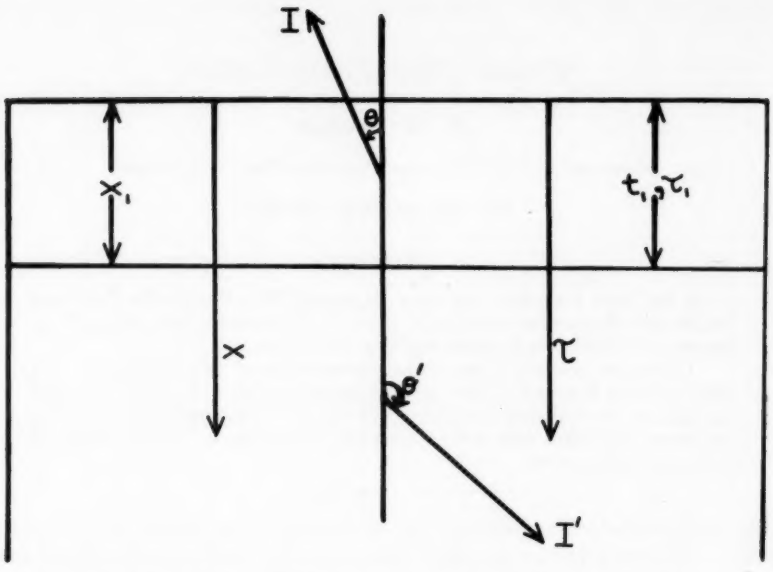

FIG. 1.—*Diagram of the solar model used. The atmosphere is of thickness x_1 and the photosphere of infinite extent. In terms of optical depth the atmosphere has thickness τ_1 and in terms of the t variable it has thickness t_1. I is used for the intensity in the atmosphere and I′ for that in the photosphere.*

comparatively simple to find an exact solution in terms of H functions, their moments, and integrals of expressions containing H functions. The coefficient ϵ is introduced to allow for thermal emission and, in the numerical results, values for the emergent intensity are found in the case of lines formed by pure scattering ($\epsilon = 0$) and pure absorption ($\epsilon = 1$).

A method of dealing with the variation of η (the ratio of the line absorption coefficient to the continuous absorption coefficient) is then developed in Section 6 for the case of lines formed by pure absorption ($\epsilon = 1$), and a formula capable of quite wide application derived*.

Finally diagrams are drawn to show the effects of veiling on line profiles.

2. *Derivation of the Milne equation of the problem.*—The problem is solved subject to certain conditions. Throughout both the atmosphere and the photosphere it is assumed that

(i) the variations of the continuous absorption coefficient κ over the range of frequencies considered may be neglected;

(ii) the variation of the Planck function $B(\nu, T)$ with the depth x below the surface of the atmosphere is such that it can be represented in the form

$$B(\nu, T) = b_0 + b_1\tau,$$

where

$$\tau = \int_0^x \kappa\rho \, dx$$

and where the variations of the coefficients b_0 and b_1 over the range of frequencies considered may be neglected.

* Similar work has been done by Eddington (6) using a Milne-Eddington approximation and for a particular type of variation of η with optical depth.

Throughout the photosphere it is assumed, in addition, that

(iii) the ratio η_ν of the line scattering coefficient to κ is independent of τ;

(iv) the scattering in the line frequencies is isotropic, and also coherent, *i.e.* the frequency re-emitted within the line depends only on the radiation absorbed at the same frequency;

(v) the coefficient ϵ, introduced to allow for thermal emission within the line, is independent of both ν and τ.

Let $\tau=\tau_1$ when $x=x_1$ (see Fig. 1). In the atmosphere, $(0\leqslant\tau\leqslant\tau_1)$, we denote the intensity in the line considered by $I_\nu(\tau,\mu)$, and in the photosphere, $(\tau>\tau_1)$, we denote it by $I'_\nu(\tau,\mu)$, a prime indicating the photosphere. In the atmosphere the intensity $I_\nu(\tau,\mu)$, at an optical depth τ and at an angle $\cos^{-1}\mu$ with the outwards drawn normal, satisfies the transfer equation

$$\mu(d/d\tau)I_\nu(\tau,\mu)=I_\nu(\tau,\mu)-(b_0+b_1\tau) \tag{2.1}$$

with the boundary conditions

$$I_\nu(0,-\mu)=0 \qquad (0\leqslant\mu\leqslant 1), \tag{2.2}$$

$$I_\nu(\tau_1,+\mu)=I'_\nu(\tau_1,+\mu) \qquad (0\leqslant\mu\leqslant 1). \tag{2.3}$$

Now consider the radiation in the photosphere in the line frequencies. Here the intensity $I'_\nu(\tau,\mu)$ satisfies the transfer equation

$$\mu(d/d\tau)I'_\nu(\tau,\mu)=(1+\eta_\nu)I'_\nu(\tau,\mu)-\tfrac{1}{2}(1-\epsilon)\eta_\nu\int_{-1}^{1}I'_\nu(\tau,\mu')d\mu'-(1+\epsilon\eta_\nu)(b_0+b_1\tau) \tag{2.4}$$

and the boundary condition

$$I_\nu(\tau_1,-\mu)=I'_\nu(\tau_1,-\mu) \qquad (0\leqslant\mu\leqslant 1). \tag{2.5}$$

If we write

$$t_\nu=(1+\eta_\nu)\tau, \qquad t_1=(1+\eta_\nu)\tau_1, \tag{2.6}$$

$$\lambda_\nu=(1+\epsilon\eta_\nu)/(1+\eta_\nu), \qquad n_\nu=1/(1+\eta_\nu), \tag{2.7}$$

and if we replace $I'_\nu(\tau,\mu)$ by $I'_\nu(t_\nu,\mu)$, then (2.4) becomes

$$\mu(d/dt_\nu)I'_\nu(t_\nu,\mu)=I'_\nu(t_\nu,\mu)-\tfrac{1}{2}(1-\lambda_\nu)\int_{-1}^{+1}I'_\nu(t_\nu,\mu')d\mu'-\lambda_\nu(b_0+b_1n_\nu t_\nu) \tag{2.8}$$

and the boundary conditions (2.2), (2.3) and (2.5) become

$$I_\nu(0,-\mu)=0 \qquad (0\leqslant\mu\leqslant 1), \tag{2.9}$$

$$I_\nu(\tau_1,+\mu)=I'_\nu(t_1,+\mu) \qquad (0\leqslant\mu\leqslant 1), \tag{2.10}$$

$$I_\nu(\tau_1,-\mu)=I'_\nu(t_1,-\mu) \qquad (0\leqslant\mu\leqslant 1). \tag{2.11}$$

We also need a condition limiting the rate of increase of $I'_\nu(t_\nu,\mu)$ for large t_ν. We make this rate so small that the homogeneous Milne equation will have no non-null solution. (This restriction is in fact necessary to obtain a result which satisfies the physical conditions of the problem. For if we take the non-null solution we would obtain a source function which was exponentially large for large t_ν, and therefore a temperature which increased exponentially for large t_ν.)

Using the condition (2.2) we first solve (2.1) for $I_\nu(\tau,-\mu)$ and obtain the following expression

$$I_\nu(\tau,-\mu)=b_0+b_1(\tau-\mu)-(b_0-b_1\mu)\exp(-\tau/\mu) \quad (0\leqslant\mu\leqslant 1), \tag{2.12}$$

and then the boundary condition (2.11) becomes

$$I'_\nu(t_1,-\mu)=b_0+b_1(\tau_1-\mu)-(b_0-b_1\mu)\exp(-\tau_1/\mu)$$
$$=b_0+b_1(n_\nu t_1-\mu)-(b_0-b_1\mu)\exp(-n_\nu t_1/\mu) \quad (0\leqslant\mu\leqslant 1). \tag{2.13}$$

We now solve (2.8) subject to (2.13). Write

$$\mathfrak{F}'(t_\nu)=\tfrac{1}{2}(1-\lambda_\nu)\int_{-1}^{+1} I'_\nu(t_\nu,\mu')d\mu'+\lambda_\nu(b_0+b_1 n_\nu t_\nu); \tag{2.14}$$

then, dropping the subscript ν for the time being, (2.8) is

$$\frac{d}{dt}I'(t,\mu)-\frac{1}{\mu}I'(t,\mu)=-\frac{1}{\mu}\mathfrak{F}'(t), \tag{2.15}$$

giving, for $0\leqslant\mu\leqslant 1$,

$$I'(t,+\mu)\exp(-t/\mu)=\int_t^\infty \mathfrak{F}'(x)\exp(-x/\mu)\mu^{-1}\,dx. \tag{2.16}$$

(This assumes $I'(t,+\mu)\exp(-t/\mu)\to 0$ as $t\to\infty$).

When $\mu<0$, write $-\mu$ for μ in (2.15). Then, for $0\leqslant\mu\leqslant 1$,

$$I'(t,-\mu)\exp(t/\mu)-I'(t_1,-\mu)\exp(t_1/\mu)=\int_{t_1}^t \mathfrak{F}'(x)\exp(x/\mu)\mu^{-1}\,dx, \tag{2.17}$$

where $I'(t_1,-\mu)$ is given by (2.13). From (2.16), (2.17) and (2.14) we obtain

$$\mathfrak{F}'(t)=\tfrac{1}{2}(1-\lambda)\int_{-1}^{+1} I'(t,\mu')d\mu'+\lambda(b_0+b_1 nt)$$
$$=\tfrac{1}{2}(1-\lambda)\left\{\int_0^1 I'(t,+\mu')d\mu'+\int_0^1 I'(t,-\mu')d\mu'\right\}+\lambda(b_0+b_1 nt)$$
$$=\tfrac{1}{2}(1-\lambda)\int_0^1 d\mu'\int_t^\infty \mathfrak{F}'(x)\exp[-(x-t)/\mu'](\mu')^{-1}\,dx$$
$$+\tfrac{1}{2}(1-\lambda)\int_0^1 d\mu'\int_{t_1}^t \mathfrak{F}'(x)\exp[-(t-x)/\mu'](\mu')^{-1}\,dx$$
$$+\tfrac{1}{2}(1-\lambda)\int_0^1 I'(t_1,-\mu')\exp[-(t-t_1)/\mu']d\mu'+\lambda(b_0+b_1 nt)$$

i.e.
$$\mathfrak{F}'(t)=\tfrac{1}{2}(1-\lambda)\int_t^\infty \mathfrak{F}'(x)dx\int_1^\infty \exp[-u(x-t)]\,u^{-1}\,du$$
$$+\tfrac{1}{2}(1-\lambda)\int_{t_1}^t \mathfrak{F}'(x)\,dx\int_1^\infty \exp[-u(t-x)]u^{-1}\,du+B(t), \tag{2.18}$$

where $u=1/\mu'$ and

$$B(t)=\tfrac{1}{2}(1-\lambda)\int_0^1 I'(t_1,-\mu')\exp[-(t-t_1)/\mu']\,d\mu'+\lambda(b_0+b_1 nt). \tag{2.19}$$

Equation (2.18) is

$$\mathfrak{F}'(t)=\tfrac{1}{2}(1-\lambda)\int_t^\infty \mathfrak{F}'(x)\,E_1(x-t)\,dx+\tfrac{1}{2}(1-\lambda)\int_{t_1}^t \mathfrak{F}'(x)\,E_1(t-x)dx+B(t), \tag{2.20}$$

where

$$E_n(s)=\int_1^\infty x^{-n}\exp(-sx)\,dx.$$

The right hand side of (2.20) is not quite

$$(1-\lambda)\Lambda_t\{\mathfrak{B}'(x)\}+B(t),$$

where

$$\Lambda_\tau\{J(t)\}\equiv\tfrac{1}{2}\int_0^\infty J(t)\,E_1(|t-\tau|)\,dt.$$

Write $t=t_1+y$; $x=t_1+u$, so that $u=y$ when $x=t$.
Then (2.20) is

$$\mathfrak{B}'(t_1+y)=\tfrac{1}{2}(1-\lambda)\int_y^\infty \mathfrak{B}'(t_1+u)\,E_1(u-y)du$$
$$+\tfrac{1}{2}(1-\lambda)\int_0^y \mathfrak{B}'(t_1+u)\,E_1(y-u)du+B(t_1+y)$$

and this is the Milne equation

$$\mathfrak{B}'(t_1+y)=(1-\lambda)\Lambda_y\{\mathfrak{B}'(t_1+u)\}+B(t_1+y), \tag{2.21}$$

where, from (2.19) and (2.13),

$$B(t)=\tfrac{1}{2}(1-\lambda)\int_0^1\{b_0+b_1(nt_1-\mu')-(b_0-b_1\mu')\exp(-nt_1/\mu')\}\exp[-(t-t_1)/\mu']d\mu'$$
$$+\lambda(b_0+b_1nt)$$
$$=\tfrac{1}{2}(1-\lambda)\{(b_0+b_1nt_1)E_2(t-t_1)-b_1E_3(t-t_1)-b_0E_2(t-t_1+nt_1)$$
$$+b_1E_3(t-t_1+nt_1)\}+\lambda(b_0+b_1nt). \tag{2.22}$$

Define $B_1(y)$ by

$$B_1(y)=B(t_1+y). \tag{2.23}$$

Then on putting $t=t_1+y$ in (2.22) we obtain

$$B_1(y)=\tfrac{1}{2}(1-\lambda)\{(b_0+b_1nt_1)E_2(y)-b_1E_3(y)-b_0E_2(y+nt_1)+b_1E_3(y+nt_1)\}$$
$$+\lambda(b_0+b_1nt_1+b_1ny). \tag{2.24}$$

On writing

$$\mathfrak{B}'(t_1+y)=F(y), \tag{2.25}$$

(2.21) becomes

$$F(y)=(1-\lambda)\Lambda_y\{F(u)\}+B_1(y). \tag{2.26}$$

From (2.16)

$$I'(t_1,+\mu)=\int_{t_1}^\infty \mathfrak{B}'(x)\exp[-(x-t_1)/\mu]\,\mu^{-1}\,dx,$$

and on writing $t_1+y=x$ this becomes

$$I'(t_1,+\mu)=\int_0^\infty \mathfrak{B}'(t_1+y)\exp[-y/\mu]\mu^{-1}\,dy, \tag{2.27}$$

i.e.

$$I'(t_1,+\mu)=\int_0^\infty F(y)\exp[-y/\mu]\mu^{-1}\,dy. \tag{2.28}$$

The next section will be devoted to finding results which are needed to find $I'(t_1,+\mu)$ when $F(\mu)$ is a solution of (2.26).

3. *Preliminary mathematics.*—We begin by solving the equation

$$(1-\varpi\Lambda)_\tau\{F_1(t)\}=E_n(\tau+a) \tag{3.1}$$

in which $\varpi=1-\lambda$, $a\geqslant 0$ and $n=2, 3\ldots$. First we consider the auxiliary equation [see (2), section 3]

$$(1-\varpi\Lambda)_\tau\{F(t,\delta)\}=\exp(-\delta\tau). \tag{3.2}$$

We can multiply by $\exp(-a\delta)d\delta/\delta^n$ and integrate with respect to δ over $(1,\infty)$ and this gives

$$(1-\varpi\Lambda)_\tau\left\{\int_1^\infty \exp(-a\delta)\,F(t,\delta)\,\delta^{-n}\,d\delta\right\}$$

$$=\int_1^\infty \exp[-\delta(\tau+a)]\,\delta^{-n}\,d\delta=E_n(\tau+a).$$

Thus

$$F_1(t)=\int_1^\infty \exp(-a\delta)\,F(t,\delta)\,\delta^{-n}\,d\delta \tag{3.3}$$

is a solution of (3.1). It is known [see (2), theorem iv] that

$$\mathscr{L}_{1/\mu}\{F(t,\delta)\}\equiv\int_0^\infty F(t,\delta)\exp(-t/\mu)\,\mu^{-1}\,dt$$

$$=\frac{H(\mu)H(\delta^{-1})}{1+\mu\delta}, \tag{3.4}$$

where $H(\mu)$ is the solution of

$$H(\mu)=1+\tfrac{1}{2}\mu\,H(\mu)\varpi\int_0^1\frac{H(\xi)}{\xi+\mu}\,d\xi \tag{3.5}$$

which is continuous for $0\leqslant\mu\leqslant 1$ [see (4), Chapter 2]. Hence, by (3.3)

$$I'_1(t_1,+\mu)\equiv\int_0^\infty F_1(y)\exp(-y/\mu)\,\mu^{-1}\,dy$$

$$=\int_0^\infty \exp(-y/\mu)\,\mu^{-1}\,dy\int_1^\infty F(y,\delta)\exp(-a\delta)\,\delta^{-n}\,d\delta$$

$$=\int_1^\infty \exp(-a\delta)\,\delta^{-n}\,d\delta\int_0^\infty F(y,\delta)\exp(-y/\mu)\,\mu^{-1}\,dy$$

and therefore, by (3.4),

$$I'_1(t_1,+\mu)=\int_1^\infty\frac{H(\mu)H(\delta^{-1})}{1+\mu\delta}\exp(-a\delta)\,\delta^{-n}\,d\delta.$$

On putting $\delta=1/\xi$, this becomes

$$I'_1(t_1,+\mu)=H(\mu)\int_0^1\frac{\xi^{n-1}}{\xi+\mu}H(\xi)\exp(-a/\xi)\,d\xi. \tag{3.6}$$

In (2), theorem v (with $\chi=1-\lambda$), it is shown that the Laplace transform of the solution of

$$F_2(y)=(1-\lambda)\Lambda_y\{F_2(t)\}+a_0\tau+a_1 \tag{3.7}$$

is

$$I'_2(t_1,+\mu)\equiv\int_0^\infty F_2(y)\exp(-y/\mu)\,\mu^{-1}\,dy$$

$$=H(\mu)\{\lambda^{-1/2}(a_0\mu+a_1)+\tfrac{1}{2}a_0\lambda^{-1}(1-\lambda)\alpha_1\}, \tag{3.8}$$

where

$$\alpha_n = \int_0^1 H(\xi)\,\xi^n\,d\xi. \tag{3.9}$$

4. *The solution for the emergent intensity.*—The results of Section 3 can now be used to find the Laplace transform $I'(t_1, +\mu)$ of the solution of (2.26) with $B_1(y)$ given by (2.24). As the operator Λ_* is linear, this solution is

$$\begin{aligned} I'(t_1, +\mu) = \tfrac{1}{2}(1-\lambda)\Big\{&(b_0 + b_1 n t_1)\,H(\mu)\int_0^1 \frac{\xi}{\xi+\mu}H(\xi)\,d\xi \\ &- b_1 H(\mu)\int_0^1 \frac{\xi^2}{\xi+\mu}H(\xi)\,d\xi \\ &- b_0 H(\mu)\int_0^1 \frac{\xi}{\xi+\mu}H(\xi)\exp(-nt_1/\xi)\,d\xi \\ &+ b_1 H(\mu)\int_0^1 \frac{\xi^2}{\xi+\mu}H(\xi)\exp(-nt_1/\xi)\,d\xi\Big\} \\ &+ H(\mu)\{\lambda^{1/2}(b_1 n\mu + b_0 + b_1 n t_1) + \tfrac{1}{2}(1-\lambda)\alpha_1 b_1 n\}. \end{aligned} \tag{4.1}$$

By using (3.5) and the relations

$$\varpi = 1-\lambda, \quad \tfrac{1}{2}(1-\lambda)\alpha_0 = 1-\lambda^{1/2}$$

[see (2), equation (4.15)] the following expressions are found which simplify equation (4.1):

$$\begin{aligned} H(\mu)\int_0^1 \frac{\xi}{\xi+\mu}H(\xi)\,d\xi &= H(\mu)\int_0^1 \frac{\xi+\mu-\mu}{\xi+\mu}H(\xi)\,d\xi \\ &= H(\mu)\,\alpha_0 - 2(1-\lambda)^{-1}[H(\mu)-1] \\ &= 2(1-\lambda)^{-1}[1-\lambda^{1/2}H(\mu)], \\ H(\mu)\int_0^1 \frac{\xi^2}{\xi+\mu}H(\xi)\,d\xi &= H(\mu)\int_0^1 \frac{\xi(\xi+\mu)-\xi\mu}{\xi+\mu}H(\xi)\,d\xi \\ &= H(\mu)\,\alpha_1 - 2\mu(1-\lambda)^{-1}[1-\lambda^{1/2}H(\mu)]. \end{aligned}$$

On substituting these in (4.1) and writing $\tau_1 = nt_1$ and

$$\begin{aligned} S(\tau_1, \mu) = \tfrac{1}{2}(1-\lambda)H(\mu)\Big\{&b_0\int_0^1 \frac{\xi}{\xi+\mu}H(\xi)\exp(-\tau_1/\xi)\,d\xi \\ &- b_1\int_0^1 \frac{\xi^2}{\xi+\mu}H(\xi)\exp(-\tau_1/\xi)\,d\xi\Big\}, \end{aligned} \tag{4.2}$$

we obtain

$$\begin{aligned} I'(\tau_1, +\mu) = (b_0 + b_1\tau_1)[1-\lambda^{1/2}H(\mu)] &- \tfrac{1}{2}(1-\lambda)b_1\alpha_1 H(\mu) \\ &+ b_1\mu\,[1-\lambda^{1/2}H(\mu)] + \lambda^{1/2}(b_1 n\mu + b_0 + b_1\tau_1)\,H(\mu) \\ &+ \tfrac{1}{2}(1-\lambda)\alpha_1 b_1 n H(\mu) - S(\tau_1, \mu), \end{aligned}$$

i.e.

$$\begin{aligned} I'(\tau_1, +\mu) = (b_0 + b_1\tau_1 + b_1\mu) &- \lambda^{1/2} b_1\mu(1-n)\,H(\mu) \\ &- \tfrac{1}{2}(1-\lambda)\,b_1\alpha_1\,(1-n)\,H(\mu) - S(\tau_1, \mu). \end{aligned} \tag{4.3}$$

The solution of (2.1) subject to (2.3) is

$$\begin{aligned} I(0,+\mu) &= \exp(-\tau_1/\mu)\, I'(\tau_1,+\mu) + \mu^{-1}\int_0^{\tau_1} \exp(-\tau/\mu)(b_0+b_1\tau)\, d\tau \\ &= \exp(-\tau_1/\mu)\, I'(\tau_1,+\mu) + b_0 + b_1\mu \\ &\quad - \exp(-\tau_1/\mu)(b_0+b_1\tau_1+b_1\mu) \end{aligned} \tag{4.4}$$

where $I'(\tau_1,+\mu)$ is given by (4.3).

For emphasis $I(0,+\mu)$ will be written as $I_{\tau_1,\nu}(0,+\mu)$, and the corresponding quantity in the *standard case* in which there is no non-selectively absorbing atmosphere will be written as $I_{0,\nu}(0,+\mu)$. The intensity in the continuum (which is the same in both cases) will be denoted by $I^*(0,+\mu)$. Let $r_{\tau_1,\nu}$ and $r_{0,\nu}$ be respectively the percentage residual intensities for the veiled line and for the line in the standard case.

Then

$$r_{\tau_1,\nu} - r_{0,\nu} = \frac{100[I_{\tau_1,\nu}(0,+\mu) - I_{0,\nu}(0,+\mu)]}{I^*(0,+\mu)}. \tag{4.5}$$

The emergent intensity in the *standard case* in which there is no non-selectively absorbing atmosphere is given by*

$$I_{0,\nu}(0,+\mu) = H(\mu)\{\lambda^{1/2}(b_0+b_1 n\mu) + \tfrac{1}{2}(1-\lambda)\alpha_1 b_1 n\}.$$

Hence, from (4.5), (4.4) and (4.3),

$$\begin{aligned} \frac{I^*(0,+\mu)}{100}[r_{\tau_1,\nu} - r_{0,\nu}] &= \exp(-\tau_1/\mu)\{b_0+b_1\tau_1+b_1\mu - \lambda^{1/2}b_1\mu(1-n)H(\mu) \\ &\quad - \tfrac{1}{2}(1-\lambda)b_1\alpha_1(1-n)\,H(\mu) - S(\tau_1,\mu)\} + b_0 + b_1\mu \\ &\quad - \exp(-\tau_1/\mu)(b_0+b_1\tau_1+b_1\mu) \\ &\quad - \lambda^{1/2}(b_0+b_1 n\mu)H(\mu) - \tfrac{1}{2}(1-\lambda)\alpha_1 b_1 n\, H(\mu) \\ &= -\exp(-\tau_1/\mu)\{\lambda^{1/2} b_1\mu(1-n)H(\mu) \\ &\quad + \tfrac{1}{2}(1-\lambda)b_1\alpha_1(1-n)H(\mu)\} + b_0 + b_1\mu \\ &\quad - \lambda^{1/2}(b_0+b_1 n\mu)\, H(\mu) \\ &\quad - \tfrac{1}{2}(1-\lambda)\alpha_1 b_1 n H(\mu) - \exp(-\tau_1/\mu)\, S(\tau_1,\mu). \end{aligned}$$

On substituting for $S(\tau_1,\mu)$ from (4.2) we get

$$\begin{aligned} \frac{I^*(0,+\mu)}{100}[r_{\tau_1,\nu} - r_{0,\nu}] &= -\exp(-\tau_1/\mu)H(\mu)\{\lambda^{1/2}(b_0+b_1\mu) + \tfrac{1}{2}b_1(1-\lambda)\alpha_1\} \\ &\quad - H(\mu)[1-\exp(-\tau_1/\mu)]\{\lambda^{1/2}(b_0+b_1 n\mu) \\ &\quad + \tfrac{1}{2}(1-\lambda)\, b_1 n\alpha_1\} + b_0 + b_1\mu \\ &\quad - \tfrac{1}{2}(1-\lambda)\exp(-\tau_1/\mu)H(\mu)\Big\{b_0\int_0^1 \frac{\xi}{\xi+\mu} H(\xi)\exp(-\tau_1/\xi)d\xi \\ &\quad - b_1\int_0^1 \frac{\xi^2}{\xi+\mu} H(\xi)\exp(-\tau_1/\xi)d\xi\Big\} \end{aligned} \tag{4.6}$$

where $I^*(0,+\mu) = b_0 + b_1\mu$ [see (5)]†.

* See (5) Section 84, equation (66). This is also obtained from (4.1) on putting $t_1 = 0$.

† The value of $I^*(0,+\mu)$ can also be obtained by letting $\tau_1 \to \infty$ in (4.4), viz. $I^*(0,+\mu) = b_0 + b_1\mu$.

In the case of lines formed by pure absorption, ($\epsilon = 1$), (4.6) can be reduced to a much simpler expression.

On putting $\epsilon = 1$ in (2.7) this gives $\lambda = 1$ and, from (3.5) with $\varpi = 1 - \lambda = 0$, we see that

$$H(\mu) \equiv 1.$$

Hence (4.6) reduces to

$$\frac{I^*(0, +\mu)}{100} [r_{\tau_1, \nu} - r_{0, \nu}] = b_1 \mu [1 - \exp(-\tau_1/\mu)] [1 - n], \tag{4.7}$$

and the expression for the percentage residual intensity in the veiled line becomes

$$\frac{I^*(0, +\mu)}{100} r_{\tau_1, \nu} = b_0 + b_1 \mu \{1 - (1 - n) \exp(-\tau_1/\mu)\}. \tag{4.8}$$

5. *Numerical results.*—A plane parallel model is not a good representation near the limb and numerical results are therefore obtained only for $0{\cdot}2 \leqslant \mu \leqslant 1$. However it is interesting to note that in every case

$$r_{\tau_1, \nu} \frac{I^*(0, +\mu)}{100} \to (b_0 + b_1 \mu)_{\mu = 0} \quad \text{as} \quad \mu \to +0.$$

Since this is $I^*(0, +\mu)_{\mu=0}$, the lines fade out completely at the limb.

As any line is formed by a mixture of absorption and scattering it was decided to consider two extreme cases, one in which the lines are formed by pure scattering ($\epsilon = 0$), and the other in which the lines are formed by pure absorption ($\epsilon = 1$). In both these cases values of $r_{\tau_1, \nu} - r_{0, \nu}$ and $r_{\tau_1, \nu}$ have been calculated for various values of η_ν and for two thicknesses of the atmosphere, using the new tables of H functions prepared by Stibbs and Weir [see (**10**)]. In the former case the electronic computer at the University Computing Laboratory was used in obtaining numerical results and my thanks are due to the Director for allowing use of these facilities. The results are given in Tables I–IV.

TABLE I

The veiling effect of the atmosphere ($\epsilon = 0$)

η \ μ	1	0·9	0·8	0·7	0·6	0·5	0·4	0·3	0·2
					$r_{0\cdot3, \nu} - r_{0, \nu}$				
1	6·11	6·54	7·03	7·61	8·31	9·16	10·25	11·68	13·68
4	10·89	11·79	12·86	14·16	15·80	17·91	20·74	24·74	30·80
9	13·20	14·37	15·79	17·54	19·74	22·62	26·53	32·14	40·70
19	14·86	16·24	17·92	20·00	22·64	26·09	30·81	37·58	47·98
99	17·20	18·88	20·92	23·45	26·66	30·88	36·64	44·94	57·66
399	18·23	20·02	22·20	24·90	28·34	32·84	39·00	47·87	61·46
					$r_{0\cdot3, \nu} - r_{0, \nu}$				
1	8·65	9·20	9·82	10·53	11·37	12·34	13·51	14·90	16·49
4	15·37	16·54	17·92	19·57	21·59	24·11	27·33	31·59	37·24
9	18·60	20·15	21·98	24·21	26·96	30·45	34·98	41·06	49·28
19	20·92	22·74	24·93	27·59	30·90	35·11	40·62	48·04	58·13
99	24·18	26·40	29·07	32·32	36·37	41·55	48·33	57·48	69·93
399	25·61	27·98	30·84	34·32	38·66	44·19	51·46	61·25	74·56

TABLE II

The centre to limb variation of the veiled lines ($\epsilon = 0$)

η \ μ	1	0·9	0·8	0·7	0·6	0·5	0·4	0·3	0·2
					$r_{0\cdot2,\,\nu}$				
1	73·71	75·10	76·66	78·43	80·47	82·83	85·61	88·94	93·02
4	53·70	55·59	57·74	60·20	63·10	66·57	70·86	76·38	83·94
9	44·24	46·14	48·35	50·93	53·90	57·80	62·65	69·20	78·59
19	37·50	39·36	41·55	44·15	47·33	51·32	56·58	63·85	74·63
99	27·99	29·81	31·98	34·65	37·99	42·33	48·19	56·56	70·28
399	23·82	25·64	27·86	30·59	34·06	38·58	44·76	53·60	67·17
					$r_{0\cdot3,\,\nu}$				
1	76·25	77·76	79·45	81·35	83·53	86·01	88·87	92·16	95·83
4	58·18	60·34	62·80	65·61	68·89	72·77	77·45	83·23	90·38
9	49·64	51·92	54·54	57·60	61·22	65·63	71·10	78·12	87·17
19	43·56	45·86	48·56	51·74	55·59	60·34	66·39	74·31	84·78
99	34·97	37·33	40·13	43·52	47·70	53·00	59·88	69·10	81·55
399	31·19	33·60	36·50	40·01	44·38	49·93	57·22	66·98	80·27

TABLE III

The veiling effect of the atmosphere ($\epsilon = 1$)

η \ μ	1	0·9	0·8	0·7	0·6	0·5	0·4	0·3	0·2
					$r_{0\cdot2,\,\nu} - r_{0,\,\nu}$				
1	5·44	5·72	6·03	6·37	6·71	7·07	7·38	7·55	7·30
4	8·70	9·16	9·66	10·19	10·74	11·31	11·80	12·08	11·67
9	9·79	10·30	10·86	11·46	12·09	12·71	13·28	13·58	13·13
19	10·33	10·87	11·46	12·09	12·76	13·42	14·01	14·34	13·85
99	10·79	11·33	11·94	12·60	13·29	13·99	14·61	14·95	14·45
399	10·85	11·42	12·04	12·70	13·40	14·09	14·72	15·07	14·55
					$r_{0\cdot3,\,\nu} - r_{0,\,\nu}$				
1	7·78	8·14	8·53	8·93	9·32	9·67	9·89	9·81	8·97
4	12·44	13·04	13·65	14·29	14·91	15·48	15·83	15·69	14·34
9	14·00	14·66	15·33	16·05	16·77	17·40	17·81	17·65	16·14
19	14·77	15·47	16·20	16·96	17·71	18·37	18·79	18·63	17·03
99	15·40	16·12	16·89	17·68	18·45	19·14	19·59	19·42	17·75
399	15·51	16·25	17·02	17·81	18·59	19·29	19·74	19·57	17·88

TABLE IV

The centre to limb variation of the veiled lines ($\epsilon = 1$)

η \ μ	1	0·9	0·8	0·7	0·6	0·5	0·4	0·3	0·2
					$r_{0\cdot2,\,\nu}$				
1	75·44	77·00	78·76	80·76	83·03	85·64	88·63	92·03	95·76
4	60·70	63·20	66·02	69·21	72·85	77·02	81·80	87·25	93·21
9	55·79	58·60	61·77	65·36	69·46	74·14	79·53	85·65	92·36
19	53·33	56·30	59·64	63·43	67·76	72·71	78·39	84·86	91·93
99	51·39	54·46	57·94	61·89	66·40	71·56	77·48	84·23	91·60
399	51·00	54·12	57·63	61·61	66·15	71·34	77·31	84·11	91·53
					$r_{0\cdot3,\,\nu}$				
1	77·78	79·42	81·26	83·32	85·64	88·24	91·14	94·29	97·43
4	64·44	67·08	70·01	73·31	77·02	81·19	85·83	90·86	95·88
9	60·00	62·96	66·24	69·95	74·14	78·83	84·06	89·72	95·37
19	57·77	60·90	64·38	68·30	72·71	77·66	83·17	89·15	95·11
99	56·00	59·25	62·89	66·97	71·56	76·71	82·46	88·70	94·90
399	55·66	58·95	62·61	66·72	71·34	76·54	82·33	88·61	94·86

6. *Variation of η_ν with optical depth.*—Since the objection may be raised that the variation of η_ν with optical depth has been neglected, a method will now be developed which will take into account this variation in the case of lines formed by pure absorption ($\epsilon = 1$).

The same notation will be used as in Section 2, except that η_ν will be denoted by $\eta_\nu(\tau)$ as it is a function of optical depth. The problem will be solved subject to conditions (i), (ii), (iv) and (v) of Section 2.

In this case equation (2.4) becomes (with $\epsilon = 1$)

$$\mu(d/d\tau)I'_\nu(\tau,\mu) = [1+\eta_\nu(\tau)]I'_\nu(\tau,\mu) - [1+\eta_\nu(\tau)][b_0+b_1\tau] \tag{6.1}$$

and from (2.1) and (2.10) the expression for the emergent intensity is

$$I_{\tau_1,\nu}(0,+\mu) = I'(\tau_1,+\mu)\exp(-\tau_1/\mu) + b_0 + b_1\mu - (b_0+b_1\tau_1+b_1\mu)\exp(-\tau_1/\mu) \quad (0 \leqslant \mu \leqslant 1). \tag{6.2}$$

Equation (6.1) has the integrating factor

$$\exp\left\{-\int_{\tau_1}^{\tau}[1+\eta_\nu(t)]\,\mu^{-1}\,dt\right\}, \tag{6.3}$$

and on writing

$$n_\nu(\tau) = 1/[1+\eta_\nu(\tau)], \quad y(\tau) = \int_{\tau_1}^{\tau}[n_\nu(t)]^{-1}\,dt, \tag{6.4}$$

(6.3) becomes

$$\exp[-y(\tau)/\mu]. \tag{6.5}$$

On multiplying (6.1) by $\exp[-y(\tau)/\mu]$ and integrating with respect to τ over (τ, ∞), the following expression is obtained when $0 \leqslant \mu \leqslant 1$:

$$\mu I'(\tau,+\mu)\exp[-y(\tau)/\mu] = \int_{\tau}^{\infty}(b_0+b_1t)\,[1+\eta_\nu(t)]\exp[-y(t)/\mu]\,dt. \tag{6.6}$$

[This assumes $I'(\tau,+\mu)$ does not increase exponentially for large τ.]

Since $\eta_\nu(\tau) > 0$, therefore

$$1/n_\nu(\tau) = 1+\eta_\nu(\tau) \geqslant 1$$

and hence, for $\tau \geqslant \tau_1$,

$$y(\tau) = \int_{\tau_1}^{\tau}[n_\nu(t)]^{-1}\,dt \geqslant \tau - \tau_1. \tag{6.7}$$

Thus $y(\tau_1) = 0$ and $y(\tau) \to \infty$ as $\tau \to \infty$. On putting $\tau = \tau_1$ in (6.6) this becomes

$$\mu I'(\tau_1,+\mu) = \int_{\tau_1}^{\infty}(b_0+b_1t)[1+\eta_\nu(t)]\exp[-y(t)/\mu]\,dt. \tag{6.8}$$

This expression can be simplified since, from (6.4),

$$(d/d\tau)y(\tau) = 1/n_\nu(\tau) = 1+\eta_\nu(\tau), \tag{6.9}$$

and therefore

$$(d/d\tau)\exp\{-y(\tau)/\mu\} = -\mu^{-1}[1+\eta_\nu(\tau)]\exp[-y(\tau)/\mu]. \tag{6.10}$$

Also, from (6.7),

$$(b_0+b_1\tau)\exp[-y(\tau)/\mu] \to 0 \qquad (\tau \to \infty).$$

Hence, on integrating (6.8) by parts, we obtain

$$\mu I'(\tau_1, +\mu) = [-\mu(b_0 + b_1 t)\exp\{-y(t)/\mu\}]_{\tau_1}^{\infty} + \mu b_1 \int_{\tau_1}^{\infty} \exp[-y(t)/\mu]\, dt$$

$$= \mu(b_0 + b_1\tau_1) + \mu b_1 \int_{\tau_1}^{\infty} \exp[-y(t)/\mu]\, dt. \qquad (6.11)$$

Then from (6.2) the emergent intensity is given by

$$I_{\tau_1,\nu}(0, +\mu) = (b_0 + b_1\tau_1)\exp(-\tau_1/\mu) + b_1 \exp(-\tau_1/\mu) \int_{\tau_1}^{\infty} \exp[-y(t)/\mu]\, dt + b_0 + b_1\mu - (b_0 + b_1\tau_1 + b_1\mu)\exp(-\tau_1/\mu)$$

$$= b_0 + b_1\mu\,[1 - \exp(-\tau_1/\mu)] + b_1 \exp(-\tau_1/\mu) \int_{\tau_1}^{\infty} \exp[-y(t)/\mu]\, dt. \qquad (6.12)$$

The expression (6.12) is an exact solution for the emergent intensity in lines formed by pure absorption, and no particular law of variation of η_ν with optical depth is presupposed.

Numerical values for the percentage residual intensity were obtained in the case in which the photosphere is divided into two layers, in the upper of which $\eta_\nu(\tau)$ was a non-zero constant and in the lower $\eta_\nu(\tau)$ was zero. The values chosen for $\eta_\nu(\tau)$ in the upper layer were some of those used in the first part of this paper, viz. 1, 4, 9 and 19, and for these the optical thicknesses of the layer were taken to be 0·5, 0·2, 0·1 and 0·05 respectively. The values 0·2 and 0·3 were again used for τ_1. By comparing the results thus obtained with similar ones obtained by I. W. Busbridge for $\tau_1 = 0$ (see (**3**)), values for the veiling effect of the atmosphere were also obtained. Since, however, all my results for this case are similar to those obtained previously (see Section 5), it seems unnecessary to insert tables of them.

7. *Conclusions.*—In the previous sections formulae have been obtained which can be used to find the percentage residual intensity in certain cases. It now remains to compare the results, so obtained, with relevant observational data and to show how a veiling atmosphere would affect a line profile*. In Fig. 2 the variation of the percentage residual intensity for $\eta = 1$ is compared with observational data for weak lines obtained by M. G. Adam for faint Fraunhofer lines (**1**). The full line shows the variation of the percentage residual intensity from centre to limb for $\epsilon = 0$ and $\tau_1 = 0{\cdot}3$ obtained from the formulae of Section 4. The scattered points show the values for the central intensity (expressed as a percentage) obtained from Miss Adam's work. The filled circles are for the line λ 5102·975, the triangles for λ 5145·470 and the crosses for λ 5147·484 (these lines have respectively Rowland Intensities of 1, 0, 0), where for each line the mean of the results from three plates is shown. These lines are weak and are chosen because they give points quite close to the full curve at $\mu = 1$.

* For observational work on line profiles see, for example, (**7**) and (**8**). Computations have been made by de Jager and Neven (**9a**) for solar lines of N I and O I. Working from curves of growth for certain lines of N I and O I, computed with the aid of the Pecker saturation function, they showed that large errors are introduced by the usual weak line approximation.

In this paper the parameter η_ν has been used to denote the ratio of the line absorption coefficient to the continuous absorption coefficient. For a line produced by a certain atom, therefore, η_ν is the ratio of the atomic absorption

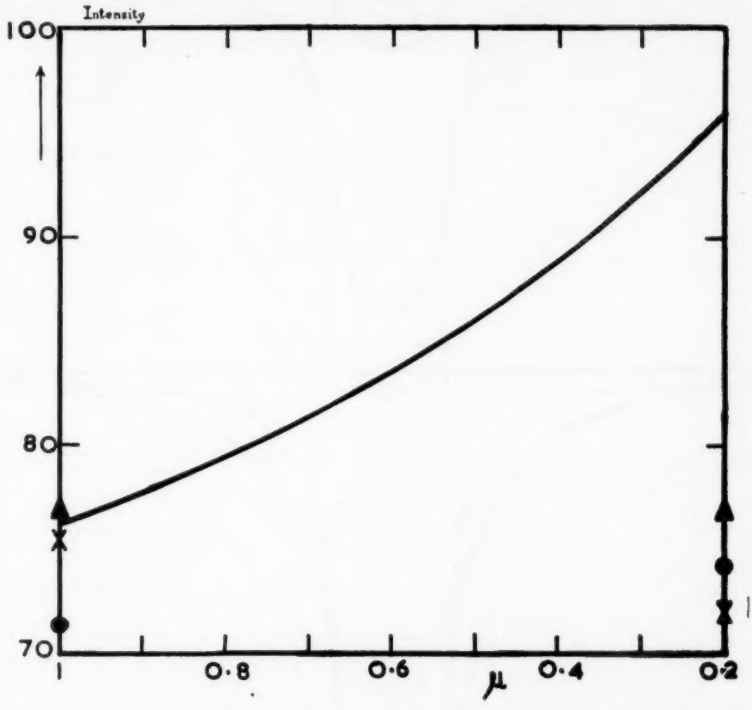

FIG. 2.—*Comparison of the variation from centre to limb of the residual intensity, obtained theoretically, with M. G. Adam's observational results. The ordinates represent residual intensity (expressed as a percentage).*

coefficient to the continuous absorption coefficient. As we can take the variation with frequency of the continuous absorption coefficient over a particular line to be negligible, the coefficient η_ν varies as the atomic absorption coefficient over the line. In the centre of the line (Doppler core), therefore, η_ν is proportional to $\exp(-\Delta\lambda^2/\Delta\lambda^2_D)$ and in the wings (damping wing) η_ν is proportional to $1/\Delta\lambda^2$, where $\Delta\lambda$ is the distance from the centre of the line in units of wavelength and $\Delta\lambda_D$ is the Doppler half width (i.e. $\Delta\lambda_D$ is the distance from the centre of the line to the point at which the intensity has e^{-1} of its value at the centre of the line).

In Fig. 3 the line profiles were drawn using $\eta = 399\exp(-v^2)$ for the central part of the line and $\eta = 9/v^2$ for the wings, and those in Fig. 4 using $\eta = 19\exp(-v^2)$ for the central part of the line and $\eta = 2{\cdot}25/v^2$ for the wings, where $v = \Delta\lambda/\Delta\lambda_D$. In each case η is taken to be independent of depth in the photosphere. These figures show how the line profile of a typical Fraunhofer line varies from centre to limb under certain circumstances. In each figure, the line profile at the centre of the Sun ($\mu = 1$) and at the limb ($\mu = 0{\cdot}2$) are shown. Fig. 3 shows the case in which the lines are formed by pure scattering ($\epsilon = 0$). In Fig. 3(*a*) there is a

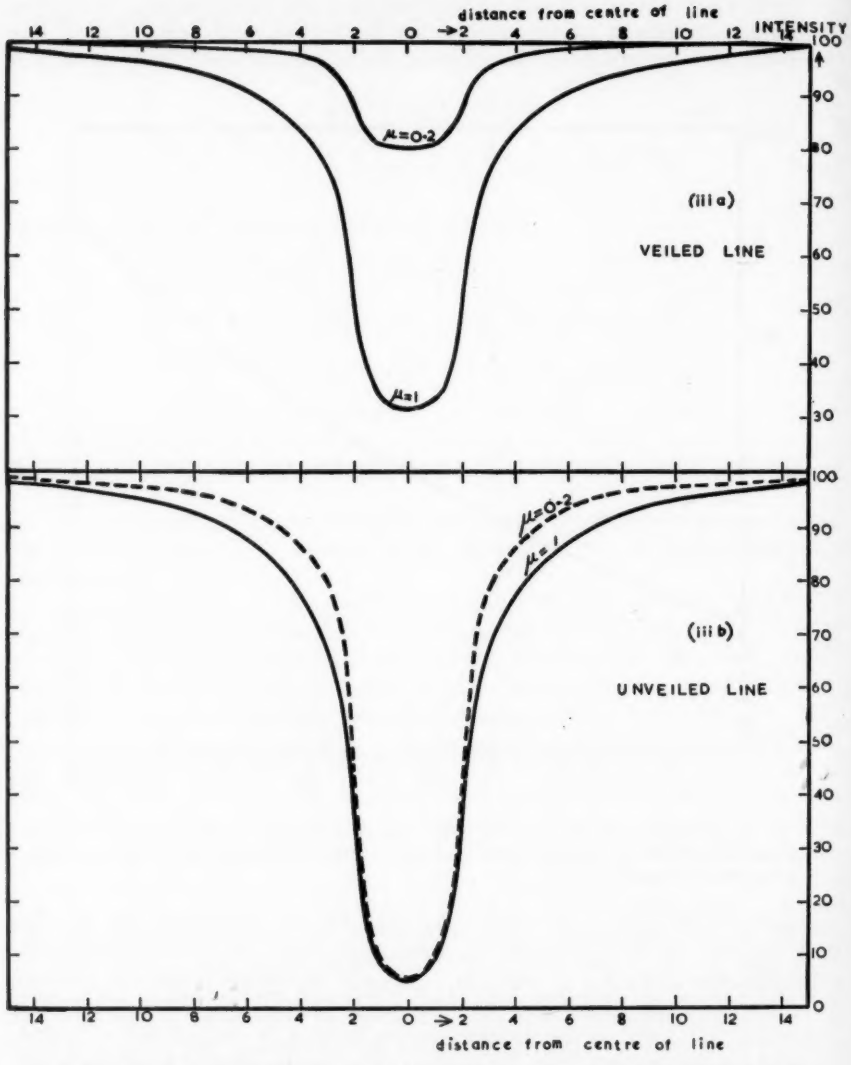

FIG. 3.—*Line profiles at the centre* ($\mu=1$) *and at the limb* ($\mu=0{\cdot}2$) *of a typical Fraunhofer line for the case in which the line is formed by pure scattering* ($\epsilon=0$). *In Fig.* 3(*a*) *there is a veiling atmosphere of optical thickness* 0·3 *and in Fig.* 3(*b*) *there is no such atmosphere. In each case the distance from the centre of the line is measured in units of* $\Delta\lambda/\Delta\lambda_D$, *and the ordinates represent percentage residual intensity.*

veiling atmosphere of optical thickness 0·3 and in Fig. 3 (*b*), which is shown for comparison, there is no such veiling atmosphere. Fig. 4 shows the case in which the lines are formed by pure absorption ($\epsilon=1$). In Fig. 4 (*a*) there is a veiling atmosphere of optical thickness 0·3 and in Fig. 4 (*b*), which is shown for comparison, there is no such veiling atmosphere.

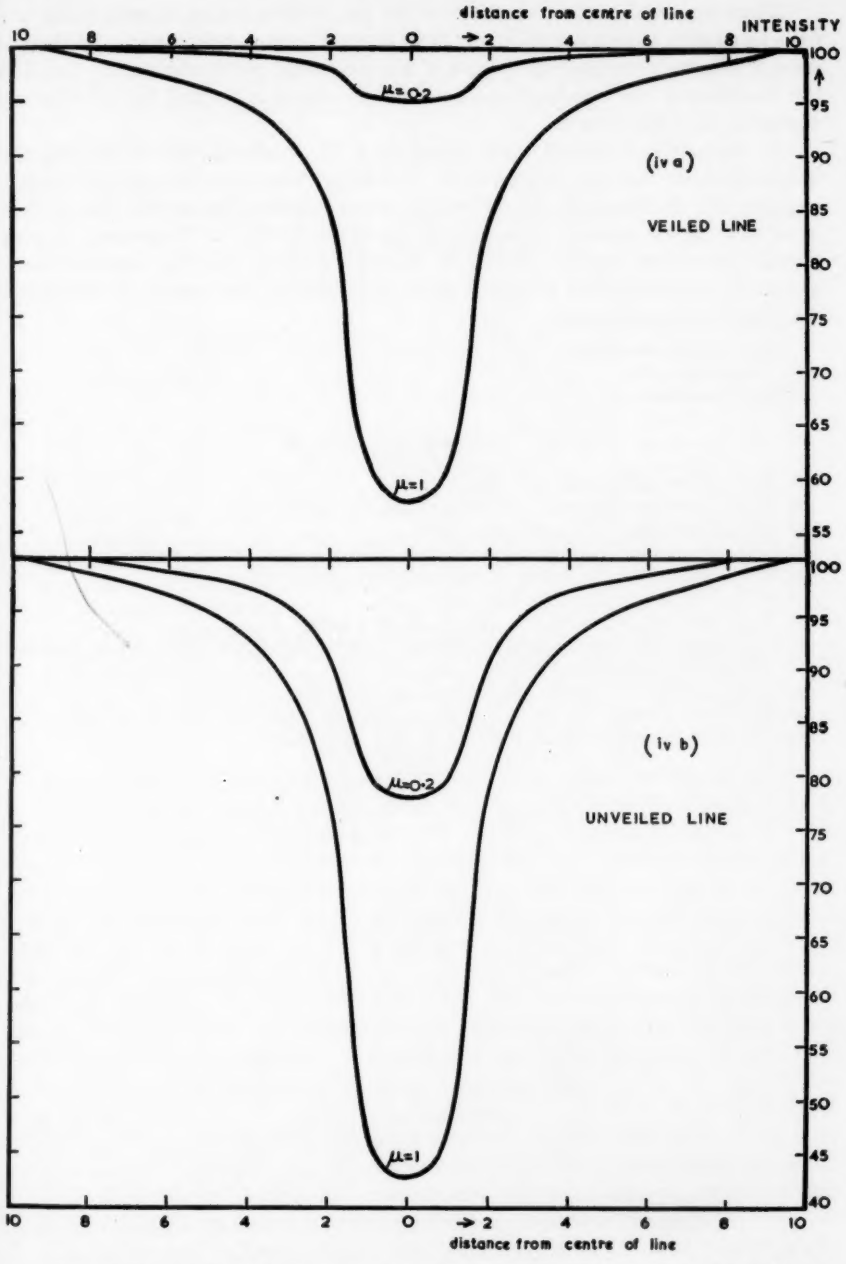

FIG. 4.—*Line profiles at the centre* ($\mu=1$) *and at the limb* ($\mu=0{\cdot}2$) *of a typical Fraunhofer line for the case in which the line is formed by pure absorption* ($\epsilon=1$). *In Fig.* 4(*a*) *there is a veiling atmosphere of optical thickness* 0·3 *and in Fig.* 4(*b*) *there is no such atmosphere. In each case the distance from the centre of the line is measured in units of* $\Delta\lambda/\Delta\lambda_D$, *and the ordinates represent percentage residual intensity.*

These figures show the behaviour of the line profiles in two extreme cases, *viz.* lines formed by pure absorption and lines formed by pure scattering. As there is some similarity between Figs. 3 (*a*) and 4 (*a*), it would not be difficult to visualize the variation of the line profile of a veiled line which is formed by a mixture of scattering and absorption.

In conclusion, I should like to thank Dr I. W. Busbridge for all her help and encouragement, and also Professor H. H. Plaskett who made several very helpful suggestions, Professor D. W. N. Stibbs who advised me about the best method of integrating expressions containing *H* functions, Dr W. R. Hindmarsh for very useful discussions on the physics of absorption lines, and the Department of Scientific and Industrial Research for awards, during the tenure of which this work has been carried out.

University Observatory,
Oxford:
1960 *September.*

References

(1) M. G. Adam, *M.N.*, **98**, 112, 1937.
(2) I. W. Busbridge, *Quart. J.* (Oxford), (2), **6**, 218, 1955.
(3) I. W. Busbridge, *M.N.*, **116**, 304, 1956.
(4) I. W. Busbridge, *Mathematics of Radiative Transfer* (Cambridge, 1960).
(5) S. Chandrasekhar, *Radiative Transfer* (Oxford, 1950).
(6) A. S. Eddington, *M.N.*, **89**, 620, 1929.
(7) G. E. Hale and W. S. Adams, *Ap. J.*, **25**, 300, 1907.
(8) J. Houtgast, *The Variations in the Profiles of Strong Fraunhofer Lines along a Radius of the Solar Disc*, thesis, Utrecht, 1942.
(9) C. de Jager and L. Neven, *Observatory*, **79**, 102, 1959.
(9a) L. Neven, *Comm. Obs. Roy. de Belgique*, **157**, 112, 1959.
(10) D. W. N. Stibbs and R. E. Weir, *M.N.*, **119**, 512, 1959.

A STUDY OF SUNSPOT VELOCITY FIELDS USING A MAGNETICALLY UNDISTURBED LINE

J. Holmes

(Communicated by the Director, University Observatory, Oxford)

(Received 1960 November 28)

Summary

The relation between magnetic lines of force and material motion is a matter of considerable importance in sunspot theory, and this investigation of sunspot velocity fields uses a line for which the Landé splitting factor $g=0$. (Fe I λ 5576·101). Doppler displacements were measured at over 100 points in the region of both a large and small sunspot. At the high dispersion value of 0·17 A/mm, measurement difficulties are presented by the broad solar lines, but a check on visual accuracy was provided by a new photo-electric method of measurement. The measured velocities were corrected for observer's motion and solar rotation and reduced to velocity components, with origin at the spot centre. Using Kinman's conclusion that the spot flow is wholly radial, we have obtained fair agreement for the maximum radial velocity in the penumbra of the small spot but found a value much smaller than that predicted by Kinman for the large spot.

The differences from the earlier measures have been attributed to the fact that we are now able to measure the true Doppler shifts, freed from the complicating effects of Zeeman splitting, and also to the " line-flare ", which appears in the penumbral region of high dispersion spectra, but was not resolved in the earlier work on Evershed effect.

Introduction.—Motion in the neighbourhood of sunspots was first investigated by Evershed in 1901, and its general form is now well established (**1, 5, 6, 7, 8, 9, 18, 19**). Detailed measurements were made by Kinman at Oxford in 1952 (**10, 11**) and again by Servajean at Meudon in 1958 (**17**). What has been neglected to date, however, is the distinction between line shifts due to velocity along the line of sight and shifts which have their origin in the line splitting produced by the magnetic field of the sunspot. The sunspot velocity fields and magnetic fields are both observed to change in a more or less regular fashion across the penumbra, and the relation between magnetic lines of force and material motion is a matter of considerable importance in sunspot theory. Plate 6 (*a*) shows the splitting of the Fe line λ6302 across a sunspot. This clearly shows that the partial suppression of one or other of the two σ components of the pattern due to instrumental polarization can easily lead to an apparent line displacement. A line such as λ6302 is an extreme case and would not be used for velocity measures, but such effects exist on a smaller scale for all lines, except those for which the Zeeman splitting factor is zero. It is only by using such a magnetically unaffected line that we can be sure that the velocities we measure are free from magnetic field effects*.

For this reason we have selected the Fe line λ5576·101 for our present study of sunspot velocity fields. This is a line first suggested by Von Klüber (**20**), for

*Servajean's work (*Ann. d'Astrophys.*, **24**, 1, 1961), using the line λ 5691·508 (Fe Ni) for which $g=0$, has been published while the present paper was in the press.

which the Landé splitting factor $g = 0$. But we have now to contend with the observational difficulties presented by such a choice. There are no terrestrial standards in this region, such as the oxygen lines which appear in Plate 6 (*a*), or the water vapour lines used by Kinman, but the difficulty has been overcome here by introducing absorption lines due to iodine vapour into the solar spectrum. These could not be introduced directly into the sunspot spectrum because the iodine line density is too high but, instead, two exposures were made in rapid succession; the first for the spot spectrum alone and the second for the spot spectrum plus iodine. The iodine lines could then be used to show slit curvature and possible slit inclination, and consequently these effects could be allowed for in the solar exposure. We then assume that at the top and bottom of the slit, far removed from the spot, the line shows only the normal photospheric velocity shift due to solar rotation, plus a possible limb effect, if we take the effect of the photospheric velocity fields to be uniform across the slit. After calculating and allowing for such effects at selected points across the slit, we have the true Evershed effect.

Observations have so far been made on one small and one large spot. Central meridian passages (kindly supplied by the Royal Greenwich Observatory) were September 11.30 and September 3.25 respectively. The observational material, together with its measurement and reduction, are described in the first two sections of the paper and we conclude with a short discussion of the velocity fields now obtained.

1. *Observations and measurements.*—The sunspot spectra for the investigation were obtained by Professor Plaskett in September 1959. The image radius ρ_0 as given by the new solar telescope was 165 mm and the slit height of 25 mm corresponds to approximately 145 seconds of arc or approximately 105 500 km on the solar surface at the disk centre. The Babcock grating was used in the 5th order with the 40 ft spectrograph, resulting in a linear dispersion of 0·17 A/mm. In each exposure, the slit passed through the spot centre and details of the measured plates are given in Table I. In this table, ρ = radial distance of the spot from the disk centre and B, L are the heliographic latitude and longitude of the spots.

TABLE I

Measured plates

Measured line λ 5576·101 $z\,^5F^0 - e\,^5D$ Fe I.
Slit height = 25 mm.
Slit width = 0·045 mm.
Dispersion = 0·17 A/mm.

Plate	Date 1959	U.T.	Exposure time	B	L	ρ/ρ_0	Umbral diameter
E22	Sept. 7	$16^h\,02^m\,16^s$	40 sec	$+17°\,02'$	$15°\,54'$	0·793	46″
E23		$16^h\,12^m\,35^s$	60 sec				34000 km.
E28	Sept. 9	$08^h\,41^m\,57^s$	30 sec			0·597	17″
E29		$08^h\,49^m\,38^s$	31 sec	$-18°\,10'$	$274°\,50'$		12000 km.
E36	Sept. 10	$08^h\,28^m\,16^s$	30 sec			0·471	
E37		$09^h\,17^m\,06^s$	30 sec				

Measurements were made using the Hilger micrometer with a transverse motion for the plate stage (**16**). The field of view, perpendicular to the dispersion,

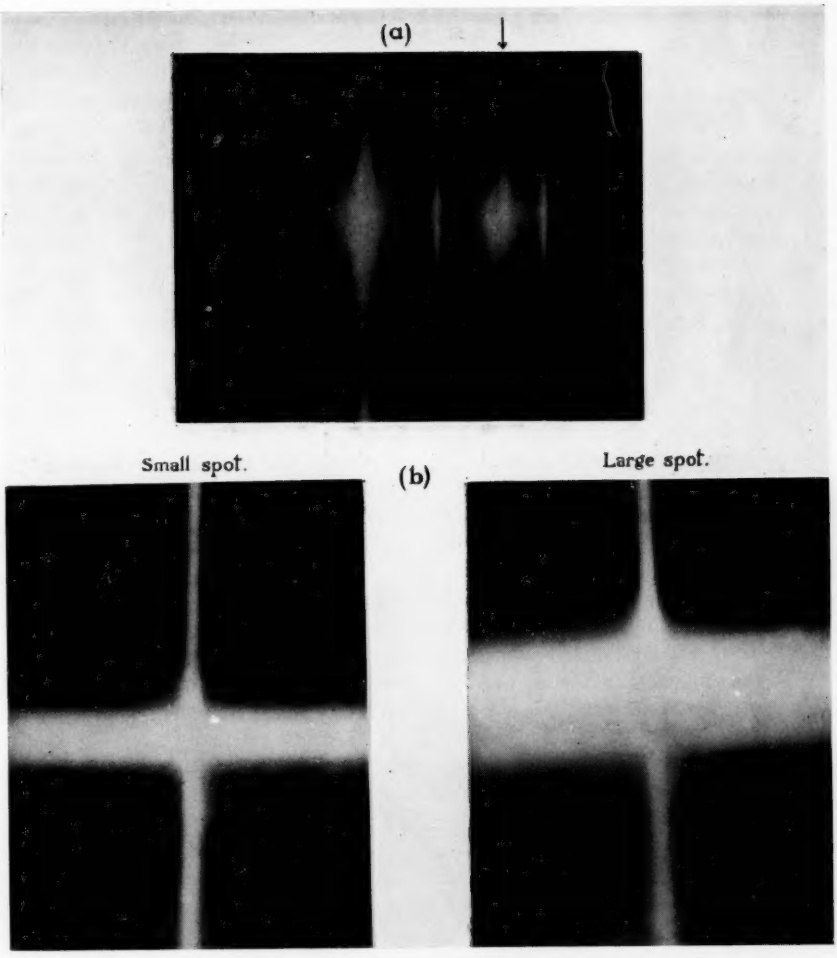

(*a*) Zeeman splitting in Fe λ 6302.
(*b*) " Line-flare " in large and small spots.

J. Holmes, A study of sunspot velocity fields using a magnetically undisturbed line.

was restricted to 0·3 mm by a diaphragm in the microscope eyepiece, so that this width of spectrum can be measured at any desired height. Since the sunspot spectra contain no atmospheric lines or lines of zero velocity, a ruled glass plate was used to provide a fiduciary line. This was permanently attached to the microscope stage and check settings were made on the ruled line throughout all the micrometer measurements of sunspot and iodine lines. Provided the sunspot spectra and iodine spectra are closely aligned at the same angle with respect to the fiduciary line, the iodine line readings give a correction curve as a function of slit height, by means of which all instrumental shifts may be removed from the observed displacements of the solar line. The six iodine correction curves were identical within the errors of measurement and were combined to give a single curve by means of a least squares solution.

All spectra were measured in the direct and reversed directions and mean readings obtained. The sunspot spectra were measured at over 100 points over the 25 mm slit height at intervals as small as 0·1 mm in the penumbral region, and wider intervals in the outer parts, where we suspect the Evershed velocities are changing less rapidly. A complete measurement of the plates was made in February and the whole set of readings repeated in April as a check, final readings being taken as the mean of these two sets. Although the high dispersion is a great advantage in the work, the solar lines are now so broad as to make visual measurements a difficult matter, especially over the restricted height our diaphragm imposes. A. D. Petford has devised a new photo-electric method of measurement (**14**) which could be used here to great advantage. In fact, the visual and photo-electric measurements made on plate E28 of our Table I are in very good agreement, as his Fig. 3 shows. The photoelectric measurements however show considerably less scatter in repeated settings and are indisputably quicker and easier to obtain.

The solar line displacements corrected for instrumental effects, as explained above, were then expressed as Doppler shifts, (1 mm displacement = 9·19 km/sec) and the results are shown in Fig. 1. Fig. 1 (*a*) is the mean of the direct and reversed readings for the February and April measurements and gives the observed curve of the small spot of Plate E28, while Fig. 1 (*b*) refers to a similar mean of the large spot of E22.

The ordinates in Fig. 1 are arbitrarily set equal to zero for the photosphere on the solar centre side of the spot and expressed in km sec^{-1}, while the abscissa is given by the spectrum height in mm. The approximate extent of the umbra and penumbra is indicated for both spots.

2.1. *Reduction to sunspot velocity fields.*—In the reduction of the observed velocities, we have followed the scheme proposed by Professor Plaskett (**15**) and followed by T. D. Kinman (**10, 11**). The first step in deducing the motion characteristic of the spot is to remove the effect of the observer's motion and to allow for the displacements which we know will arise from solar rotation and limb effect. The Mercury computor of the Oxford University Computing Laboratory was used to calculate the corrections at representative points up the slit height, and interpolations were made for the remaining measured points. The corrections for the observer's motion may be calculated immediately from the observed epoch of exposure and the polar coordinates of the slit. For solar rotation at latitude B, we have used (**2**)

$$R_B = 2(1 - 0{\cdot}229 \sin^2 B) \text{ km sec}^{-1}.$$

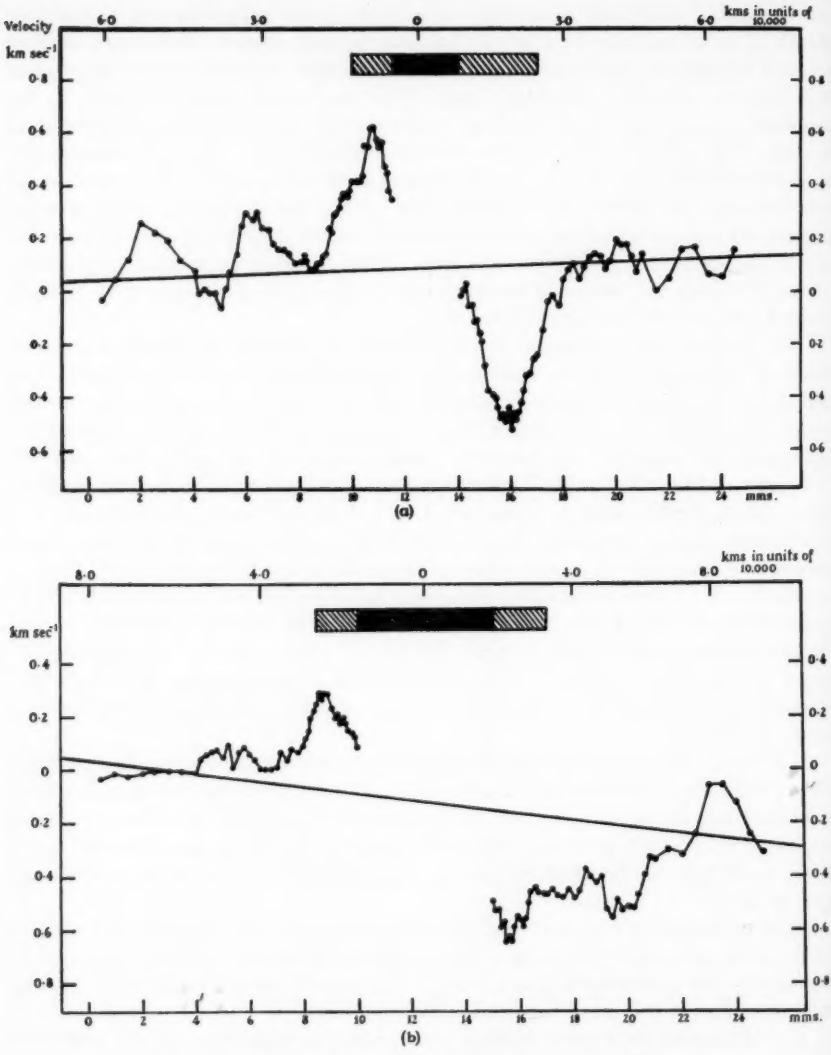

FIG. 1. (*a*) *Observed velocities and correction line for small spot.*
(*b*) *Observed velocities and correction line for large spot.*
Ordinate: observed velocity in km sec^{-1}.
Abscissa: 1. *Spectrum height in mm* (lower).
2. *Distance from spot centre in units of* 10 000 *km* (upper).

The limb effect corrections (2) were found to be negligible for the disk positions considered. These corrections show what velocity shift would occur across the slit height in the undisturbed photosphere. The lines in Fig. 1 show the run of these velocity corrections across the slit and are positioned for the small and large spots to give zero photospheric velocity on either side of the spot. It is the shifts above and below these lines which we believe represent the true sight-line velocities in the spot.

To deduce the spatial motion in the spot region from the sight-line velocities, we transform the coordinates of the measured points on the projected disk to polar coordinates (r, ϕ) on the solar surface and origin at the centre of the umbra. In this system, r is the horizontal radius from the centre of the umbra and ϕ is the position angle measured counter clockwise from the direction of solar rotation. If ΔB and $\Delta\lambda$ are the differential heliographic coordinates measured from the centre of the umbra (heliographic coordinates B, L) then:

$$r = R_0 [(\Delta\lambda \cos B)^2 + (\Delta B)^2]^{1/2} \quad \text{and} \quad \tan\phi = \frac{\Delta B}{\Delta\lambda \cos B}$$

where R_0 = radius of the Sun in kilometres.

Motion in the sunspot is conveniently considered in terms of the cylindrical velocity components $u = \dot{r}$, $v = r\dot{\phi}$, $w = \dot{z}$, which are the radial, tangential and vertical velocity components respectively. If can be shown (**11**) that the sight-line velocity V is given in terms of these components by the linear relation

$$V = u(\cos\phi \cos\gamma_1 + \sin\phi \cos\gamma_2) + v(\cos\phi \cos\gamma_2 - \sin\phi \cos\gamma_1) + w \cos\gamma_3$$

where $\cos\gamma_i$ is a direction cosine which depends upon the position of the points of measurement on the disk and is defined (**15**) as follows:

$$\cos\gamma_1 = \sin(L - L_0) \cos B_0 \sin(\theta + \theta_1) \operatorname{cosec}\theta$$

$$\cos\gamma_2 = [\sin B \cos B_0 \cos(L - L_0) - \cos B \sin B_0] \sin(\theta + \theta_1) \operatorname{cosec}\theta$$

$$\cos\gamma_3 = -\cos(\theta + \theta_1)$$

where $\theta_1 \simeq \frac{\rho}{\rho_0} S$ $\quad S$ = angular semi-diameter of Sun

and

$$\sin(\theta + \theta_1) \simeq \frac{\theta_1}{S}.$$

Ideally, we should have liked to make a complete least squares solution for the three unknowns u, v, w, but our observational material was insufficient to provide a satisfactory set of equations. (It is hoped to attempt such a complete solution in future investigations.) We have therefore based our calculations on Kinman's conclusions, which were obtained from 12 least squares solutions for u, v, w, at four values of r for each of three plates. These showed that the tangential component v is entirely due to random error and that the vertical component w, relative to the photosphere, is zero.

As a first description of the velocity field, we have then assumed that the motion is entirely a radial flow outward from the centre of the umbra ($v = 0$, $w = 0$). Fig. 2 (*a*) shows the results of the calculation for the small spot of E28, and Fig. 2 (*b*) is a similar plot for the large spot of E22. Positive velocities are now shown for both sides of the spot, since both refer to outflow velocities. For the small spot, where we have four sections of the same spot, we may go further and attempt a solution for another component of motion. Assuming that the spot has radial symmetry about the centre of the umbra, the two sides of the spot on four plates lead to eight observational equations for the state of motion at any one r value. Still assuming $v = 0$ (**10, 17**), we have used these equations to obtain a least squares solution for finding components u and w. These solutions were carried out for eight r values and lead to the results shown in Fig. 3.

We find as Kinman did, that w is zero within the limits of error. We see also that the values of the radial velocity thus obtained for the four plates are quite similar to those shown in Fig. 3 (*a*) for plate E28 only.

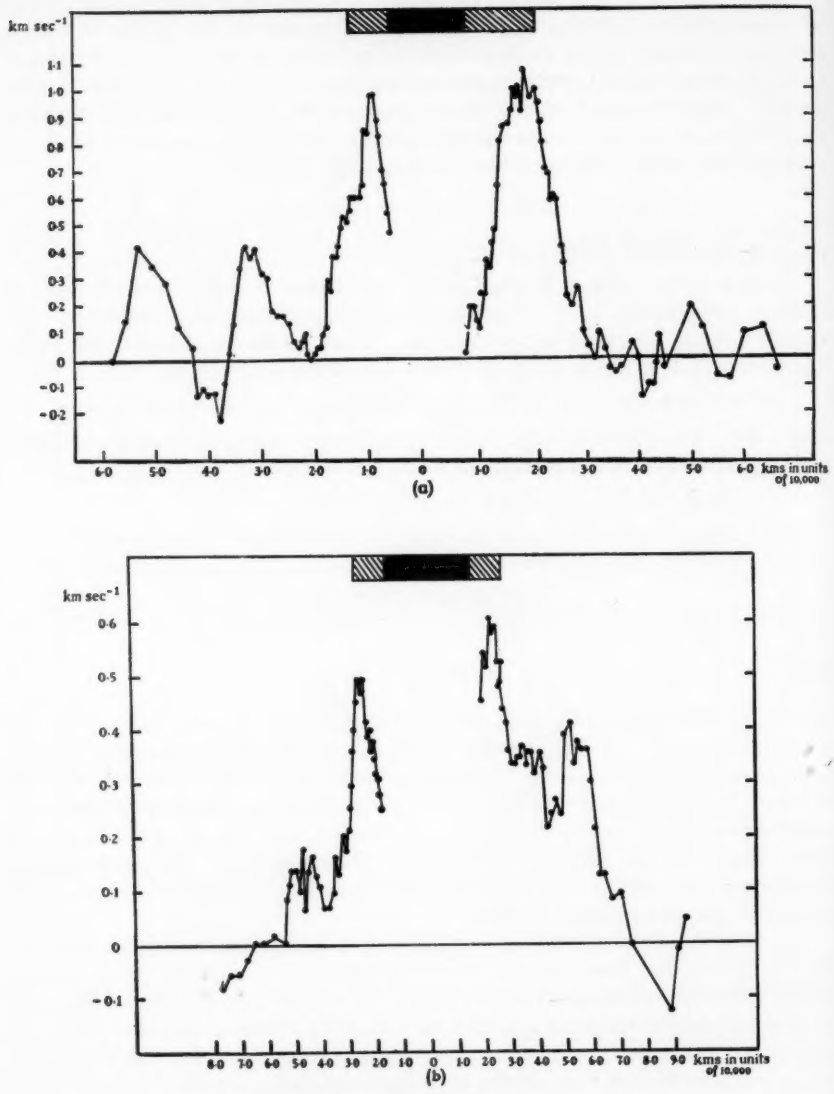

FIG. 2. (*a*) *Radial velocity for small spot, assuming* $v=0$, $w=0$.
(*b*) *Radial velocity for large spot, assuming* $v=0$, $w=0$.
Ordinate: Radial velocity in km sec^{-1}.
Abscissa: Distance from spot centre in units of 10 000 *km.*

2.2. *Errors.*—The error in setting on the solar lines after taking direct and reversed readings and the mean of two sets of readings is approximately 10 microns, which is equivalent to a velocity error of 0·1 km/sec. The comparison of photo-electric and visual measurements on one plate indicated a velocity difference of about 0·15 km/sec in the penumbra (the most difficult place to make a setting) and

the discrepancy was considerably less in the region away from the penumbra. We can thus consider a line setting error 0·15 km/sec throughout as a generous estimate. No correction has been applied to the observed sight-line velocities for scattered light, but Kinman (**10**) gives an estimate for a reduction in the observed penumbral velocities of about 9 per cent due to this effect. However, as Plate 6 (*a*) shows, the definition of our spectra is good and observations have shown that the instrumental scatter for the 35 m telescope is very similar to that for the 19 m telescope used by Kinman.

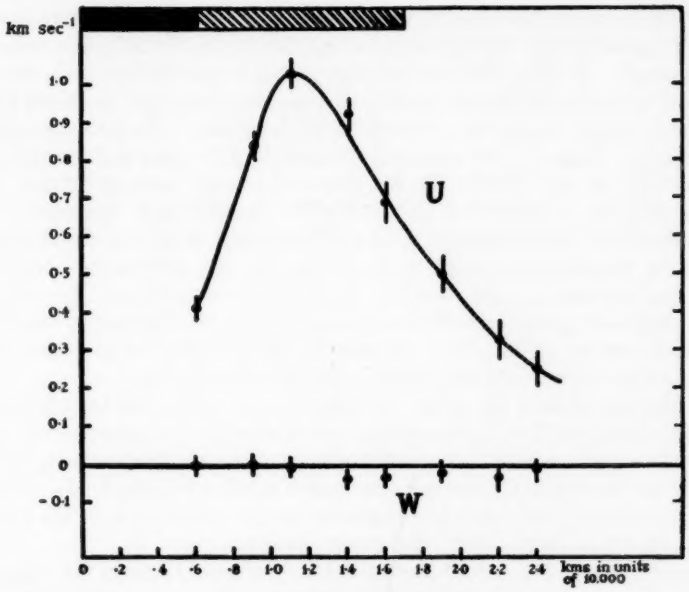

FIG. 3.—*Least squares solution for the velocity field of small spot.*
Ordinate: Velocity component in km sec⁻¹ (Radial velocity u above; vertical velocity w below.)
Abscissa: Mean distance (for the 4 small spot plates) from spot centre in units of 10 000 km.

Discussion.—The general form of motion in the small spot is very like that obtained by Kinman, and within the limits of our observational material, it again appears that the flow is wholly radial. The maximum radial velocity (mean uncorrected value of 1·1 km sec^{-1}) is achieved towards the edge of the penumbra, and we see that the flow extends well beyond the penumbral region, falling to zero at approximately 30 000 km from the spot centre. Considering Kinman's linear relation (**11**) between maximum radial velocity and spot size, we see that there is fair agreement for the small spot, but our maximum radial velocity for the large spot (mean uncorrected value approx. 0·6 km sec^{-1}) falls well below the value (approx. 3·5 km sec^{-1}) which may be estimated from the linear relation. In addition, the velocity field for the large spot is of quite a different form from that of a the small spot. The large spot pattern is much more spread out, falling to zero at approximately 70 000 kms from the spot centre, and it does not show such well defined maxima in the penumbra.

The high dispersion spectra (0·17 A/mm) reveal a phenomenon (discovered at the McMath-Hulbert Observatory (**12**)) which is unobservable in the low

dispersion spectra. This feature, which appears in Plate 6 (*b*) for the large and the small spot, will be referred to as "line-flare". The appearance of the plate indeed suggests that the main line is undisturbed and that the measured shift is caused by this diffuse "flare". The line-flare now observed extends over some 120 mA from the centre of the undisturbed line, corresponding to a sight-line velocity up to 6 km sec^{-1}. Evershed (**9**) first observed that spectral lines showed diffusive widening in the direction of displacement near the penumbral limits, but he remarked that this phenomenon might well be involved with Zeeman widening. The line-flare cannot be due to Zeeman splitting here, but is probably a Doppler effect due to turbulence, with a mean motion of matter away from the umbra (as shown by the flare appearing on opposite sides of the line on either side of the umbra). The same feature has been recently noted in Bumba's investigation (**3**) of spot velocity distributions. A complete account of his work (**4**) has come to our notice during the preparation of this paper. He also suggests that the line-flares ("flags" in his notation) are a result of Doppler shifts, and that the line as a whole is not shifted. In low dispersion work, such as Kinman's, the line-flare and the undisturbed line would be blended and consequently the amalgamated flare would contribute in a different way to the measured Doppler shift. This phenomenon could well account for the differences observed in velocity displacements in high and low dispersion investigations. In measuring the high dispersion plates, it is difficult to say exactly to what part of the line the micrometer setting refers, but presumably (Plate 6 (*b*)) it is closer to the undisturbed line than would be possible with lower dispersion.

The plates used here for radial velocities are not calibrated for photometry, but high dispersion calibrated plates have been obtained in the early summer of this year for a full-scale study of the intensity and extent of line-flare, and to investigate more fully the part it plays in our measurement of sunspot velocity fields. Further possible considerations in such investigations are the effects of spot age and disk position (**13**, **17**) on the sunspot velocity components.

Acknowledgments.—I should like to thank Professor Plaskett for suggesting this investigation and obtaining the sunspot spectra and also Dr M. G. Adam for constant advice, encouragement and guidance. I am grateful to Mr L. A. Higgs for his help with the Mercury computor calculations and to the Director of the Computing Laboratory for the use of the computor. My thanks are also due to the Department of Scientific and Industrial Research for the provision of a maintenance grant during this research period.

University Observatory,
Oxford:
1960 *October* 29.

References

(1) G. Abetti, *Publ. R. Osserv. Arcetri*, **50**, 47, 1932.
(2) M. G. Adam, *M.N.*, **119**, 460, 1959; *Comm. Un. Obs. Oxford*, No. 71.
(3) V. Bumba, *Bull. Astron. Inst. Czechoslovakia*, **10**, 5, 1959.
(4) V. Bumba, *Isvestiya Crimea Ap. Obs.*, **23**, 253, 1960.
(5) J. Evershed, *Kodaikanal Obs. Bull.*, **15**, 63, 1909.
(6) J. Evershed, *M.N.*, **69**, 454, 1909.
(7) J. Evershed, *M.N.*, **70**, 217, 1910.
(8) J. Evershed, *Mem. Kodaikanal Obs.*, **1**, Part 1, 1909.
(9) J. Evershed, *Kodaikanal Obs. Bull.*, **51**, 167, 1916.
(10) T. D. Kinman, *M.N.*, **112**, 425, 1952; *Comm. Univ. Obs. Oxford*, No. 35.

(11) T. D. Kinman, *M.N.*, **113**, 613, 1953; *Comm. Univ. Obs. Oxford*, No. 41.
(12) R. McMath, *Ap. J.*, **122**, 565, 1955.
(13) R. Michard, *Ann. d'Astrophys.*, **14**, 101, 1951.
(14) A. D. Petford, *M.N.*, **121**, 519, 1960; *Comm. Univ. Obs. Oxford*, No. 76.
(15) H. H. Plaskett, *M.N.*, **112**, 414, 1952; *Comm. Univ. Obs. Oxford*, No. 34.
(16) H. H. Plaskett, *M.N.*, **114**, 251, 1954; *Comm. Univ. Obs. Oxford*, No. 44.
(17) R. Servajean, *C.R.*, **248**, No. 14, 1959.
(18) C. E. St. John, *Ap. J.*, **37**, 322, 1913.
(19) C. E. St. John, *Ap. J.*, **38**, 341, 1913.
(20) H. von Klüber, *Zeit. für Ap.*, **24**, 121, 1947.

OSCILLATOR STRENGTHS OF NEUTRAL AND IONIZED TITANIUM FROM A VORTEX-STABILIZED ARC

J. B. Tatum

(Communicated by the Director of the University of London Observatory)

(Received 1960 November 30)

Summary

Relative oscillator strengths of 200 lines of Ti I and Ti II have been measured from spectra of a vortex-stabilized arc running in titanium tetrachloride at 10 080 °K. Comparison is made between the present measurements and those of other workers; these data are summarized on a scale which is approximately absolute. It is shown in the case of titanium that the excitation potential effect discovered by Allen and Asaad is merely a selection effect.

---

1. *Introduction.*—The measurement of oscillator strengths in the laboratory continues to be an essential prerequisite to the quantitative interpretation of astronomical spectra. The intensity of a spectrum line emitted or absorbed by an element in given physical conditions depends not only on N, the number of atoms present, but on gfN, where g is the statistical weight of the initial level, and f is the oscillator strength of the transition. In general, g is known accurately from the level designation, but not f. In complex spectra detailed values of gf may be obtained only by measurement. The present paper describes some gf measurements in titanium, which is of great astrophysical importance.

2. *Equipment.*—The main piece of apparatus used was a modification of the "water-stabilized arc", originally developed by Maecker (**13**) and Jürgens (**8**). The basic unit, which we shall call the "vortex", is drawn diagrammatically in Fig. 1. It is constructed from a short solid brass cylinder down the axis of which is a hole of diameter 8 mm, widening into a central chamber of diameter 16 mm. Liquid is injected tangentially into the chamber through two orifices; there it forms a little whirlpool and then flows out through the ends of the axial hole, where it spreads, without splashing, over the ends of the vortex, which are shaped like telephone earpieces. An 80 amp. D.C. arc, powered by a heavy generator, was struck down the axis of the vortex between two hollow carbon electrodes, and the plasma was observed end-on through one of the electrodes.

The advantages claimed for this type of arc are three-fold:

(*a*) Stability. Although the stability of the vortex arc has been questioned (**12**) there can be little doubt that when it is running correctly it is far more stable than an ordinary arc in air.

(*b*) Composition. If the arc is run at a known temperature and pressure in a liquid of known chemical composition, the composition of the plasma may be computed.

(*c*) Temperature. Since the plasma is constricted by the vortex, the temperature is high. Further, since the outside of the plasma is cooled by the liquid, thus reducing the electrical and thermal conductivities, most of the current is carried in the middle of the plasma and the heat generated there does not escape. The middle becomes extremely hot, thus permitting the excitation of high-level lines. The high radial temperature gradient is not necessarily an advantage, however.

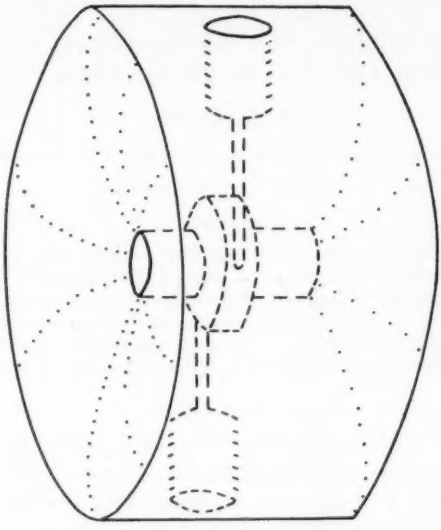

FIG. 1.—*The vortex-stabilized arc.*

It might be thought that the excitation of a metallic spectrum could be achieved simply by running the arc in a solution of salt. Experiment shows that in these circumstances the salt does not penetrate suitably to the plasma (**12, 24**). However, one may obtain a metallic spectrum by using a liquid which contains the metal in molecules held together by covalent or coordinate bonds. Examples of such compounds are the organometallic compounds such as $Pb(C_2H_5)_4$ lead tetraethyl, the carbonyls such as $Fe(CO)_5$ iron pentacarbonyl, and some chlorides such as $TiCl_4$ titanium tetrachloride. Such compounds are usually rare and dangerous. Exhaustive search in the chemical literature revealed that titanium tetrachloride was almost the only suitable liquid, and it is a happy coincidence that titanium is of considerable astrophysical interest. The nearest rival to titanium tetrachloride appears to be $SnCl_4$ stannic chloride, which is more expensive but less objectionable. The tetrachlorides of vanadium and germanium might also be suitable, but on the whole it seems that the future of vortex arc lies with the non-metals, for which there are many suitable liquid compounds.

The spectrum was recorded photographically with a Littrow-type quartz-prism spectrograph having a dispersion of 16 A/mm at Hγ and 6 A/mm at 3200A. The plates used were 10 in. × 4 in. Ilford Long-Range Spectrographic. Line intensities were compared with the spectrum of the standard radiator described by Euler (**6**). This is a carbon arc whose positive pole is at 3995°K and whose emissivity has been given by Euler. Measurements were made with a Hilger H670 recording microphotometer. In order to calibrate the plates, a rhodium-on-quartz step filter, having densities of 0 to 1·2 dex (i.e. in 10-based logarithms) in steps of 0·2 dex, was placed in front of the spectrograph slit and the spectrum of the carbon arc was photographed. The lines of the titanium spectrum have an intensity range of more than 1·2 dex and, to calibrate the plates over the whole intensity range, three exposures of 1, 8 and 32 sec were made. The resulting partial characteristic curves were combined into one complete curve.

3. *Experiment.*—Preliminary experience with the vortex arc was obtained by running it in water and in carbon tetrachloride. Experiments in which salts were dissolved in water or in carbon tetrachloride produced only a few feeble metallic lines.

In 1959 June the arc was run for the first time in pure titanium tetrachloride. Dense white fumes were produced as soon as the liquid came in contact with the air. The vortex arc seemed to run fairly well except that there was quite a lot of light outside the vortex. This suggested that some arcing might have taken place between an electrode and the vortex instead of from electrode to electrode *through* the vortex. When the apparatus was examined afterwards a quantity of a friable yellow solid, probably a mixture of titanium dioxide and titanium oxychloride, was found to be clogging up the vortex and the space between vortex and electrodes. It was thought that most of this was not present while the spectrographic exposures were being made, but was formed shortly afterwards when the water vapour in the air had had sufficient time to react with the titanium tetrachloride. The spectrum showed many hundreds of neutral and ionized titanium lines but no chlorine lines. The titanium lines were rather diffuse and in many cases strongly self-absorbed.

During the course of the next few months many more spectra were taken of the vortex running in pure $TiCl_4$. On some occasions it was known that undesirable arcing between electrodes and vortex had occurred, whilst on other occasions the arc was thought to have run correctly. The spectra usually had approximately the appearance described above, but sometimes when the arc was running incorrectly the spectrum showed a strong continuum crossed by *absorption* lines. Because of the uncertainty in knowing how the arc would run with this liquid which hydrolyses so readily when exposed to the air, it was decided to use a solution of titanium tetrachloride in carbon tetrachloride. The solution which was found to be most suitable was one part of titanium tetrachloride to four parts of carbon tetrachloride. The tendency for the above-mentioned yellow solid to form and short the arc was considerably reduced.

When the arc was running in such a solution it was possible to approach fairly closely and examine the plasma. On nearly every occasion the arc was running satisfactorily. The spectrum lines were much sharper than in the case of pure $TiCl_4$ and were rarely self-reversed. The stronger lines were, however, self-absorbed, and all lines suffered from the general absorption of the fumes. Lines of neutral chlorine were present and they were noticeably broader than the titanium lines.

4. *Composition of the plasma.*—The composition of a plasma resulting from the evaporation of a mixture of composition $a CCl_4 + TiCl_4$ is given by the solution of the following seven equations:

$$
\begin{aligned}
n_1 + n_2 + n_3 + n_4 + n_5 + n_6 + n_e - \frac{P}{kT} &= 0 \quad (1)\\
4(a+1)n_1 + 4(a+1)n_2 - n_5 - n_6 &= 0 \quad (2)\\
4(a+1)n_3 + 4(a+1)n_4 - an_5 - an_6 &= 0 \quad (3)\\
n_2 + n_4 + n_6 - n_e &= 0 \quad (4)\\
S_{Ti}n_1 - n_e n_2 &= 0 \quad (5)\\
S_C n_3 - n_e n_4 &= 0 \quad (6)\\
S_{Cl}n_5 - n_e n_6 &= 0 \quad (7)
\end{aligned}
$$

where n_1, n_2, n_3, n_4, n_5, n_6, are the numbers per unit volume of the atoms Ti, Ti^+, C, C^+, Cl, Cl^+ and n_e is the number per unit volume of electrons. P is the total pressure (equal to atmospheric pressure in the present work), T the absolute temperature and k Boltzmann's constant. S_X denotes the Saha function for the element X.

Equation (1) is a statement of the perfect gas law. Equations (2) and (3) follow from the molecular composition of $TiCl_4$ and CCl_4. Equation (4) expresses the fact that the plasma is electrically neutral. Equations (5), (6), (7) are Saha's equations for Ti, C, Cl.

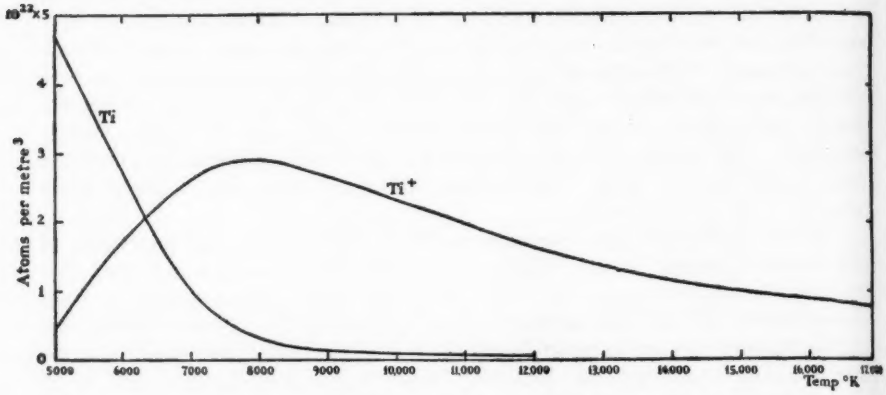

FIG. 2.—*Concentration of neutral and ionized titanium resulting from the evaporation of a solution of composition $TiCl_4$: CCl_4 = 1 : 4 by volume.*

The Saha function is given by

$$\log S = -(\chi - \Delta\chi)\Theta - \tfrac{3}{2}\log\Theta + 27{\cdot}24 + \log\frac{u_+(T)}{u_0(T)} \text{ metres}^{-3} \qquad (8)$$

where $\Theta = \dfrac{5040}{T}$, χ is the ionization potential in volts, and $u_+(T)$ and $u_0(T)$ are the partition functions of the ion and neutral atom. Partition functions were obtained from Claas (**5**) for the lower temperatures and by calculation for the higher temperatures. Unsöld (**25**) has shown that the ionization potential should be lowered by

$$\Delta\chi = 7\times10^{-5}n_e^{1/3} \text{ volts}$$

where n_e is in electrons per metre^3. $\Delta\chi$ was at first neglected in the equations (5–7) and an approximate value of n_e was obtained. The Saha functions were then adjusted and the equations were solved again. A further iteration was thought to be unnecessary.

The numbers per unit volume of neutral and ionized titanium atoms and of electrons are shown in Fig. 2 for the mixed plasma. It should be noted that equations (2, 3) and Fig. 2 are valid only if the $TiCl_4$ and CCl_4 evaporated into the plasma at the same rate.

5. *Analysis of the spectra.*—Six spectra were chosen for measurement and analysis, all of the mixed $TiCl_4 + CCl_4$ plasma. Absolute intensity measurements were made of as many Ti I and Ti II lines, free from blending, as was possible. Some of these lines had previously been measured by the Kings (**9**, **10**), others were new.

Measurement of the temperature was one of the most important and difficult tasks. Three methods were used by the writer. Comparison of his intensities with the titanium oscillator strengths published by the Kings (**9**, **10**) gave the excitation temperature. The ionization temperature was measured by comparing the intensities of Ti I and Ti II lines. A further check on the order of magnitude came from an examination of the variation of intensity of Ti I lines from the centre of the edge of the plasma. The first of these methods must be regarded as the most important; the other two provide good confirmatory evidence.

The intensities of emission lines are related to their oscillator strengths by

$$\log \frac{\lambda^3 I}{gf} = \text{const.} - \Theta V \qquad (9)$$

where λ is the wavelength of a line, I its intensity, and V the excitation potential of the upper level in volts. As before, $\Theta = 5040/T$. In Fig. 3 we have converted King's Ti II *gf*-values to relative intensities at four different temperatures, and have compared them with our measured intensities from spectrum No. QP 145(1).

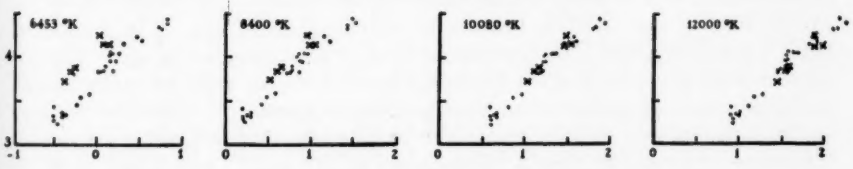

FIG. 3.—*Comparison of measured log intensities with intensities calculated at different temperatures from King's f-values. The ordinate gives the logarithm of the measured intensity in watt* m^{-2} *sterad*$^{-1}$*; the abscissa gives the logarithm of the calculated intensity in arbitrary units.*

Least scatter is expected to occur at the temperature of our experiment. At lower temperatures, lines of high excitation potential (E.P.), marked by crosses in Fig. 3, will be displaced to the left; at higher temperatures, to the right. We see that our temperature cannot have been far from 10080°K. The Ti I lines give the same temperature. A direct plot of $\log\frac{\lambda^3 I}{gf}$: V, which, for optically thin lines, should be a straight line of slope $-\Theta$, confirms this result. It should be noted that any error in King's determination of his furnace temperature will be perpetuated by a similar error in our temperature. The writer is of the opinion that the experiments of the Kings are still the best ever done on titanium oscillator strengths; this does not obscure the fact that independent temperature measurement is most desirable. It may be noted that R. B. King (**11**) still believes "that no very large systematic error was made in the furnace temperature measurement", and further evidence for this is presented in the section of this paper dealing with the excitation potential effect.

In order to calculate the ionization temperature it is necessary to put King's *gf*-values for Ti I and Ti II on a single scale. Using the formulae of Allen (**3**), it was possible to put King's *gf*-values on the absolute scale. This will be discussed in the section on absolute values. The ionization temperature is then given by the solution of:

$$\left\{\log\left(\frac{\lambda^3 I}{gf}\right)_0 + \Theta V_0\right\} - \left\{\log\left(\frac{\lambda^3 I}{gf}\right)_+ + \Theta V_+\right\} = \log n_e - 27{\cdot}24 + 1{\cdot}5\log\Theta + \Theta V \qquad (10)$$

where the suffixes o and + refer to the neutral atom and the ion, V_0 and V_+ are the excitation potentials of the upper levels of an atomic and ionic line, V is the ionization potential, and n_e is the number of electrons per cubic metre. Mean values of the braces on the left-hand-side were calculated for all measured atomic and ionic lines at various temperatures. The required temperature is obtained when the difference between the mean values of the braces is equal to the right-hand-side. Ionization temperatures obtained in this way were in satisfactory agreement with excitation temperatures for the three spectra for which such an analysis was possible. The degree of agreement is indicated by the following table:

Spectrum No.	Excitation temperature	Ionization temperature
QP 145(1)	10080 °K	9500 °K
QP 145(2)	9500	9500
QP 146B	9500	9900

The principle of the third method of temperature measurement was to measure the change of intensity of neutral titanium lines from the cool perimeter of the plasma to the hot interior. With increasing temperature, the intensities of the neutral lines at first increase because of increasing excitation. The intensities reach a maximum and then decrease because of increasing ionization. From a measurement of the ratio of the maximum intensity to the intensity in the middle of the plasma, it is possible to deduce the central temperature. Certain difficulties in this measurement made it possible to obtain only a lower limit to the central temperature; thus the central temperature of QP 145(1) was found to be at least 9500 °K.

6. *Results and comparison with previous observations.*—Relative log *gf*-values were calculated from measured intensities by equation (9), assuming temperatures from 9500°K to 10080°K for the different plates. The scales on which the *gf*-values were calculated were those of King and King (**9**) for Ti I and of King (**10**) for Ti II, but they have been reduced to absolute values as described in the next section. Comparison of our values with previously published values has been made in detail, and this has been satisfactory. In particular the standard deviation of our log *gf*-values from the Kings' values is about $\pm 0{\cdot}2$ dex in Ti I and $\pm 0{\cdot}1$ dex in Ti II. 200 lines were measured in all, of which 113 are not on the Kings' lists.

Oscillator strengths for Ti I have been published previously by King and King (**9**), van Stekelenburg (**22**), Ostrovskii (**18**), Hefferlin *et al.* (**7**), Mitrofanova (**15**), Allen (**1**) and Boyarchuk and Boyarchuk (**4**); and for Ti II by King (**10**), van Stekelenburg (**22**), Mitrofanova (**15**), Rountree (**20**), Allen (**1**) and Boyarchuk and Boyarchuk (**4**). The published values are of variable quality and nearly all on different scales. In view of this and of the 1955 I.A.U. Report on line intensities (**14**), which stresses the need to "make available all theoretical and experimental data from various sources critically balanced and combined", the writer has compiled a table (**23**) which lists all published titanium oscillator strengths known to him. This table gives 884 measurements of 420 lines in 137 Ti I multiplets and 369 measurements of 202 lines in 67 Ti II multiplets, all reduced to a scale which is approximately absolute, as described in section 7. The table gives also the weighted mean of all the measurements.

The present paper gives only those lines which have been measured by the writer. Tables I and II give the results for Ti I and Ti II respectively. The

successive columns are the multiplet number and wavelength written in the same order as in the Revised Multiplet Table (**16**), our measurement of log *gf*, and the weighted mean of all published values, omitting the astrophysical measurements of Allen (**1**) and Boyarchuk (**4**) and the laboratory values of Mitrofanova (**15**).

TABLE I

Absolute log gf-values in Ti I

Mult.	λ	Tatum	Mean	Mult.	λ	Tatum	Mean
6	4681·9	−1·32	−1·09	115	3789·3	−0·65	−0·65
	4667·6	−1·42	−1·24		3798·3	−1·02	−1·02
9	4112·7	−1·64	−1·63	126	4820·4	−0·47	−0·47
12	3998·6	−0·12	−0·06	129	4186·1	−0·22	−0·22
	3989·8	−0·18	−0·20	130	3919·8	−1·22	−1·22
	3981·8	−0·27	−0·33	131	3724·6	−0·85	−0·08
	3964·3	−1·08	−1·14	133	3547·0	−0·80	−0·80
	3962·9	−1·18	−1·15	145	4617·3	+0·25	+0·29
13	3958·2	−0·14	−0·18		4623·1	−0·06	−0·01
	3956·3	−0·45	−0·45		4629·3	−0·44	−0·44
	3948·7	−0·46	−0·48		4650·0	−0·94	−0·76
	3929·9	−1·00	−1·07		4645·2	−0·92	−0·76
14	3947·8	−0·81	−0·93	146	4481·3	−0·35	+0·04
	3921·4	−1·52	−1·52		4496·1	−0·23	−0·23
17	3752·9	−0·23	−0·10	148	4276·4	−0·46	−0·46
	3729·8	−0·36	−0·39	157	4885·1	+0·03	+0·22
	3771·7	−0·74	−0·99		4899·9	−0·07	+0·10
18	3689·9	−1·03	−1·24	161	4404·9	+0·08	+0·08
	3669·0	−1·34	−1·37	162	4263·1	+0·18	+0·18
19	3653·5	−0·13	+0·11		4282·7	−0·09	−0·09
	3642·7	−0·19	+0·01		4265·7	−0·80	−0·80
	3635·5	−0·11	−0·04	185	4030·5	−0·03	−0·03
	3671·7	−0·91	−1·07		4021·8	−0·50	−0·50
24	3354·6	−0·55	−0·13	189	3822·0	−0·25	−0·25
	3341·9	−0·99	−0·39	206	4151·0	−0·02	−0·02
27	3199·9	+0·05	+0·12		4159·6	−0·43	−0·43
38	4981·7	−0·14	+0·61	207	4099·2	−0·42	−0·42
	5007·2	−0·41	+0·64	220	4203·5	−0·45	−0·45
42	4555·5	−0·59	−0·52		4200·8	−0·65	−0·65
	4544·7	−0·62	−0·55		4188·7	−0·49	−0·49
	4512·7	−0·52	−0·45	221	4154·9	−1·02	−1·02
	4518·0	−0·39	−0·33	231	4856·0	+0·37	+0·37
	4522·8	−0·46	−0·37	233	4742·8	+0·16	+0·12
44	4305·9	+0·35	+0·41	246	3938·0	−0·33	−0·33
53	4840·9	−0·75	−0·62	252	4256·0	−0·56	−0·56
56	3904·8	+0·13	+0·14	253	4137·3	−0·26	−0·26
57	3786·0	+0·17	+0·02		4143·1	−0·42	−0·42
59	3598·7	−0·92	−0·92		4131·2	−0·69	−0·69
62	3292·1	−0·31	−0·23	254	4071·2	−0·36	−0·36
75	4698·8	−1·07	−1·04	260	4805·4	+0·73	+0·73
	4722·6	−1·07	−1·29		4792·5	+0·40	+0·40
80	4078·5	−0·10	−0·16	284	4237·9	0·00	0·00
	4082·5	−0·81	−0·74	291	4278·2	+0·11	+0·11
83	3710·0	−0·31	−0·39	292	3926·3	+0·26	+0·33
113	4457·4	+0·15	+0·15	296	4127·5	+0·26	+0·48
	4455·3	−0·22	−0·22	301	4224·8	−0·28	−0·28

TABLE II

Absolute log gf-values in Ti II

Mult.	λ	Tatum	Mean	Mult.	λ	Tatum	Mean
1	3361·2	−0·01	+0·05	32	4341·4	−2·22	−2·22
	3372·8	−0·05	−0·05	34	3900·5	−0·08	−0·08
	3383·8	−0·26	−0·19		3913·5	−0·20	−0·20
	3380·3	−0·69	−0·71		3932·0	−1·53	−1·53
	3387·8	−0·65	−0·66	36	3232·3	−0·06	−0·12
	3394·6	−0·74	−0·76	40	4417·7	−1·15	−1·15
	3407·2	−1·89	−1·88	41	4312·9	−1·14	−1·14
	3409·8	−1·84	−1·89		4307·9	−1·00	−1·00
2	3234·5	+0·04	+0·07		4315·0	−0·96	−0·96
	3236·6	−0·11	−0·07	45	3276·8	−0·68	−0·68
	3242·0	−0·40	−0·35	50	4563·8	−0·84	−0·84
	3254·3	−0·65	−0·70		4590·0	−1·81	−1·81
	3252·9	−0·56	−0·60	51	4399·8	−1·20	−1·20
	3251·9	−0·72	−0·72	52	3641·3	−0·15	−0·15
	3217·1	−0·52	−0·58		3624·8	−0·16	−0·16
	3222·8	−0·50	−0·74	53	3402·4	−0·98	−0·98
3	3197·5	−1·52	−1·52	54	3352·1	−1·02	−1·02
4	3157·4	−1·41	−1·41	55	3337·9	−1·12	−1·12
	3130·8	−0·48	−0·48	65	3332·1	−0·04	−0·06
6	3444·3	−0·93	−0·91		3321·7	−0·30	−0·30
	3461·5	−0·97	−0·99		3315·3	−0·64	−0·64
	3477·2	−1·04	−1·06	66	3248·6	+0·24	+0·24
	3491·1	−1·17	−1·21		3261·6	+0·32	+0·24
7	3322·9	−0·39	−0·33		3271·7	+0·01	+0·01
	3329·5	−0·48	−0·48		3278·3	−0·17	−0·18
	3335·2	−0·58	−0·60		3282·3	−0·23	−0·25
	3340·3	−0·72	−0·74	72	3741·6	+0·27	+0·27
	3343·8	−1·21	−1·24		3776·1	−1·04	−1·04
	3346·7	−1·14	−1·16	73	3706·2	−0·38	−0·38
	3308·8	−1·21	−1·23	75	3659·8	−0·26	−0·26
	3318·0	−1·14	−1·16		3662·2	−0·28	−0·28
	3326·8	−1·12	−1·20		3679·7	−1·25	−1·25
10	3168·5	−0·36	−0·36	82	4549·6	−0·14	−0·14
	3162·6	−0·49	−0·50		4572·0	−0·24	−0·24
	3161·8	−0·88	−0·76	84	3224·2	+0·16	+0·16
	3161·2	−1·07	−0·92		3218·3	+0·13	+0·13
11	4012·4	−1·59	−1·59	87	4028·3	−0·81	−0·81
12	3813·4	−1·75	−1·75		4053·8	−0·98	−0·98
	3814·6	−1·53	−1·53	88	3504·9	+0·59	+0·59
13	3721·6	−0·98	−1·04		3510·8	+0·26	+0·26
15	3587·1	−1·43	−1·43	89	3287·7	+0·38	+0·38
	3561·6	−1·81	−1·81	94	4350·8	−1·69	−1·69
	3573·7	−1·36	−1·36	98	3535·4	+0·24	+0·24
16	3341·9	−0·04	−0·04		3520·3	−0·02	−0·02
19	4395·0	−0·30	−0·30	99	3456·4	−0·04	−0·04
	4443·8	−0·64	−0·64		3452·5	−0·53	−0·53
	4450·5	−1·46	−1·46		3465·6	−0·84	−0·84
20	4294·1	−0·92	−0·92	105	4163·6	+0·01	+0·01
	4337·9	−0·89	−0·89		4171·9	−0·15	−0·15
	4344·3	−1·94	−1·94	107	3748·0	−0·24	−0·24
26	3190·1	+0·11	+0·15	114	4911·2	−0·42	−0·42
	3202·5	+0·10	+0·10	115	4488·3	−0·46	−0·46
31	4468·5	−0·52	−0·52		4411·1	−0·60	−0·60
	4501·3	−0·79	−0·79	125	3480·8	+0·32	+0·32

7. *Absolute gf-values.*—It has not been possible to obtain absolute *gf*-values from the present experiment. Line intensities were measured in absolute units since the absolute intensity of the carbon arc standard radiator was known. It was possible to calculate the numbers per unit volume of atoms and ions of each species in the plasma, and since it is believed that most of the lines were optically thin it should therefore have been possible to calculate absolute *gf*-values. When this was done, however, values were obtained which were of the order of about 10^{-3} of what one might reasonably expect. There are two possible reasons for this discrepancy. The rate of evaporation of the titanium tetrachloride into the plasma may have been much lower than that of the carbon tetrachloride, so that the concentration of titanium atoms was much less than calculated. On the other hand the very dense fumes which arose from the liquid during the experiments may have caused serious loss of light. The writer believes that fumes accounted for by far the greater part of the light loss, and that differential evaporation was negligible; but the matter is not yet settled. Comparison of the present log *gf*-values with those of the Kings shows that any wavelength dependence of the extinction due to the fumes was certainly less than 0·15 dex in the range 3000–5000 A, and therefore this caused no serious systematic wavelength dependence of the present log *gf*-values.

According to Allen (**3**), the conversion factor from the scale of King and King for Ti I to absolute values is given by:

$$\log gf \text{ (abs.)} = \log gf \text{ (rel.)} - 3{\cdot}22.$$

Allen does not give a conversion factor for Ti II but it is possible to calculate one from his empirical formulae. The most reliable of these formulae is the one for $d^n s - d^n p$ multiplets, viz:

$$\sum gf = 0{\cdot}233 g_{\text{ut}}$$

where g_{ut} is the statistical weight of the upper term. The multiplets 1, 2, 13, 14, 16, 24, 26, 65, 88, 98, 99 are all $d^2 s - d^2 p$ multiplets; none of them is intercombination or interparental, and the writer has been able to estimate total multiplet strengths on King's relative scale for them, either from his own or from published data. The mean difference between the calculated absolute $\log \Sigma gf$ and the measured relative $\log \Sigma gf$ is $2{\cdot}37 \pm 0{\cdot}15$. The small standard deviation gives an indication of the reliability of Allen's formula in this case. The conversion from King's relative scale for Ti II (**10**) to the absolute scale is therefore:

$$\log gf \text{ (abs.)} = \log gf \text{ (rel.)} - 2{\cdot}37.$$

Absolute *gf*-values calculated on these bases were used to compute an ionization temperature for the vortex (Section 5), and the agreement between this and the excitation temperature seems to confirm the correctness of both the excitation temperature and Allen's formula.

8. *Oscillator strengths and excitation potential.*—It was pointed out by Allen and Asaad (**2**) that there is a tendency for experimental oscillator strengths of iron-group atoms to increase with excitation potential. I have examined the effect in titanium.

There are several things which could cause the excitation potential effect and we may group them under the following headings:

A. The effect may be a systematic experimental error, such as:

(i) Wrong temperature estimation.

(ii) Failure to allow for self-absorption.

B. It may be a selection effect. This has been suggested by Traving (**26**).

C. It may be real in either of the following senses:

(i) There happens to be a strong array with high E.P.

(ii) Oscillator strength is a function of E.P.

Before we consider the effects to which these might give rise, we notice the following. Underestimation of temperature would produce an apparent increase of gf with E.P.; overestimation would produce a decrease. If A(i) is the explanation then we must believe that no experimenters have overestimated but all have underestimated their temperatures, and indeed very grossly underestimated them. A(ii) could give rise to the E.P. effect, if self-absorption, acting only on low-lying lines, were neglected. This would affect only emission experiments, whereas the E.P. effect is known to occur also conspicuously in absorption experiments. A selection effect, in which lines of high E.P. and low gf are too faint to measure, *must* operate; the only question is how important selection is. King (**11**) has pointed out that the array $d^n s - d^n p$, which might be expected to have strong lines, has many high-lying multiplets, and this undoubtedly contributes to the E.P. effect. A similar suggestion has been made by Allen (**26**). C(i) and B are not entirely separable. As for C(ii) there is no theoretical reason for believing gf to be a function of E.P. and we must consider this only after we have eliminated all other possibilities. Thus we are led at the outset strongly to suspect that the E.P. effect is a selection effect.

We can predict qualitatively and quantitatively what type of E.P. effect A and B would give rise to, on the assumption that gf is not a function of E.P. Let us suppose that, for all E.P., all gf-values lie roughly between the limits α and β. Fig. 4 shows how we might expect measured values of $\log gf$ apparently to vary with E.P. In Fig. 4 (*b*) is shown the expected increase of $\log gf$ with E.P. if the temperature were underestimated. For emission experiments the abscissa is the upper E.P., for absorption experiments it is the lower E.P. Fig 4 (*a*) shows how one might underestimate $\log gf$ for lines ending at the ground term if one did not allow for self-absorption in these lines. This would occur only in an emission experiment; the abscissa in Fig. 4 (*a*) is the lower E.P. In Fig. 4 (*c*), in which the abscissa is as in Fig. 4 (*b*), we see the effect of selection. The upper limit of measured oscillator strengths remains the same, but for high E.P.'s we cannot measure the lines of small oscillator strength. We can measure lines right up to the point of the triangular area in Fig. 4 (*c*), but not beyond. We may write equation (9) as:

$$\log gf = \log \lambda^3 I - \text{const.} + \Theta V$$

and we see that lines of slope Θ are lines of constant $\lambda^3 I$ or roughly of constant intensity. Thus we see that the hypotenuse of Fig. 4 (*c*) represents the lower limit of measurable intensity and should have a slope of $\frac{5040}{T}$. For a number of reasons the lower limit should not be expected to be as clear-cut as indicated, but nevertheless selection should give rise to an E.P. effect roughly as shown.

Fig. 5 shows the E.P. effect actually obtained by various workers. A line of slope Θ is drawn in each diagram for comparison with the observed distribution of $\log gf$-values. These graphs speak for themselves and indicate that selection is the main cause of the E.P. effect in titanium.

The solar and stellar *gf*-values of Allen (1) and Boyarchuk (4) require additional comment, however. The ratio of the solar and stellar values to laboratory values shows a slight residual dependence on E.P. which cannot be explained by selection. Thus log *gf* (Allen) − log *gf* (laboratory) decreases slightly with E.P. Allen used $\Theta = 0{\cdot}9$ for the reciprocal excitation temperature in the Sun. If we adjust his *gf*-values to $\Theta = 1{\cdot}0$ the residual E.P. dependence disappears. Log *gf* (Boyarchuk) − log *gf* (laboratory) increases slightly with E.P. Boyarchuk used $\Theta = 1{\cdot}1$ for the Sun. If we adjust his *gf*-values to $\Theta = 1{\cdot}0$, again the residual E.P. dependence disappears.

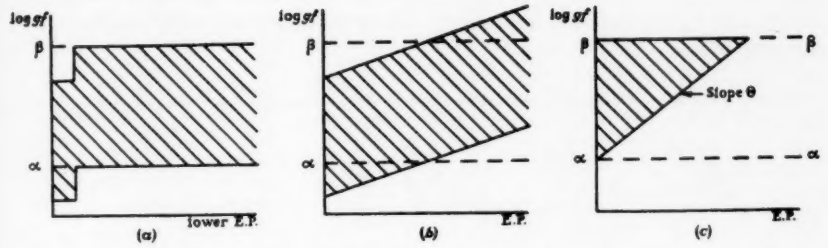

FIG. 4.—*Apparent increase of log gf with E.P., due to:*

(*a*) *Non-allowance for self-absorption in the low-level lines*
(*b*) *Underestimation of temperature*
(*c*) *Observational selection.*

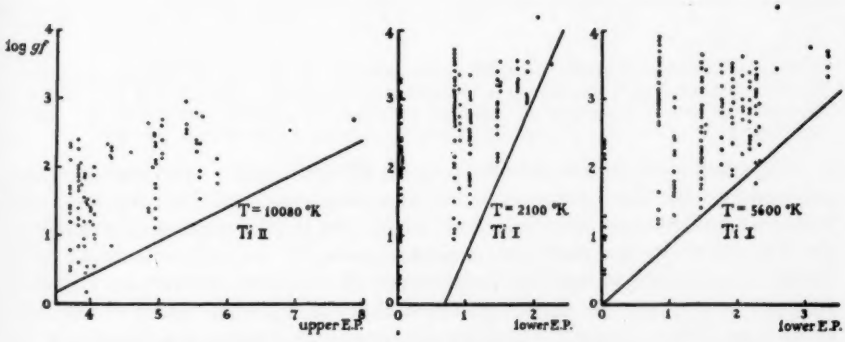

FIG. 5.—*Observed increase of log gf with E.P. in volts. The observers are respectively Tatum (this work), King and King* (9), *and Allen* (1). *The straight lines are drawn corresponding to the temperature quoted by each author.*

The corrections are small, however, and there is no doubt that the major reason for the apparent increase of oscillator strength with excitation potential is observational selection. This result is important in that it shows that published *f*-values in titanium are not marred by serious systematic error (reference (15) is an exception) and are therefore trustworthy. It is expected that the same would be found for other atoms in the iron group.

9. *Comparison with theory.*—There are two classifications of the spectrum of Ti I extant; that of Russell (in 17) and that of Rohrlich (19). The main differences in these classifications are in the configuration assignments of the

singlet and triplet terms of odd parity. Rohrlich computed multiplet strengths based on his assignments, and it is accordingly of much interest to compare his multiplet strengths with the observed values. He computed strengths not only for multiplets allowed by the *LS*-coupling rules, but also for some multiplets which are, on his assignment, interparental; he did not include configuration interaction and did not compute strengths of intercombination multiplets. Before we compare laboratory values with Rohrlich's values, we should note that the purpose for which Rohrlich computed multiplet strengths was primarily to guide him in making his assignments and not necessarily to produce accurate multiplet strengths for astrophysical purposes; in his own words, referring more particularly to interparental multiplets, "these values are only very rough approximations".

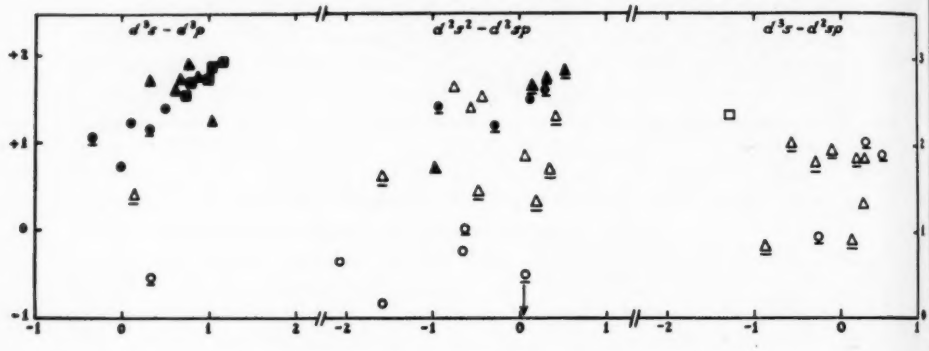

FIG. 6.—*Comparison of observed multiplet strengths with the calculated strengths of Rohrlich, for three different arrays. The abscissa is the observed log* Σgf *on the absolute scale. The ordinate is Rohrlich's calculated log* Σgf *on a relative scale which is different for each array. The left-hand scale refers to* $d^3s - d^3p$ *and* $d^2s^2 - d^2sp$*; the right-hand scale refers to* $d^3s - d^2sp$.

The comparison has been made in Table III and Fig. 6. The multiplets are grouped into the three arrays of Rohrlich's classification. The columns of the table are: multiplet number from the R.M.T. (**16**) and the multiplet designation; the logarithm of the multiplet oscillator strength, $\log \Sigma gf$, calculated from Rohrlich's multiplet strengths; the logarithm of the observed multiplet oscillator strength from (**23**). It should be noted that the Rohrlich values are relative and are on different scales for each array; the observed values are intended to be absolute. A colon after the multiplet designation indicates that Russell's assignment (i.e. Russell's 1947 assignment given by Moore (**17**), not the 1927 Russell assignment (**21**) which is given in Rohrlich's paper) differs from Rohrlich's. A comma indicates that the multiplet is interparental on Rohrlich's assignment. A semi-colon indicates both. Note also that in multiplet 284, the upper term designation is u^1D^0, not v^1D^0 as given in the R.M.T. (**16**). The reason has been stated by Moore (**17**). In Fig. 6, singlets, triplets and quintets are indicated by circles, triangles and squares. Underlined multiplets are those for which Russell's assignment differs from Rohrlich's. Open symbols are interparental on Rohrlich's assignment, full symbols are *LS*-permitted.

The trends which appear from Fig. 6 seem to indicate that for *LS*-permitted multiplets, the agreement between Rohrlich's values and experimental values is tolerably good, including those multiplets for which Rohrlich's and Russell's

TABLE III

Total multiplet strengths

	Multiplet	Rohrlich	Laboratory
	$3d^34s-3d^34p$		
238	$b^1G-z^1H^0$:	+1·09	−0·36
240	$-y^1G^0$:	+1·19	+0·30
284	$b^1D-u^1D^0$	+0·75	0·00
286	$a^1H-y^1G^0$;	−0·52	+0·34
288	$-z^1I^0$	+1·40	+0·50
291	$-x^1H^0$	+1·24	+0·11
157	$a^3G-y^3H^0$	+1·74	+0·66
160	$-v^3G^0$	+1·73	+0·32
162	$-t^3F^0$	+1·61	+0·59
220	$b^3P-u^3P^0$;	+0·42	+0·13
231	$a^3H-z^3I^0$	+1·90	+0·77
233	$-x^3H^0$	+1·76	+0·81
260	$c^3P-s^3D^0$	+1·27	+1·04
38	$a^5F-y^5G^0$	+1·95	+1·14
42	$-y^5F^0$	+1·89	+1·03
44	$-x^5D^0$	+1·75	+0·94
145	$a^5P-w^5D^0$	+1·71	+0·77
146	$-y^5P^0$	+1·53	+0·70
	$3d^34s-3d^24s4p$		
244	$b^1G-y^1H^0$;	+0·96	−0·25
287	$a^1H-x^1G^0$;	+2·04	+0·30
289	$-y^1H^0$;	+1·90	+0·52
102	$b^3F-x^3F^0$;	+2·03	−0·57
104	$-y^3G^0$;	+0·90	+0·13
106	$-w^3D^0$;	+1·86	+0·18
108	$-x^3G^0$;	+0·86	−0·86
109	$-v^3D^0$;	+1·95	−0·10
115	$-u^3D^0$;	+1·80	−0·29
154	$a^3G-z^3H^0$,	+1·34	+0·26
156	$-v^3F^0$,	+1·84	+0·26
37	$a^5F-y^5D^0$,	+2·38	−1·30
	$3d^24s^2-3d^24s4p$		
48	$a^1D-z^1D^0$,	−0·82	−1·54
49	$-z^1F^0$,	−0·35	−2·04
53	$-y^1D^0$;	+0·01	−0·62
56	$-y^1F^0$	+1·54	+0·14
57	$-z^1P^0$;	−∞	+0·02
58	$-y^1P^0$:	+1·21	−0·29
59	$-x^1D^0$:	+1·42	−0·92
126	$a^1G-y^1F^0$,	−0·21	−0·63
131	$-x^1G^0$:	+1·68	+0·31
4	$a^3F-z^3F^0$,	+1·55	−0·44
5	$-z^3D^0$,	+1·41	−0·56
6	$-z^3G^0$,	+1·67	−0·74
12	$-y^3F^0$;	+0·72	+0·36
13	$-y^3D^0$;	+0·36	+0·19
17	$-x^3F^0$:	+1·76	+0·32
19	$-y^3G^0$:	+1·84	+0·53
23	$-w^3D^0$:	+1·62	+0·14
24	$-x^3G^0$;	+1·31	+0·41
26	$-v^3D^0$;	+0·61	−1·60
69	$a^3P-z^3S^0$	+0·71	−0·97
72	$-y^3D^0$;	+0·48	−0·46
75	$-w^3D^0$;	+0·47	−0·46
83	$-y^3S^0$,	+0·89	+0·06

assignments differ. An exception is multiplet 59, which has, however, low experimental weight. The scatter of points is worse for the interparental multiplets, although there is no great systematic difference from interparental to permitted. Many of the interparental multiplets in Fig. 6 have different assignments on Rohrlich's and Russell's classifications. This makes it difficult to decide whether the large scatter is due to the "very rough approximations" of Rohrlich's interparental multiplet strengths or to inappropriate assignments. The most serious discrepancies are for multiplets 37 and 57, both of which have high experimental weights. The reason for the discrepancy in multiplet 37 is not clear. Multiplet 57 is $a\ ^1D-z\ ^1P^0$. Rohrlich assigns $z\ ^1P^0$ to $3d^24s(b^2P)4p$ and therefore the multiplet is interparental and should have zero intensity. Russell assigns $z\ ^1P^0$ to $3d^24s(a^2D)4p$; the multiplet would therefore be permitted and strong, as is observed. It would seem that the latter assignment is more appropriate. However, we should then have to follow Russell and assign $y\ ^1P^0$ to $3d^24s(b^2P)4p$; multiplet 58 would then be interparental, whereas it is observed to be strong. This situation is typical of any attempt to improve the observed-calculated agreement by changing assignments. It would probably be fair to conclude that there is not necessarily a unique "correct" assignment for some multiplets.

Acknowledgments.—The author is greatly indebted to the constant encouragement, advice and optimism of Professor C. W. Allen; to Mr E. W. Foster for introducing the vortex arc technique to this Observatory; to Dr R. H. Garstang for many conversations on the theory of spectra; to Mr E. P. Hayne for able assistance in the laboratory; to the magical skill of Mr C. R. Spratt in the workshop; and to University College London for the award of the Perren Studentship.

This work was carried out in partial fulfilment of the requirements for the degree of Ph.D.

University of London Observatory,
Mill Hill Park,
London, N.W.7:
1960 *November.*

References

(1) C. W. Allen, Memoir No. 5 part 2, *Commonwealth Solar Physics Observatory*, 1934.
(2) C. W. Allen and A. S. Asaad, *M.N.*, **115**, 571, 1951.
(3) C. W. Allen, *M.N.*, **121**, 299, 1960.
(4) M. E. and A. A. Boyarchuk, *Izv. Krimskoi Astr. Obs.*, **22**, 234, 1960.
(5) W. J. Claas, *Rech. Obs. Utrecht*, **12**, part 1, 1951.
(6) J. Euler, *Ann. der Physik*, (6), **11**, 203, 1953.
(7) R. Hefferlin, B. Cobb, D. Hall, C. Lehman, *Ap. J.*, **132**, 259, 1960.
(8) G. Jürgens, *Z. Phys.*, **134**, 21, 1952.
(9) R. B. and A. S. King, *Ap. J.*, **87**, 24, 1938.
(10) R. B. King, *Ap. J.*, **94**, 27, 1941.
(11) R. B. King, personal communication, 1960.
(12) W. Lochte-Holtgreven, *Rep. Prog. Phys.*, **21**, 312, 1958, Section 2.1.5.
(13) H. Maecker, *Z. Phys.*, **129**, 108, 1951.
(14) G. J. Minnaert, *Trans. I.A.U.*, **9**, 214, 1955.
(15) L. Mitrofanova, *Ivz. Glav. Astr. Obs., Pulkovo*, No. 153, 107, 1955.
(16) C. E. Moore, *Princeton Contr.* No. 20, 1945.
(17) C. E. Moore, *Atomic Energy Levels, N.B.S. Circ.* No. 467, 1949.
(18) Yu. Ostrovskii, *Diss. Leningrad*, 1958; *Optika i Spektroskopiya*, **1**, 821, 1956.
(19) F. Rohrlich, *Phys. Rev.*, **74**, 1381, 1948.
(20) J. C. Rountree, *Ann. d'Ap.*, **23**, 633, 1960.
(21) H. N. Russell, *Ap. J.*, **66**, 347, 1927.
(22) L. van Stekelenburg, *Diss. Utrecht*, 1943; *Physica*, **14**, 189, 1948.
(23) J. B. Tatum, Communications from the Univ. London Observatory, No. 41, 1961.
(24) J. B. Tatum, Thesis, University of London, 1961.
(25) A. Unsöld, *Zeit. Ap.*, **24**, 355, 1948.
(26) *Trans. I.A.U.* **10**, 233, 1958.

THE SCORPIO–CENTAURUS ASSOCIATION

II. Spectral Types and Luminosities of 220 O, B and A Stars

Pamela M. Morris

(Received 1960 December 3)

Summary

Spectral types and luminosities on the revised Yerkes (MK) system are given for 6 stars of type O, 201 of type B, and 13 of type A, in the region of the Scorpio–Centaurus Association. Microphotometer tracings were used to estimate the line ratios. A mean modulus is determined for the certain members of the Association, and variations of the mean modulus with type and luminosity are discussed briefly.

As a part of an extensive study of the Scorpio–Centaurus Association, the spectral classification of early-type stars in the region of the Association was undertaken. The distance modulus obtained from the spectral type and luminosity is a sensitive criterion for membership of the Association.

Spectrograms of the brighter stars were obtained with a three-prism spectrograph at the Cassegrain focus of the 30-inch reflector (dispersion 36 A/mm at Hγ), while for the fainter stars a two-prism spectrograph was used at the Newtonian focus of the 74-inch reflector (dispersion 90 A/mm at Hγ). These will be referred to as 'Cassegrain' and 'Newtonian' spectra respectively. The Cassegrain spectra were obtained primarily for radial velocity measurements and were too narrow for reliable classification by visual inspection, whereas the Newtonian spectra were sufficiently wide and well resolved to be classified visually. However, in order that the classification system should be as homogeneous as possible, all spectra were treated in the same way. They were recorded with a Hilger microphotometer at enlargements of $\times 7$ for Cassegrain and $\times 15$ for Newtonian spectra, and relative line intensities were estimated from the tracings. In addition, the wings of the hydrogen lines and any peculiar features were examined with a binocular microscope. To retain homogeneity the classification of Cassegrain spectrograms has been suspended since the recent installation of a new set of camera and collimator optics, and will not be resumed until a new library of standard spectra has been built up.

The standard stars for classification were selected from the work of H. L. Johnson and W. W. Morgan (**1**), M. L. Woods (**2**), and A. de Vaucouleurs (**3**). A comprehensive list of standard stars suitable for use in the southern hemisphere has been compiled by W. Buscombe (**4**). The distribution of the standards observed is given in Table I, which shows that the main gaps occur in luminosity class II.

TABLE I

Classification standards recorded

	Cassegrain					Newtonian				
L	I	II	III	IV	V	I	II	III	IV	V
T										
O7										1
O9			1				1	1		1
O9·5	2				2					1
B0	2				1	1				
B0·5	1		1		1			2	1	
B1	3				2	2				1
B2		1	1	2	1				2	
B2·5					1	1				
B3	1	1		1	1		1		1	1
B5	3		1	1	1			1	1	1
B6			1		1			1	1	
B7			2		1	1			1	
B8	1	1	2		3			1		2
B9		1	1	1	2			1	1	2
B9·5					1					1
A0	2			1	2	2				2
A1	1				2					
A2				1	2	2			1	1
A2·5					1					
A3			1		1					
A4					1				1	1
A5	1	1	1		1	1	1	1		1
A7			1		1					
A9			1							

Totals:	O	5		O	5	
	B	45		B	28	
	A	22		A	14	
		72			47	

The 220 southern stars which have been classified on the MK system (1) are listed in Tables II and III. Table II gives those stars for which Harvard photovisual magnitudes (5) are available, while the magnitudes of stars in Table III have been derived from various other sources. The columns show:

(1) the star name, or Gould number (6), or, if these are lacking, the Durchmusterung number;

(2) the Henry Draper Catalogue number (7);

(3) and (4) the galactic longitude and latitude to the nearest hundredth of a degree, on the revised system (8);

(5) the spectral type and luminosity class;

(6) the Harvard photovisual magnitude, or, in Table III, magnitude derived from other sources as shown by reference numbers in the final column; an asterisk indicates that the magnitude has been corrected for duplicity by +0·3, and a dagger that it has been corrected by +0·6;

(7) the colour excess derived from various sources, all converted to the $B-V$ system; the values of the intrinsic colours for MK types were taken from (**9**), (**10**) and (**11**):

(8) the modulus $m_0-M=m-3E_y-M$, where M is the visual absolute magnitude corresponding to the spectral type and luminosity as given by H. L. Johnson and B. Iriarte (**12**);

(9) the spectrograph used; C indicates Cassegrain and N Newtonian;

(10) remarks, and references to notes at the end of the Tables.

TABLE II

Star	HD	l^{II}	b^{II}	Sp. & Lum.	$m(HP_V)$	E_y	m_0-M	Sp.	Notes
72G Col	41534	238·43	−23·37	B2 IV	5·62	+0·02	8·86	C	
83G Col	43071	243·55	−23·08	B3 V	6·83	...	8·53	N	
90G Col.	44506	241·63	−20·78	B1 Vn	5·86*	+0·03	9·37	C	
42G CMa	46189	236·17	−16·47	B4 IV	5·83	0·00	8·03	C	
50G CMa	46936	241·29	−17·54	B8 V	5·91*	+0·05	5·66	C	
70G CMa	49028	240·12	−14·67	B8 IV	6·43	0·00	7·13	N	
30G Pup	49336	247·15	−17·19	B3 V	6·06	+0·05	7·61	C	
80G CMa	50012	237·51	−12·36	B3 IV	6·90	−0·02	9·40	N	
82G CMa	50093	236·11	−11·62	B3 V	6·24	−0·01	7·94	C	
21° 1655	51200	233·15	− 8·99	B3 IV	7·11*	...	9·61	N	
104G CMa	51925	238·12	−10·67	B3 V	6·19	−0·02	7·89	N	
21° 1695	52437	233·73	− 8·04	B4 Vne	6·33	−0·04	7·73	N	Em. Hβ
27° 3540	52812	238·50	−10·02	B3 V	6·66	+0·03	8·27	N	
26° 3880	54224	238·51	− 8·68	B1 V	6·38	+0·06	9·80	C	
124G CMa	54669	236·33	− 7·15	B3 V	6·85*	−0·01	8·55	N	
136G CMa	55857	239·81	− 7·65	B3 IV	5·86	...	8·36	C	
79G Pup	56733	250·09	−11·92	B5 IV	5·71	+0·02	7·45	C	
80G Pup	56779	248·52	−11·12	B2 V	5·32*	+0·05	7·67	C	
149G CMa	56876	239·73	− 6·58	B5 Vn	6·34	−0·01	7·34	C	
157G CMa	57573	236·55	− 4·12	B3 V	6·45	+0·04	8·01	C	
96G Pup	59550	245·05	− 6·52	B2·5 IV	6·10*	0·00	9·00	C	
y Pup	59635	251·64	− 9·91	B3 IV	5·70*	+0·04	8·08	C	
115G Pup	60606	249·85	− 7·96	B3: Vnek	6·13†	+0·08	7·59	N	(*a*)
118G Pup	60753	262·80	−14·42	B6 IV	6·70	...	8·20	N	
125G Pup	61068	235·53	+ 0·60	B2 II	5·66	0·00	10·56	C	
26° 4723	61687	242·13	− 2·37	B7 IV	6·74	−0·02	7·94	N	
146G Pup	61925	251·53	− 7·46	B3 IV	6·26*	+0·14	8·34	N	
163G Pup	62753	254·33	− 8·13	B2 Vne	6·54	+0·12	8·68	C	(*b*)
55G Car	62758	270·92	−16·71	B5 IV	6·63*	+0·05	8·28	N	
168G Pup	63028	240·55	+ 0·21	B3 IV	6·55	...	9·05	C	
178G Pup	63271	239·20	+ 1·33	B1 IV	5·84	+0·05	9·79	C	
181G Pup	63308	254·36	− 7·55	B3 V	6·64	...	8·34	N	
b Pup	64503	253·89	− 5·93	B3 V	4·84*	+0·01	6·51	C	
75G Car	66546	268·38	−12·48	B4 V	6·17*	+0·08	7·33	N	
14 Pup	66834	238·88	+ 6·27	B3 V	6·05	+0·01	7·72	C	

TABLE II—(*continued*)

Star	HD	l^{II}	b^{II}	Sp. & Lum.	$m(HP_V)$	E_y	m_0-M	Sp.	Notes
79G Car	67536	276·11	−16·14	B4 Vn	6·30	+0·02	7·64	N	
254G Pup	67698	242·66	+ 4·94	B5 Ve	6·64	...	7·64	N	(*c*)
258G Pup	67888	254·52	− 2·64	B5 III	6·30	+0·08	8·26	C	
10G Vel	68324	263·33	− 7·97	B3 V	5·58*	−0·03	7·28	C	
36° 4359	69106	254·50	− 1·33	Bo·5 III	7·22*	+0·17	11·61	N	
35° 4413	69620	254·15	− 0·53	B6 V	6·92	+0·13	7·23	N	
87G Car	70839	272·87	−11·91	B3 III	6·25*	+0·08	8·91	C	
32° 5245	71015	252·32	+ 2·62	B3 III	7·03	+0·10	9·63	N	
36G Vel	72350	262·69	− 3·21	B5 IV	6·37	...	8·18	N	
95G Car	73390	274·15	−10·51	B3 Vn	5·58*	+0·04	7·16	C	
50G Vel	74067	260·18	+ 0·91	B9 V	5·12	+0·13	4·13	C	
55G Vel	74196	270·31	− 6·85	B8 IV	5·91*	−0·03	6·61	C	
60G Vel	74455	266·59	− 3·61	B3 Vn	5·67*	0·00	7·37	C	
61G Vel	74535	270·57	− 6·67	B9 III	5·59	...	5·99	C	
62G Vel	74560	270·59	− 6·67	B4 IV	4·92	+0·02	7·06	C	
D Vel	74753	268·10	− 4·48	Bo Vn	5·37*	+0·06	9·59	C	
68G Vel	75149	265·32	− 1·69	B2 II	5·46	+0·45	9·01	C	
f Car	75311	273·90	− 8·42	B2 Vn	4·81*	+0·09	7·04	C	
η Cha	75416	292·40	−21·65	B9 IV	5·83*	+0·04	5·91	C	
82G Vel	76161	267·88	− 2·44	B6 : Vn	6·29*	−0·02	6·99	C	
92G Vel	77320	264·81	+ 1·95	B2·5 Vn	5·97	+0·03	7·98	C	
103G Vel	79186	267·36	+ 2·24	B3 Ib	4·90	+0·33	9·81	C	
124G Car	80094	277·65	− 6·56	B7 IV	6·24*	+0·03	7·35	C	
125G Vel	80781	275·75	− 3·92	B7 IV	6·32	+0·03	7·43	C	
ζ Cha	83979	295·58	−21·05	B5 IV	5·42*	...	7·22	N	
157G Vel	84816	271·85	+ 6·66	B3 V	5·92*	+0·03	7·53	C	
166G Vel	85980	273·25	+ 7·13	B4 V	5·69	+0·06	6·91	C	
ϕ Vel	86440	279·34	+ 0·10	B5 II	3·58	+0·03	7·49	C	
172G Vel	86466	278·19	+ 1·65	B3 V	6·03	+0·06	7·55	C	
167G Car	86659	288·39	−11·30	B4 IV	6·22	+0·06	8·24	C	
186G Vel	88206	279·13	+ 3·39	B2 V	5·28*	+0·08	7·54	C	
206G Car	91533	285·72	− 0·50	A2 I	6·13	+0·26	12·35	C	
205G Car	91619	285·55	− 0·05	B5 Ia	6·14	+0·52	11·58	C	
24G Cha	93237	297·19	−18·39	B5 V	6·36*	+0·13	6·97	C	
238G Car	93607	289·96	− 4·68	B3 IV	4·98	+0·04	7·36	C	
240G Car	93737	288·04	− 0·65	Ao Ia	6·06	+0·18	12·52	C	
261G Car	96919	291·14	− 1·44	B9 Ia	5·34	+0·24	11·42	C	
264G Car	97583	292·43	− 3·33	B9 V	5·40	+0·06	4·62	C	
5G Mus	99264	296·31	−10·50	B3 III	5·54	+0·21	7·81	C	
36G Cen	100198	293·45	+ 0·10	Ao Ia	6·30	...	13·30	N	
42G Cen	100673	291·78	+ 6·93	B9 V	5·00*	0·00	4·40	C	
λ Cen	100841	294·47	− 1·39	B9 II	3·24	+0·01	6·21	C	
54G Cen	101189	294·38	− 0·16	B9 IV	5·24	+0·09	5·17	C	
j Cen	102776	296·17	− 1·72	B3 Vne	4·70*	+0·04	6·28	C	Em. Hβ
70G Cen	102878	295·98	− 0·60	A2 Ia	5·59	+0·23	12·10	C	

TABLE II—(*continued*)

Star	HD	l^{II}	b^{II}	Sp. & Lum.	$m(HP_V)$	E_y	$m_0 - M$	Sp.	Notes
ϵ Cha	104174	300·20	−15·62	B9 Vn	5·25*	+0·11	4·32	C	
θ^2 Cru	104841	297·64	− 0·76	B3 IV	5·09*	+0·10	7·29	C	
25G Mus	104878	298·61	− 5·83	A0 V	5·94†	+0·11	4·61	C	
92G Cen	105382	295·93	+11·63	B6 III	4·68	−0·03	6·58	C	
93G Cen	105416	295·62	+13·57	A1 V	5·80*	+0·03	4·21	C	
95G Cen	105509	294·94	+17·89	A3 III	5·88	+0·35	3·63	C	
δ Cru	106490	298·22	+ 3·78	B2 III	2·93	0·00	6·53	C	
24G Cru	107696	299·09	+ 4·99	B8 Vp	5·78*	−0·01	5·68	C	(*d*)
118G Cen	108114	296·93	+27·38	B9 III	5·75	+0·03	6·06	C	
α Mus	109668	301·65	− 6·29	B2 IV	3·09*	+0·03	6·30	C	
132G Cen	110073	300·53	+22·84	B8 IV	5·02*	+0·01	5·69	C	
39G Cru	110335	301·73	+ 3·17	B7 IV	4·92	+0·10	5·82	C	
41G Cru	110461	301·70	+ 6·90	B9 V	6·43*	+0·11	5·50	C	
42G Cru	110506	301·77	+ 6·67	B9 Vn	6·14	+0·04	5·42	C	
β Mus	110879	302·44	− 5·24	B2·5 V	3·42*	+0·05	5·37	C	
145G Cen	111774	303·02	+23·20	B7 V	6·07	+0·07	6·26	C	
48G Cru	111904	303·16	+ 2·55	B9 Ia	5·74	+0·36	11·46	C	
H Cen	112409	303·82	+11·67	B8 V	5·48*	+0·12	5·02	C	
55G Mus	113120	303·86	− 8·61	B1 Vne	6·11*	+0·22	9·05	N	(*e*)
ξ^1 Cen	113314	304·95	+13·30	A0 V	5·24*	+0·14	3·82	C	
171G Cen	113703	305·46	+14·33	B5 IV	5·11*	+0·01	6·88	C	
183G Cen	114529	305·53	+ 2·85	B8 V	4·95*	+0·01	4·82	C	
η Mus	114911	305·18	− 5·12	B8 V	5·14*	0·00	5·04	N	
202G Cen	115823	307·39	+ 9·88	B5 III	6·15†	+0·03	8·26	C	
207G Cen	116072	306·69	+ 1·67	B4 Vn	6·66*	+0·04	7·94	N	
210G Cen	116226	308·31	+13·99	B7 IV	6·33	+0·02	7·47	C	
251G Cen	118978	309·45	+ 3·44	B9 IV	5·73*	+0·04	5·81	C	
250G Cen	118991	310·24	+ 7·60	B8 V	5·60*	+0·12	5·14	C	
253G Cen	119159	309·97	+ 5·40	B2 IV	6·15	+0·08	9·21	C	
ν Cen	120307	314·41	+19·90	B2 IV	3·76*	+0·01	7·03	C	
277G Cen	120642	312·13	+ 8·98	B9 Vn	5·64*	+0·07	4·83	C	
288G Cen	121190	312·75	+ 9·50	B8 V	6·03*	+0·04	5·81	C	
310G Cen	122879	312·26	+ 1·80	B0 II	6·35	+0·30	11·15	N	
7G Cir	124197	311·35	− 4·19	B6 V	6·88	...	7·58	N	
ι Lup	125238	318·47	+14·14	B3 IV	4·02	+0·01	6·49	C	
4G Lup	125721	318·19	+11·83	B3 V	6·11	+0·01	7·78	N	
342G Cen	125823	321·56	+20·03	B5 III	4·51	−0·04	6·71	C	
τ^1 Lup	126341	319·91	+14·51	B3 III	4·85*	+0·02	7·69	N	
379G Hya	126769	326·93	+28·83	B8 IV	5·24*	+0·02	5·88	C	
14G Lup	126981	320·55	+14·16	B6 IV+A1:	6·01†	+0·11	7·18	C	
13G Lup	126983	318·95	+10·26	A0 V+B	6·06†	...	5·06	C	
368G Cen	129116	325·88	+20·11	B3 IV	4·36*	+0·02	6·80	C	
22G Cir	129954	314·22	− 6·31	B2 V	5·90	+0·12	8·04	C	
ζ Cir	131058	315·02	− 6·05	B4 V	6·31*	+0·05	7·56	N	
376G Cen	131120	327·93	+19·12	B6 V	5·10	0·00	5·80	C	

TABLE II—(*continued*)

Star	HD	l^{II}	b^{II}	Sp. & Lum.	$m(HP_V)$	E_y	$m_0 - M$	Sp.	Notes
36G Lup	131562	321·27	+ 5·56	A2 V	5·80*	...	3·90	N	
37G Lup	131657	323·62	+ 9·91	B9 V	5·98*	+0·09	5·11	C	
40G Cir	135160	319·67	− 2·83	B1 V	5·80	+0·09	9·13	C	
δ Cir	135240	319·69	− 2·90	O8 n	5·39*	+0·20	9·99	N	
45G Cir	135591	320·12	− 2·64	O9 II	5·66*	+0·13	11·37	N	
7G TrA	135737	316·50	− 8·62	B3 V	6·65*	+0·08	8·11	C	
ϵ Lup	136504	329·22	+10·32	B3 IV	4·25†	0·00	6·75	C	
κ^1 Aps	137387	313·85	−13·99	B3 IV	5·82*	+0·03	8·23	C	
κ^2 Aps	138800	314·33	−14·42	B8 IV	5·65	+0·05	6·20	C	
2G Nor	139129	326·98	+ 2·52	B9 V	5·40	+0·18	4·26	C	
94G Lib	139160	343·25	+23·31	B9 IV	6·30*	+0·05	6·35	C	
12G Nor	141168	327·83	+ 0·80	B8 V	5·86	+0·08	5·52	C	
19G TrA	142139	323·84	− 5·33	A1 V	6·21*	+0·04	4·59	C	
6G Sco	142250	345·55	+20·01	B7 V	6·01	+0·08	6·17	C	
7G Sco	142301	347·12	+21·51	B8 IV	5·85	0·00	6·55	C	
116G Lib	142378	351·62	+25·66	B5 V	6·20*	+0·14	6·78	N	
10G Sco	142883	350·90	+24·09	B3 V	5·88	+0·20	6·98	C	
11G Sco	142990	348·12	+21·21	B8 V	5·65*	−0·04	5·55	C	
η Lup	143118	338·76	+11·03	B2 V	3·86*	+0·01	6·33	C	
δ Sco	143275	350·09	+22·50	B0 V	3·11†	+0·14	7·09	C	
23G TrA	143448	324·54	− 5·95	B3 IV	6·84	+0·04	9·22	N	
151G Lup	143699	339·12	+10·43	B5 IV	5·26*	+0·01	7·03	C	
β^2 Sco	144218	353·18	+23·61	B3 V	4·98	+0·14	6·26	C	
θ Lup	144294	340·82	+11·33	B3 IVn	4·27	+0·01	6·74	C	
19G Sco	144334	350·35	+20·85	B8 V	5·87	−0·01	5·77	N	
ι^2 Nor	144480	326·79	− 4·53	B9 V	5·71	+0·12	4·75	C	
24G Sco	144661	350·00	+19·98	B7 V	6·31	+0·03	6·62	N	
ν^2 Sco	145501	354·61	+22·70	A0 IV	6·12	+0·04	5·70	C	
ν^1 Sco	145502	354·61	+22·70	B3 IV	4·50*	+0·22	6·34	C	
41G Nor	145782	327·46	− 5·11	A0 IV	6·10*	+0·09	5·53	C	
41G Sco	145792	350·99	+19·04	B6 V	6·31	+0·18	6·47	C	
46G Sco	146001	350·38	+18·13	B8 IV	6·09	+0·16	6·31	C	
52G Nor	147152	334·01	+ 0·13	B6 IV	5·36	...	6·86	C	
σ Sco	147165	351·31	+17·01	B1 III	3·63*	+0·33	7·04	C	
66G Sco	147628	342·87	+ 8·27	B8 IV	5·69*	+0·04	6·27	C	
ρ^1 Oph	147933	353·68	+17·69	B3 IV	5·42*	+0·35	6·87	N	
ρ^2 Oph	147934	353·67	+17·68	B3 V	6·12*	...	7·82	N	
55G Nor	147977	328·10	− 6·77	B9 III	5·98*	+0·13	5·99	C	
59G Nor	148379	337·23	+ 1·57	B2 Ia	5·61*	+0·84	10·19	C	
μ Nor	149038	339·38	+ 2·51	B0·5 Iab	5·38*	+0·26	10·90	C	
1G Ara	149485	327·23	− 9·35	B8 V	6·11	+0·04	5·89	C	
η^1 TrA	149671	321·70	−14·28	B7 IV	5·91	+0·07	6·90	C	
62G Nor	149711	340·38	+ 2·36	B3 IV	5·99	+0·18	7·95	C	
97G Sco	151804	343·59	+ 1·95	O8 fk	5·59*	+0·26	10·01	N	
41° 11021	152235	343·31	+ 1·10	B0·5 Ia	6·03	+0·78	10·49	C	

TABLE II—(*continued*)

Star	HD	l^{II}	b^{II}	Sp. & Lum.	$m(HP_V)$	E_y	m_0-M	Sp.	Notes
106G Sco	152408	343·55	+ 1·06	O7 f	5·88	+0·38	10·24	C	
32G Ara	153716	331·88	− 9·86	B5 V	5·74	+0·08	6·50	C	
140G Sco	156325	353·75	+ 2·93	B6 IV	6·34	+0·31	6·91	C	
31° 14091	158186	355·90	+ 1·61	B3 IV	6·81	+0·13	8·92	N	
151G Sco	158320	354·18	+ 0·25	B4 IV	6·67	...	8·87	N	
υ Sco	158408	351·27	− 1·84	B3 Ib	3·04*	−0·02	8·94	C	
μ Oph	159975	17·00	+12·35	B9 III	4·53	+0·09	4·66	C	
32° 13072	160124	356·43	− 0·67	B3 IV	7·03	+0·04	9·41	N	
4G Sgr	161756	1·99	+ 0·48	B3 IV	6·46*	+0·32	8·00	C	
22° 4478	163892	7·15	+ 0·63	Bo IV	7·44*	+0·40	11·24	N	
22° 4484	164002	7·12	+ 0·47	Bo·5 IV	7·45*	+0·23	11·36	N	
21G Sgr	164402	7·14	− 0·01	Bo Ib	5·72	+0·12	11·56	C	
23° 13804	164492	7·00	− 0·23	O7	6·91	+0·40	11·21	N	
22G Sgr	164637	7·34	− 0·22	B1 IIk	6·89*	+0·12	11·83	N	
24° 13816	164816	6·05	− 1·18	Bo V	7·34	+0·22	11·08	N	
22° 4533	164833	7·34	− 0·46	Bo Ia	7·16*	+0·14	12·34	N	
θ Ara	165024	343·32	−13·80	Bo·5 II	3·76	+0·14	8·84	C	
19G Ser	165402	20·29	+ 6·14	B8 IV	6·06*	...	6·76	N	
30G Sgr	165516	8·92	− 0·43	B1 Ibk	6·26	+0·21	11·73	N	
33G Sgr	165793	355·74	− 8·15	B1 Ibk	6·50	+0·05	12·45	N	
16° 4736	166286	13·42	+ 1·13	Bo II	7·58	+0·52	11·72	N	
52G Sgr	167771	12·69	− 1·12	O8 k	6·67*	+0·31	10·94	N	
18° 4896	168021	12·70	− 1·44	Bo Ibk	6·68*	+0·32	11·92	N	
24° 14462	170978	9·37	− 6·98	B3 IV	6·75	+0·18	8·71	N	
17° 5310	173375	16·59	− 6·64	B6 V	7·06	+0·26	6·98	N	
47° 12565	173994	348·45	−19·61	B8 Vk	7·17	...	7·07	N	
σ Sgr	175191	9·56	−12·42	B4 IV	2·07	−0·02	4·27	C	
6° 5005	176630	28·54	− 5·03	B4 IV	7·69	+0·25	9·14	N	
47G CrA	178628	358·54	−20·23	B8 III	6·48*	+0·12	7·12	N	
53G Tel	180183	340·88	−25·93	B3 IV	6·83	...	9·33	N	
179G Sgr	182180	10·68	−19·03	B5 IV	6·20*	+0·04	7·88	C	
191G Sgr	183133	23·35	−14·90	B5 V	6·99*	...	7·99	N	

TABLE III

Star	HD	l^{II}	b^{II}	Sp. & Lum.	m_v	E_y	m_0-M	Sp.	Notes
58° 969	62805	270·96	−16·70	B9 V	6·7	...	6·1	N	(7)
18G Vel	69168	262·54	− 6·67	B3 IV	7·3	...	9·8	N	(7)
40° 4212	71216	258·81	− 1·79	B8 V	7·1	...	7·0	N	(7)
57° 1513	71634	273·32	−11·52	B7 IV	7·0	...	8·2	N	(7)
46° 4267	72555	264·83	− 4·53	B4 V	7·0	...	8·4	N	(7)
59° 3017	96248	289·92	+ 0·30	B1 II	6·56	+0·34	10·8	C	(13) (14)
59° 3038	96446	290·08	+ 0·28	B2 IIIp	6·64	+0·09	10·0	N	(14)
59° 3193	97557	290·76	+ 0·84	B3 IV	7·18	+0·16	9·2	N	(14)
59° 4080	105580	297·66	+ 2·69	B6 V	7·0	+0·14	7·3	N	(7)
68° 1777	111558	302·91	− 6·77	B7 Ia	7·13	+0·11	13·6	N	(13)

TABLE III—(*continued*)

Star	HD	l^{II}	b^{II}	Sp. & Lum.	m_v	E_y	m_0-M	Sp.	Notes
66° 2171	115846	305·80	− 4·83	B4 V	7·1	...	8·5	N	(7)
73° 1184	119109	306·70	−11·15	B7 V	7·0	...	7·4	N	(7)
65° 2652	124182	311·21	− 4·62	B6 IV	7·0	...	8·5	N	(7)
16G Cir	128293	312·72	− 7·42	B5 : V : e	6·70	+0·16	7·2	C	(15) (*f*)
55° 6509	136003	322·68	+ 0·92	B2 III	6·72	+0·31	9·4	N	(13) (14)
41° 10925	151515	342·81	+ 1·73	B3 II	7·4	...	11·8	N	(7)
22° 4500	164359	7·70	+ 0·36	Bo IIIk	8·2	+0·30	12·7	N	(7)
18° 4871	167411	12·70	− 0·68	Bo IIk	8·6	+0·47	12·9	N	(7)

Notes

(*a*) HD 60606. Emission in Hβ, Hγ and λ 4267.

(*b*) HD 62753. Emission in Hβ, Hγ, Hδ and Hϵ. Very broad, badly-defined lines.

(*c*) HD 67698. Emission in Hβ and Hγ.

(*d*) HD 107696. λ 4072 is extremely strong for the type, and appears the same on four plates of this star.

(*e*) HD 113120. Emission in Hβ and Hγ.

(*f*) HD 128293. Emission in Hβ, Hγ, Hδ and Hϵ. Both class and luminosity are uncertain. There may also be emission at λ 3933, but this region is not well-resolved on the spectra available.

The majority of the colours were found in the work of Schilt and Jackson (**16**) and the Cape Mimeograms (**17**). Some were taken from the work of Oosterhoff (**13**), Hoffleit (**14**), Stoy (**15**), Hogg (**18**), Hiltner (**19**), Stebbins *et al.* (**20**), and Cousins (**21**). All conversions to the *B–V* system were linear, with the exception of the Schilt and Jackson values, which were converted by comparison with colours derived from other sources. A recent paper by T. Walraven and J. H. Walraven (**22**) and a private communication from R. H. Hardie and D. L. Crawford arrived too late to be conveniently incorporated. However, it was noted in both cases that the colours given were in good agreement with those from other sources.

The criteria used for type and luminosity classification were the same as those quoted by Mrs de Vaucouleurs (**3**). For B stars the most prominent criterion of spectral type is the rapid decrease in strength, from B2 to B9, of the He I line at λ 4026. An estimate of the strength of this line compared with that of Hδ quickly gives a good first approximation for the type.

Some stars from Mrs de Vaucouleurs's list have been re-classified as spectra of improved quality were obtained. In spite of the poor quality of some spectra used by Mrs de Vaucouleurs, there is little change in the assigned type and luminosity. A new mean modulus for the stars with normal spectra which were considered to be *certain members* of the Scorpio–Centaurus Association by Blaauw (**23**) has been computed using some revised classifications and the improved absolute magnitude values (**12**). The moduli for the individual stars are given in Table IV. Three stars, HD 105435, 120324, and 151890, which have peculiar spectra, have been omitted, but none of the stars with normal spectra has a distance modulus which deviates excessively from the mean on Chauvenet's criterion.

TABLE IV

Certain members of the Scorpio–Centaurus Association

HD	Sp.	$m_0 - M$	HD	Sp.	$m_0 - M$
79351	B2 IV	7·18	130807	B6 III	6·33
85980	B4 V	6·91	132200	B2 III	6·79
103884	B3 V	7·39	132955	B4 IV	7·39
105382	B6 III	6·58	136298	B3 IV	6·13
106983	B3 IV	6·55	136664	B3 IV	7·34
109668	B2 IV	6·30	138764	B6 IV	7·11
112078	B5 Vn	6·00	140008	B6 V	6·08
113703	B5 IV	6·88	142669	B3 IV	6·47
120307	B2 IV	7·03	143118	B2 V	6·33
120709	B5 IV	6·30	147165	B1 III	7·04
120908	B5 V	6·37	148703	B2 V	6·93
120955	B5 IV	6·74	149438	B0 V	7·15
121743	B2 V	6·73	151985	B2 IV	6·88
122980	B2 V	6·88	153716	B5 V	6·50
125823	B5 III	6·71	172910	B3 V	6·46
129056	B1 III	7·34	175362	B8 IV	6·12
129116	B3 IV	6·80			

Mean $m_0 - M = 6{\cdot}72 \pm 0{\cdot}05$ p.e.

Division into luminosity classes and intervals of spectral type leads to the following mean moduli:

	III	IV	V	B0–2	B3–4	B5–8
$\overline{m_0 - M}$	6·80	6·75	6·64	6·85	6·83	6·50
p.e., ±	0·13	0·07	0·08	0·06	0·10	0·10
n	6	15	12	12	9	12

This shows that the use of the new calibration of absolute magnitudes for the MK types has eliminated the systematic luminosity effect noted by Mrs de Vaucouleurs. The barely significant excess in the mean distance modulus for the B stars of earliest sub-classes may indicate that the adopted intrinsic colours are not sufficiently blue. On the other hand, Blaauw (**24**) has suggested that the stars embedded in the interstellar clouds of Scorpius and Ophiuchus have evolved more toward the right from the main sequence in the Hertzsprung–Russell diagram. Two of the stars earlier than B2, HD 129056 and HD 147165, are pulsating stars of the β CMa type. There is as yet no secure evidence that the distance from the Sun varies significantly from its mean value of 220 parsecs in any section of the 60° of galactic longitude subtended by the Association.

From the distance moduli it will be seen that many of the early-type stars examined in this paper lie beyond the Scorpio–Centaurus Association, while some of the late B and early A stars are in the foreground. Further studies of the radial velocities of possible member stars are in progress.

Acknowledgments.—Dr S. C. B. Gascoigne has given very helpful advice and assistance in the computation of galactic coordinates using the Observatory's IBM 610 computer. Dr W. Buscombe, Dr H. Gollnow and Dr A. Przybylski have willingly made available plates from their individual programmes and have obtained spectra of the standard stars. Special thanks are due to Dr Buscombe, who has not only obtained almost all the Newtonian spectra used but has given valuable advice and assistance throughout.

Mount Stromlo Observatory,
Canberra, Australia:
1960 *November.*

References

(1) H. L. Johnson and W. W. Morgan, *Ap. J.*, **117**, 313, 1953.
(2) M. L. Woods, *Mem. Comm. Obs.*, **3**, No. 12, 1955.
(3) A. de Vaucouleurs, *M.N.*, **117**, 449, 1957.
(4) W. Buscombe, Mt. Stromlo Mimeogram No. 3, 1959.
(5) C. P. Gaposchkin, Harvard Mimeograms Ser. III, Nos. 1 and 2, 1938.
(6) B. A. Gould, *Cordoba Resultados*, **1**, 1879.
(7) A. J. Cannon, *Harvard Annals*, **91–99**.
(8) A. Blaauw *et al.*, *Ap. J.*, **130**, 702, 1959.
(9) H. L. Johnson and W. A. Hiltner, *Ap. J.*, **123**, 267, 1956.
(10) H. L. Johnson, *Lowell Obs. Bull.*, **4**, 37, 1958.
(11) A. Feinstein, *Zs. f. Ap.*, **47**, 218, 1959.
(12) H. L. Johnson and B. Iriarte, *Lowell Obs. Bull.*, **4**, 47, 1958.
(13) P. Th. Oosterhoff, *B.A.N.*, **11**, 299, 1951.
(14) D. Hoffleit, *Ap. J.*, **124**, 61, 1956.
(15) R. H. Stoy, *M.N.A.S.S.A.*, **14**, 34, 1955; **14**, 82, 1955; **15**, 27, 1956; **17**, 142, 1958; **18**, 136, 1959.
(16) J. Schilt and C. Jackson, *A.J.*, **56**, 209, 1952.
(17) A. W. J. Cousins, Cape Mimeogram No. 1, 1953.
(18) A. R. Hogg, Mt. Stromlo Mimeogram No. 2, 1958.
(19) W. A. Hiltner, *McDonald Contr.* No. 269, 1956.
(20) J. Stebbins, C. M. Huffer and A. E. Whitford, *Ap. J.*, **91**, 20, 1940.
(21) A. W. J. Cousins, *M.N.A.S.S.A.*, **17**, 134, 1958.
(22) T. Walraven and J. H. Walraven, *B.A.N.*, **15**, 67, 1960.
(23) A. Blaauw, *Pub. Kapteyn Astr. Lab. Groningen* No. 52, 1946.
(24) A. Blaauw, *Ann. Astrophys.* Supp. No. 8, 105, 1959.

ON TWO METHODS OF BROWN AND SHOOK

Harold Jeffreys

(Received 1960 December 15)

Summary

A method given by Brown and Shook for the elimination of short-period terms from the disturbing function is essentially an extension of one given by von Zeipel. A slight further extension is given here. It is shown that the method of Brouwer for the motion of artificial satellites is a case of that of Brown and Shook.

Another method of Brown and Shook uses the orbital true longitude as independent variable. The motion of an artificial satellite appeared to provide a particularly suitable case for the application of this method, but on trial it proved to be extremely laborious.

Some suggestions are offered with regard to sign conventions in Hamiltonian theory.

1.—Brouwer's solution (1959) of the problem of the motion of an artificial satellite uses Hamilton–Delaunay theory, and eliminates terms of short period by a method of von Zeipel (1916). In the application concerned this method is equivalent to one given by E. W. Brown and C. A. Shook (1933), which however appears to be more general and to need less preliminary explanation. I shall restate it here in a slightly more general form than that given by Brown and Shook.

Let the Hamiltonian be

$$H = H_0(p) + m\sum_s H_s(p)\cos(l_{rs}q_r + n_s t), \tag{1}$$

with

$$\frac{dp}{dt} = -\frac{\partial H}{\partial q}, \qquad \frac{dq}{dt} = \frac{\partial H}{\partial p}, \tag{2}$$

and m small. Neglect of m gives the first approximation

$$\frac{dq_r}{dt} = \frac{\partial H_0}{\partial p_r} = a_r(p), \qquad \frac{dp_r}{dt} = 0. \tag{3}$$

Write

$$l_{rs}a_r + n_s = \nu_s \tag{4}$$

and consider the transforming function

$$J = p_r'\, q_r - m\sum_s{}' \frac{H_s(p')}{\nu_s}\sin(l_{rs}q_r + n_s t) \tag{5}$$

summation being over any set of terms with $\nu_s \neq 0$, and usually also not with ν_s small. Then

$$p_r = \partial J/\partial q_r = p_r' - m\sum_s{}' \frac{H_s(p')}{\nu_s} l_{rs}\cos(l_{rs}q_r + n_s t) \tag{6}$$

$$q_r' = \partial J/\partial p_r' = q_r - m\sum_s{}' \frac{\partial H_s(p')}{\partial p_r'}\frac{1}{\nu_s}\sin(l_{rs}q_r + n_s t), \tag{7}$$

and the new Hamiltonian is

$$H' = H + \frac{\partial J}{\partial t} = H_0(p) + m\sum H_s(p)\cos(l_{rs}q_r + n_s t)$$

$$- m\sum{}' H_s(p')\frac{n_s}{\nu_s}\cos(l_{rs}q_r + n_s t). \quad (8)$$

Substitution for p in H_0 and using (6) gives

$$H_0(p) = H_0(p') - \sum_k m a_k \sum_s{}' \frac{H_s(p')}{\nu_s} l_{ks}\cos(l_{rs}q_r + n_s t) + O(m^2). \quad (9)$$

Then in H' the terms under the sign $\sum'$ of order m are

$$m\sum{}' H_s(p')\cos(l_{rs}q_r + n_s t) - m\sum{}' H_s(p)\frac{n_s}{\nu_s}\cos(l_{rs}q_r + n_s t)$$

$$- m\sum_k a_k \sum{}' \frac{H_s(p')}{\nu_s} l_{ks}\cos(l_{rs}q_r + n_s t). \quad (10)$$

On summation with regard to k and reference to (4) we see that all these terms cancel except for the difference between p_r and p'_r. Hence

$$H' = H_0(p') + \sum_0 m H_s(p')\cos(l_{rs}q_r' + n_s t) + O(m^2) \quad (11)$$

where $\sum_0$ denotes summation over terms in $\sum$ not included in $\sum'$. Thus all short-period terms of order m can be removed in one operation and the further interest is usually in secular terms and terms of long period. For the latter it is well known that a further differentiation with regard to t simplifies the further analysis and covers the case of libration.

If H_0 is a function of p_1 only, so that $a_r = 0$ for $r \neq 1$, and if H does not contain t explicitly, so that $n_s = 0$, ν_s is simply $l_{1s}a_1$, and

$$J = p_r' q_r - m\sum{}' H_s(p')\frac{\sin(l_{1s}q_1)}{l_{1s}a_1} \quad (12)$$

$$= p_r' q_r - \frac{m}{a_1}\sum{}' \int H_s(p')\cos(l_{1s}q_1)\,dq_1. \quad (13)$$

In the problem of an artificial satellite, where the Earth's field is supposed to have axial symmetry, q_1 is the mean longitude and J is found by direct integration. The series can be summed exactly, as is done by Brouwer, who integrates as in (13). His transforming function is therefore identical with that found by this method. I have verified this directly.

2.—Brown and Shook give another method, which uses v, the total angular distance described, as independent variable. They reduce the problem to a set of differential equations, the left sides of which, except for that for t, are all linear with constant coefficients in the unknowns, while the right sides all contain derivatives of the disturbing function as factors. u, the reciprocal of the radius vector, is treated as one of the unknowns, so that its variation includes those of the eccentricity and pericentre. The method has not, so far as I know, been much used in planetary theory, apparently on account of the difficulty of expressing the coordinates of the disturbing body as harmonic series in v. But it seemed likely that the method would be very suitable for the artificial satellite problem, since the disturbing function depends only on the position of the satellite itself. The method introduced by King-Hele (1958), which gave the short-period terms to the first order and the secular motion of the node to the second order, depends on the same principles. The method has the further apparent advantage in this problem

that u appears on the right side only in positive powers, except in the equation for t, so that the other variables, to any order in J of the theory of the figure of the Earth, consist of finite sums of harmonic terms whose coefficients are powers of e.

When I tried the method I found that it gave the first order terms very easily. The second order terms, however, appeared prohibitively difficult. It might be expected that, since the expressions on the right sides of the equations all contain the factor J, it would be easy to pick out the terms of order J^2 that are secular or of long period. In the equation for u this would imply a search for terms of speed near n to get the motion of the perigee. Actually, the first approximations contain several terms and the terms on the right are products of three or four such sums. To pick out the relevant terms therefore needed all multiplications but the last to be carried out in full. The energy equation and an equation given by Brown and Shook ((10), p. 174) for the sine of the declination could be used as checks, but only at the very end, and would be of little help towards tracing any mistake.

In comparison with the transformation method, which also involves much algebra, the latter has the advantages that at each stage the disturbing function is worked out and is used in every equation, and that elimination of short period terms simplifies it. In the true longitude method the different partial derivatives have to be worked out separately, to the required order, before multiplication by the other factors, and become more complicated at each approximation. My final conclusion was that the labour of the method would not be justified by the results.

After this disappointing conclusion I noticed a passage in Brouwer's obituary notice of E. W. Brown (1939), which seems to imply that Brown himself had abandoned the method for very similar reasons. As the artificial satellites should provide an exceptionally favourable case for the method my attempt may be regarded as reinforcing Brown's conclusion.

These remarks of course do not apply to the later work of King-Hele and his collaborators on atmospheric resistance, where only a first-order theory is involved.

3.—The standard works on Hamilton–Delaunay theory suffer from a hopeless confusion of signs, and it seems worth while to point out that there is a choice with, apparently, substantial advantage over the others. In the first place some authors write

$$\frac{\partial S}{\partial \alpha_r} = \beta_r, \tag{1}$$

but almost as many use a negative sign. If the initial coordinates q_{r0} are identified with the α_r the above gives $\beta_r = -p_{r0}$. This is not, however, an argument for taking the negative sign. The β_r in planetary theory are angles and best regarded as analogous to coordinates, and therefore the α_r as analogous to momenta. Then if a modified Hamiltonian is

$$H = H_0 + mH_1 \tag{2}$$

and $S_0\,(q, \alpha, t)$ is the solution of the Hamiltonian equation with $H = H_0$, the transforming function according to the rules

$$J = S_0, \partial J/\partial \alpha = \beta, \quad \partial J/\partial q = p, \tag{3}$$

$$H' = H + \frac{\partial J}{\partial t} \tag{4}$$

eliminates H_0 from the Hamiltonian. So far there is no negative sign.

Further, most theoretical writers write further transforming functions as $J(q, q', t)$, leading to the transforming equations

$$p = \frac{\partial J}{\partial q}, \qquad p' = \frac{\partial J}{\partial q'}. \tag{5}$$

This has an unfortunate consequence. The function $J = q_r q_r'$ leads to

$$p_r = q_r', \quad p_r' = q_r, \tag{6}$$

so that coordinate-like and momentum-like variables are interchanged at every transformation. To take the transforming function as

$$J(q, p', t) \quad \text{or} \quad J(q', p, t) \tag{7}$$

is however perfectly satisfactory; and

$$J = q_r p_r', \qquad p = \frac{\partial J}{\partial q}, \qquad q' = \frac{\partial J}{\partial p'} \tag{8}$$

leads to $q_r' = q_r$, $p_r = p_r'$, so that the identical transformation does not interchange coordinates and momenta.

One consequence of this form of the theory is that in the equations of motion, when the mean longitude l is taken as one coordinate, the principal term in the Hamiltonian will be $-\mu^2/2L^2$, and the disturbing function R, which is an addition to the gravitational potential, appears with a negative sign. We could compensate this, if we want to do so, by reversing the sign in the definition of H, and something could be said for this (it is done in part in Routh's modified Lagrangian function); in works on celestial mechanics, however, it is usually achieved by interchanging the p's and q's at some stage, not generally with much clarity. For myself I doubt whether either method of compensation is worth while.

160 *Huntingdon Road,*
Cambridge:
1960 *December* 14.

References

D. Brouwer, 1939, *M.N.*, **99**, 306.
—— 1959, *A.J.*, **64**, 378–397.
E. W. Brown and C. A. Shook, 1933, *Planetary Theory*, Camb. Univ. Press.
D. G. King-Hele, 1958, *Proc. Roy. Soc.* A, **247**, 49–72.
H. von Zeipel, 1916, *Ark. Astr. Mat. Fys.*, **11**, No. 1.

THE EFFECT OF TIDAL FRICTION ON ECCENTRICITY AND INCLINATION

Harold Jeffreys

(Received 1961 January 26)

Summary

Darwin's analysis for the effects of tidal friction on the eccentricity and inclination of a satellite's orbit is adapted to modern laws of imperfect elasticity and of friction in ocean currents. It appears that as the conditions make the lags in the tides nearly proportional to the speeds his results for small viscosity are qualitatively correct, since these have the same property. In particular the eccentricity and inclination of the Moon's orbit should now be increasing.

In a classical paper Darwin (1880, 1908 (esp. p. 342)) studied the variations of the orbital elements of the Earth and Moon, and also considered incidentally the case of a planet attended by several satellites. His work was quite general, but the only case worked out to quantitative results, except for the variation of the mean distance and the rotation of the planet, was for a fluid planet of small viscosity. Since it appears that most of the tidal friction in the Earth–Moon system is in turbulent sea currents it has long appeared desirable that this case also should be considered; and since there are now plausible laws of imperfection of elasticity in a solid planet they also need examination.

In the first place we neglect the inclination. The tidal potential due to a body at distance R in the plane of the equator is

$$U=\frac{fmr^2}{R^3}\{\tfrac{3}{4}\sin^2\theta\cos 2(\phi-v)+\tfrac{1}{2}(\tfrac{1}{2}-\tfrac{3}{2}\cos^2\theta)\} \tag{1}$$

where v is the true longitude of the body and (r, θ, ϕ) are polar coordinates. To refer to the rotating planet we must replace ϕ by $\omega t+\lambda$, where ω is the speed of rotation and λ the longitude of the place. We take

$$R=c(1-\alpha\cos pt), \qquad v=nt+\beta\sin pt, \tag{2}$$

where in elliptic motion, to the first order,

$$p=n, \ \alpha=e, \ \beta=2e. \tag{3}$$

Then

$$U=\frac{fmr^2}{c^3}[\tfrac{3}{4}\sin^2\theta\{\cos(2\lambda+2\omega t-2nt)+(\tfrac{3}{2}\alpha+\beta)\cos(2\lambda+2\omega t-2nt-pt)$$
$$+(\tfrac{3}{2}\alpha-\beta)\cos(2\lambda+2\omega t-2nt+pt)\}+\tfrac{1}{2}(\tfrac{1}{2}-\tfrac{3}{2}\cos^2\theta)(1+3\alpha\cos pt)]. \tag{4}$$

The elastic tide raised by a potential

$$U=k_2r^2S_2 \tag{5}$$

in a homogeneous planet of radius a is λbS_2, where

$$\left(1+\frac{2g\rho a}{19\mu}\right)\lambda=\frac{5}{19}\rho a^2k_2. \tag{6}$$

We shall however write it at present by replacing $\frac{3}{4}fma^2/\lambda c^3$ by H, and inserting lags $2\epsilon_0$, $2\epsilon_1$, $2\epsilon_2$, $2\epsilon_3$ in the periodic terms. If there is imperfect elasticity the coefficients in the amplitudes will also need corrections, but these can be adjusted later.

A surface inequality HS_2 produces an external potential

$$\tfrac{3}{5}fMa\frac{HS_2}{r^3}. \tag{7}$$

As the results will be applied to a satellite as affected by the tides raised by another I shall not necessarily identify the disturbed satellite with the tide-raising one, and consequently state the results in a more general form than is needed for the immediate problem. The part due to friction is

$$U=\tfrac{3}{5}\frac{fMaH}{r^3}[2\sin^2\theta\{\epsilon_0\sin(2\lambda+2\omega t-2nt)+\epsilon_1(\tfrac{3}{2}\alpha+\beta)\sin(2\lambda+2\omega t-2nt-pt)$$
$$+\epsilon_2(\tfrac{3}{2}\alpha-\beta)\sin(2\lambda+2\omega t-2nt+pt)\}+\tfrac{4}{3}(\tfrac{1}{2}-\tfrac{3}{2}\cos^2\theta)\epsilon_3\alpha\sin pt], \tag{8}$$

and if accents now refer to the tide-raising body, R and v to the disturbed one, and $\theta=\frac{1}{2}\pi$,

$$U_1=\frac{6fMaH}{5}\frac{}{R^3}[\epsilon_0\sin(2v-2n't)+\epsilon_1(\tfrac{3}{2}\alpha'+\beta')\sin(2v-2n't-p't)$$
$$+\epsilon_2(\tfrac{3}{2}\alpha'-\beta')\sin(2v-2n't+pt)+\epsilon_3\alpha'\sin p't]. \tag{9}$$

For the disturbed body we take

$$R=c\{1-e\cos(l-\varpi)\},\quad v=l+2e\sin(l-\varpi), \tag{10}$$

where l is the mean longitude. Rates of change of the elements can be calculated as usual. We have

$$n^2c^3=fM, \tag{11}$$

defining n. Then

$$U_1=\frac{6}{5}\frac{fMaH}{c^3}[\epsilon_0\{\sin(2l-2n't)+\tfrac{7}{2}e\sin(3l-\varpi-2n't)-\tfrac{1}{2}e\sin(l+\varpi-2n't)\}$$
$$+\epsilon_1(\tfrac{3}{2}\alpha'+\beta')\{\sin(2l-2n't-p't)+\tfrac{7}{2}e\sin(3l-\varpi-2n't-p't)$$
$$-\tfrac{1}{2}e\sin(l+\varpi-2n't-p't)\}$$
$$+\epsilon_2(\tfrac{3}{2}\alpha'-\beta')\{\sin(2l-2n't+p't)+\tfrac{7}{2}e\sin(3l-\varpi-2n't+p't)$$
$$-\tfrac{1}{2}e\sin(l+\varpi-2n't+p't)\}$$
$$+\tfrac{3}{2}\epsilon_3e\alpha'\{\sin(l-\varpi+p't)-\sin(l-\varpi-p't)\}]. \tag{12}$$

The perturbations are, to the first order,

$$\left.\begin{aligned}
\delta\frac{dl}{dt}&=\delta n-2\sqrt{\left(\frac{c}{fM}\right)}\frac{\partial U_1}{\partial c}+\tfrac{1}{2}\frac{e}{\sqrt{(fM)}}\frac{\partial U_1}{\partial e}\\
\delta\frac{dc}{dt}&=2\sqrt{\left(\frac{c}{fM}\right)}\frac{\partial U_1}{\partial l},\\
\delta\frac{de}{dt}&=-\frac{1}{\sqrt{(fMc)e}}\left(\tfrac{1}{2}e^2\frac{\partial U_1}{\partial l}+\frac{\partial U_1}{\partial\varpi}\right)\\
e\delta\frac{d\varpi}{dt}&=\frac{1}{\sqrt{(fMc)}}\frac{\partial U_1}{\partial e}.
\end{aligned}\right\} \tag{13}$$

For a single satellite perturbed by its own tides

$$\alpha'=e',\ \beta'=2e', \tag{14}$$

where we must put $e'=e$, $c'=c$, $l=nt$, $p't=l-\varpi$ after differentiation.

Then the secular terms are

$$\left.\begin{aligned}\delta\frac{dl}{dt}&=\delta n,\quad \delta\frac{d\varpi}{dt}=0,\\ \delta\frac{dc}{dt}&=\frac{24}{5}\frac{(fM)^{1/2}aH}{c^{5/2}}aH\epsilon_0\\ \delta\frac{de}{dt}&=-\frac{6}{5}\frac{(fM)^{1/2}aH}{c^{7/2}}e\left(\epsilon_0-\frac{49}{4}\epsilon_1+\tfrac{1}{4}\epsilon_2+\tfrac{3}{2}\epsilon_3\right).\end{aligned}\right\}\qquad(15)$$

The change in dc/dt gives the usual secular variation of mean distance.

In the case where all speeds are such that the lag is proportional to the speed, $\delta\, de/dt$ has the sign of

$$-e\{(2\omega-2n)-\frac{49}{4}(2\omega-3n)+\tfrac{1}{4}(2\omega-n)-\tfrac{3}{2}n\}=e(22\omega-36n).\qquad(16)$$

Thus e increases or decreases according as n is less or greater than $11\omega/18$. This is Darwin's result. All direct satellites except Phobos should be receding; all except Deimos should have increasing eccentricities.

For the type of linear elastic afterworking that I have considered (Jeffreys 1957 a, b), the rigidity μ is replaced by the operator

$$\mu=\mu_0\frac{1+1/\tau' p}{1+1/\tau p},\qquad(17)$$

where p is the Heaviside symbol and τ, τ' are two constants with the dimensions of time, and $\tau'>\tau$. For a motion with speed σ, p must be replaced by $i\sigma$. In the disturbance produced by a tidal potential the elastic properties enter through a factor λ as in (6), and H contains

$$\frac{\tau'(i\sigma\tau+1)}{(19\mu_0+2g\rho a)\tau\tau' i\sigma+19\mu_0+2ga\tau'}.\qquad(18)$$

The lag is proportional to the imaginary part of this. If $\sigma\tau$ is large (and therefore $\sigma\tau'$ large)

$$\epsilon=\frac{19\mu_0(\tau'-\tau)}{\sigma(19\mu_0+2g\rho a)\tau\tau'}.\qquad(19)$$

The lags are as $1/\sigma$.

For $\sigma\tau$ and $\sigma\tau'$ small the lag is

$$\epsilon=\frac{19\mu_0\sigma\tau(1-\tau/\tau')}{19\mu_0\tau/\tau'+2g\rho a}.\qquad(20)$$

The amplitude is as for rigidity $\mu_0\,\tau/\tau'$ and the lags are proportional to σ. In both cases the lag is small, and the correction to H for imperfect elasticity is $O(\epsilon^2)$.

In Darwin's case the amplitude H is proportional to $\cos 2\epsilon$ and therefore the frictional effect to $\sin 4\epsilon$, and is also proportional to σ for small lags. Thus his result on the sign of de/dt stands without alteration for the case of $\sigma\tau$, $\sigma\tau'$ small. This however is clearly wrong for the Earth–Moon system since $2\pi/\sigma$ is of the order of 12^h or 27^d and τ might be of the order of 20^d or 200^d.

In the opposite case where $\sigma\tau$ and $\sigma\tau'$ are large for all the relevant tides, the corresponding factor in de/dt is

$$e\left(\frac{44\omega^2-63\omega n+20n^2}{(2\omega-n)(2\omega-2n)(2\omega-3n)}-\frac{3}{2n}\right).\qquad(21)$$

This has a complicated behaviour on account of the infinities at $n = \frac{2}{3}\omega$, ω and 2ω. Near these the corresponding speeds are small and the approximation fails, but it appears that if $\omega\tau$ and $n\tau$ are both large de/dt must change sign three times as n/ω varies. But it is worth while to notice that the coefficient is negative for both Phobos and Deimos. It is negative whenever $n/\omega < 0{\cdot}2$ and therefore for most satellites.

I no longer think that either of the above cases is realized in the solar system, but the results may be worth recording.

For friction in turbulent ocean currents, where one tidal component has greater amplitude than the others, it is known (Jeffreys 1959, Section 8.03) that if the current is of the form

$$u = a\sin pt + av\sin rpt \quad (v \leqslant 1) \tag{22}$$

the corresponding terms in the frictional resistance following a quadratic law are, to order v,

$$\tfrac{1}{4}ka^2\left(\frac{8}{3}\sin pt + 4v\sin rpt\right) \tag{23}$$

at least as long as rv is small. The relevant terms in the dissipation are in the ratio $\frac{3}{2}v^2$.

Now it is likely that in the present state of the Earth–Moon system the semi-diurnal tides are somewhere near resonance, their amplitudes being largely controlled by friction. Then for the ocean ϵ_0, ϵ_1, ϵ_2 will be large angles, and since the monthly tide produces velocities proportional to its speed it is likely that ϵ_3 will contain an extra factor n/ω. In that case the tide of speed $2\omega - 3n$ will remain the dominant one in the effect on the eccentricity, on account of the large coefficient of ϵ_1, and e should at present be increasing. The complications of the problem are great, but the main conclusion seems highly probable.

For the modified Lomnitz law, in which the creep under constant stress increases like t^α, with α about $0{\cdot}25$ (Jeffreys and Crampin 1961) the lag in a periodic disturbance increases by a factor of about 3 over a range of period from $0{\cdot}25^{\mathrm{d}}$ to 100^{d}. This is insufficient to upset the dominance of the term in ϵ_1. Even if $2\omega - 3n$ is small, this is a case of an exceptionally large lag and the relative magnitude of the term is accentuated.

The general conclusion is that de/dt is in general positive except when n/ω is more than about 2/3.

This conflicts with the results of G. W. Groves (1960) who finds that e always increases. As however he gets de/dc to be independent of ω it appears that his hypotheses must have oversimplified the problem, since de/dt and dc/dt involve n and ω in quite different ways.

The treatment of the inclination is much more complicated, but the essential results are in Darwin's papers. The semidiurnal, diurnal, and fortnightly tides all contribute; the semi-annual tide is negligible. However we see from Darwin's (35), p. 58, that the fortnightly term enters di/dt with a factor $\sin^3 i$, and what matters is the ratio of the lags for the semidiurnal and diurnal tides. For both the reasonable laws the ratio of the lags will remain substantially the same as on Darwin's theory. Thus his main result, that the inclination should now be increasing, will stand: for small obliquities the obliquity increases if the month is more than twice the day, otherwise decreases.

160 *Huntingdon Road,*
Cambridge:
1961 *January* 25.

References

Darwin, G. H., 1880, *Phil. Trans.*, **171**, 713–891.
—— 1908, *Sci. Papers* 2, Ch. 6.
H. Jeffreys, 1957 a, *M.N.*, **117**, 506–515.
—— 1957 b, *M.N.*, **117**, 585–589.
—— 1959, *The Earth*, C.U.P.
H. Jeffreys and S. Crampin, 1961, *M.N.*, **121**, 571–577.
G. W. Groves, 1960, *M.N.*, **121**, 497–502.

DISSIPATIVE INTERACTION BETWEEN SATELLITES

Harold Jeffreys

(Received 1961 January 26)

Summary

Mutual influence of satellites through tidal friction is considered, and with modern evidence on the rate of tidal friction it appears that the effect is insufficient to explain approximate commensurabilities of mean motions. There is less difficulty in supposing that mutual influence through a resisting medium can have been important.

Kuiper's theory of the origin of Trojan planets appears to be inconsistent with the result that the triangular position is secularly unstable.

The problem of the effect of the tides raised by one satellite on the motion of another was discussed by Darwin (1908, Chapter 8). Since there are several pairs of satellites whose mean motions are nearly commensurable, we might expect that some dissipative action has produced this state. Any such explanation would require the state to be secularly stable. Tidal friction and a resisting medium both need to be considered.

Darwin's remarks on tidal friction in this connection are rather discouraging. He points out that on account of incommensurability of mean motions the tides raised by one satellite cannot ordinarily have any secular effect on another; thus the orbital elements of all vary independently. The exception would be when the mean motions are commensurable, but Darwin says (p. 408) " it is not credible but that such relationship should be broken down by tidal friction ". That is to say, he assumes secular instability; for if the state is secularly stable it will be preserved through further changes of the mean distances.

On both points his arguments need amplification. In the first place, it appears impossible to say without detailed examination whether the state of commensurable mean motions is secularly stable or not. In the second, perturbations of satellite A by satellite B will affect the tides raised by A, and some of the subsidiary tides will have such speeds that they can affect B. It is for this reason that in the previous paper (Jeffreys 1961) p was not immediately identified with n. If the mean motions of A and B are n and n' the mean longitude of A will contain terms with $p = \pm 2\,(n-n')$, arising from perturbations, and terms in $\sin(2l-2n't\pm pt)$ in (12) of the foregoing paper will not contain n', and these tide components can affect B. What is true, as indeed Darwin points out, is that the amplitude of such tides will contain the product of the masses as a factor, and their effect will in general be much less than the effect on either satellite of its own tides. Thus the orbital elements of the satellites will indeed vary nearly, but not exactly, independently. But this statement need not hold when the mean motions are nearly commensurable, since the perturbations of A by B may then be much larger than the ratio of the masses of B and the primary. For instance, the mass of Titan is only about 1/4000 of that of Saturn, but it forces an eccentricity of about 0·1 in the

orbit of Hyperion. This type of state can occur if the mean motions are such that $pn - qn'$ is small compared with n and n', where p and q are integers satisfying $p = q$ or $p = q \pm 1$. The former case is that of the Trojan planets. The latter is that of the pairs J I, J II; J II, J III; Mimas, Tethys; Enceladus, Dione; Titan, Hyperion.

I have pointed out (1957) that the only satellites whose orbits can have been affected to any important extent by tidal friction are the Moon and possibly J I. It appears to follow that the commensurabilities, except possibly for the pair J I, J II, cannot have arisen through tidal friction, and a detailed treatment of the secular stability seems unnecessary, though it might be relevant to an explanation of how the commensurability, once established, could have persisted.

The effect of a resisting medium depends greatly on the motion of the medium. For the solar system as a whole, if there is anything in the nature of a pressure, and if the medium is at rest, the density must increase rapidly inwards, to such an extent that if the mass within 0·1 astronomical unit of the Sun was of the order of the mass of the Sun, that outside the orbit of Mars would be a negligible fraction of a gram (Jeffreys 1929, p. 51). I have considered a medium effectively in rigid body rotation (1917), but this depends on Jeans's theorem on statistically steady motions, which I maintain to be totally erroneous (Jeffreys 1937). It would obviously imply that if the rate of rotation was adapted to the motion of one planet, the matter at $2^{1/3}$ times the distance would have a parabolic velocity; and closer to the Sun it meets the same difficulty as a medium at rest. If a medium is to have an appreciable affect on more than one planet or satellite the pressure must be everywhere small, and the steady motion of most of the medium must be such that the matter at any point has nearly the velocity of a particle in a circular orbit through the point. Near a planet the velocity must correspond to that in a variational orbit.

Since any satellite orbit is essentially an oscillation about a variational orbit it appears that secular effects of a resisting medium will be confined to the eccentricities and inclinations; any effect on the mean distances can arise only through the small departures of the medium from the velocity in the variational orbit.

Interaction between satellites may be due either to viscous or turbulent drag, the formation of shock waves, or accretion. The resistance will depend mainly on the surface of the bodies, so that it may for small bodies be more important than any interaction due to tidal friction. If satellites A, B have different mean motions n, n', it appears that resistance to a perturbation may well give rise to secular terms in the mean distances; these must be small, but not so small as for tidal friction, for two reasons. First, we have no upper bound to the total amount of the effect of a resisting medium, and the fact that most near satellites have small eccentricities and inclinations suggests that it has been large. Secondly, the fact that surfaces rather than masses will occur in the [illegible]action favours it for small bodies.

I considered the effect of a resisting medium on a Trojan planet in three early papers (1915 a, 1916, 1917). In (1915 a) I took the medium to be at rest. In (1917) I took it to be rotating like a rigid body with angular velocity equal to the mean motion of Jupiter. In (1916) I took it to have the velocity appropriate to a circular orbit. On all hypotheses the amplitude of the faster oscillation about the equilateral triangle position would decrease. On those of (1915 a) and (1917) that of the slower oscillation would also decrease; on that of (1916) it would increase.

But (1915a) and (1917) are quite out of the question: (1916) is right, and Lagrange's particles are secularly unstable.

Now Kuiper (1956) has argued that the primitive planets were much more massive than the present ones, and have lost mass; and that Jupiter in consequence failed to control some of its outer satellites, which escaped and became Trojans. This would require that if a satellite enters the region where Trojan orbits are possible, the subsequent oscillations will diminish. But this is contrary to the result that the equilateral triangle position is secularly unstable. Even if the motion near the third point is largely controlled by Jupiter, there will be some influence of the rest of the medium, which would tend to give a compromise between the variational motion and that due to the Sun alone.

Again, if m is the mass of Jupiter, the speed of the slower oscillation is $O(m^{1/2})$. Many cases have been worked out where a motion satisfies a differential equation of the form

$$\ddot{x}+m\chi(t)x=0$$

where χ varies slowly (Jeffreys 1915 b; Jeffreys and Jeffreys 1956, Section 17. 13) and the general rule is that the speed varies like $\chi^{1/2}$ and the amplitude like $\chi^{-1/4}$. That is, if Jupiter has lost mass the amplitude should have *increased*.

In fact Kuiper's hypothesis leads to just the opposite conclusion to what he draws. If the existence of the Trojans is to be attributed to change of the mass of Jupiter, that change must have been an increase sufficient to counteract the effect of a resisting medium. An escaped satellite would become an ordinary asteroid and not a Trojan.

160 *Huntington Road,*
Cambridge:
1961 *January* 25.

References

G. H. Darwin, 1908, *Scientific Papers* 2, Chapter 8.
H. Jeffreys, 1915 a, *M.N.*, **75**, 580–583.
—— 1915 b, *Mem. R.A.S.*, **60**, 187–217.
—— 1916, *M.N.*, **77**, 107–109.
—— 1917, *M.N.*, **77**, 447–448.
—— 1929, *The Earth*, Second Edition, C.U.P.
—— 1937, *M.N.*, **98**, 59–64.
—— 1957, *M.N.*, **117**, 585–9.
—— 1961, *M.N.*, **122**, 339–343.
H. and B. S. Jeffreys, 1956, *Methods of Mathematical Physics*.
G. P. Kuiper, 1956, *Vistas in Astronomy*, 2, 1662–6.

AN EXAMINATION OF THE STEADY-STATE MODEL IN THE LIGHT OF SOME RECENT OBSERVATIONS OF RADIO SOURCES

M. Ryle and R. W. Clarke

(Received 1961 January 30)

Summary

The results of some recent observations of radio sources have been used to investigate the " luminosity function " for the sources. Without making any assumptions about their nature, it can be shown from radio observations alone that most of the sources lying in any given range of flux density are extragalactic with an emission at 178 Mc/s which exceeds 10^{24} watts $(c/s)^{-1}$ $ster^{-1}$. If it is assumed either that the physical dimensions or that the optical luminosities of the sources are comparable with those of the Galaxy, then the emission must lie in the range 3×10^{25}–10^{27} watts $(c/s)^{-1}$ $ster^{-1}$.

From these figures it is possible to derive the expected number-flux density relationship according to different cosmological models and special consideration has been given to the predictions of the steady-state model.

With the new Cambridge interferometer it has become possible to observe sources considerably weaker than those reached in earlier surveys, and hence to make a more accurate determination of the actual number-flux density relationship; the new data has also allowed more detailed corrections for the effects of extended sources and source clustering to be made.

A comparison of these observational results with those predicted by the steady-state model shows a marked discrepancy, the number of sources observed with a flux density in the range 0·5 to 2×10^{-26} watts $(c/s)^{-1}$ m^{-2} being at least $3 \pm 0{\cdot}5$ times that predicted by the model.

No attempt has been made to select an alternative model to account for the observations, but the results appear to provide conclusive evidence against the steady-state model.

---

1. *Introduction.*—Previous observations of radio sources situated more than 20° from the galactic equator have shown there to be an isotropic distribution, with some evidence for non-uniformity in depth (Shakeshaft, Ryle, Baldwin, Elsmore and Thomson 1954; Mills, Slee and Hill 1958; Edge, Scheuer and Shakeshaft 1958; Edge, Shakeshaft, McAdam, Baldwin and Archer 1959). The possibility that this latter result is due to effects of the red-shift was first discussed by Ryle and Scheuer (1955).

A new series of observations has now been made at the Mullard Radio Astronomy Observatory with an instrument having considerably greater resolving power and sensitivity than those used in the previous surveys.

The results obtained are reliable over a considerably greater range of flux density than those of the earlier surveys, and they also allow an examination to be made of selection effects which may have been present previously. In particular analyses have been made of the distribution of the sources in relation to their

surface brightness (Leslie 1961 a) to find the effect of partial resolution of extended sources, and also the effects which might be caused by source clustering (Leslie 1961 b).

The combination of the results obtained from "whole-sky" surveys made with intermediate resolving power (Elsmore, Ryle and Leslie 1959; Leslie 1961 a) with those of a number of limited areas of sky made with the full resolving power of the instrument (Scott, Ryle and Hewish 1961) make it possible to obtain a greatly improved determination of the number–flux density ($N-S$) relationship (Scott and Ryle 1961). This relationship has been extended to still smaller flux densities by applying to the survey of high resolution the statistical method of analysis introduced by Scheuer (1957). This technique has been developed by Hewish (1961) who has shown that if, as in the present observations, the noise level is small, the method can provide information on the $N-S$ relationship even when there is about one source per beam area. A number of authors have shown that a study of individual sources can only give a reliable estimate of source counts for flux densities at which there is not more than one source per 20 beam areas.

In the present observations it has been possible to extend the analysis to flux densities at which there are about 2×10^4 sources per steradian. The results confirm the previous conclusion of an apparent non-uniformity in depth.

In addition to these observations at a frequency of 178 Mc/s, further measurements of the spectral distribution both of radio sources (Whitfield 1957; Harris and Roberts 1960) and of the background emission (Costain 1960) are now available which are relevant to the present investigation.

Before applying the new data to the cosmological problem it is necessary to re-examine the question of the radio luminosity function of the sources. In a previous paper (Ryle 1958) it was shown that, even in the absence of optical identifications, a number of different radio observations could be combined to set restrictions on the ranges of luminosity within which the majority of the observed sources must lie. Although the number of optical identifications has since been increased, it still represents only a small fraction of the sources known; as will be shown in Section 2, however, the optical data are valuable in extending the rigorous, though more conservative, restrictions on the radio luminosity function set by the new radio data. It is now clear that few of the sources are within the Galaxy, and that most of those observed are extra-galactic objects having a radio luminosity approaching that of the Cygnus-A source.

The importance of the red-shift in modifying the number–flux density counts is then evident and consideration is given in Section 3 to the predicted curves for two particular cosmological models: (*a*) the steady-state model and (*b*) the Einstein-de Sitter model.

The results of these computations are compared in Section 4 with the observed counts of sources paying particular attention to the observational test of the steady-state model.

2. *The derivation of the radio luminosity.*—Considerable progress has been made in the identification of radio sources with optical objects (Dewhirst 1958, 1961; Bolton 1960), although the number of identified sources is still only a small fraction of the total. It is, however, now clear that most sources are extremely faint optical objects (Minkowski 1960; Long and Marks 1961) and the observations are consistent with a radio luminosity function in which most of the sources observed in a given range of flux density produce a radio emission which

is at least 5 per cent that of Cygnus-A. This interpretation is supported by theoretical arguments concerning the mechanism and supply of energy for the emission, the gravitational potential of the source, and the minimum optical emission expected (Tunmer 1960).

As will be seen later, the luminosity function derived from optical work is entirely consistent with the limits derived from the radio data, but since it must be based on a small fraction of the sources the distribution might be seriously in error if a class of radio source exists having a low intrinsic optical luminosity.

The observation of additional sources of small angular size in the area of sky covered by the "spur" of galactic emission at $I^{II}=30°$ was first reported by Edge *et al.* (1959) and this result has been confirmed by recent unpublished observations at Cambridge. The presence at high galactic latitudes of radio sources which are presumably in the Galaxy and which are apparently unrelated to optical objects must raise the question of whether there are other optically invisible galactic sources.

A further difficulty is illustrated by the problem of accounting for the source Hercules-A, which recent observations have shown to be a double source with an angular separation of about 2′ arc between the components (Boishot 1960; Williams, Dewhirst and Leslie 1961); the sources may represent a similar situation to the Cygnus-A object, although this explanation would require a physical separation of the two emitting regions about 200 kpc to either side of the optical galaxy. If the intensities of the two components had differed by more than 3:1 it would have been difficult to recognize the source as double and the apparent radio position would have been displaced from the optical galaxy by several times the probable error. In such circumstances a very low limit would have been wrongly attributed to the optical luminosity of the related object.

Similar difficulties also apply to the derivation of the distance and hence the radio luminosity from measurements of the angular diameter of a source. The complex nature and large extent of Hercules-A (and to a lesser degree Cygnus-A) suggest that the distances of similar but more remote objects might be seriously underestimated. On the other hand a source of small physical size but having a large volume emissivity might be interpreted as a more powerful and distant source if it were assumed to be of galactic dimensions.

For these reasons it is important to re-examine the limits which may be set to the radio luminosity function from radio observations alone. Having established definite but perhaps less stringent limits in this way, the evidence provided by optical observations and from theories of the radio emission may allow closer restrictions to be set.

(*a*) *The evidence from radio observations*

In an analysis based on the results of earlier surveys it was shown (Ryle 1958) that limits could be set to the radio luminosity (P) from a correlation of the following information:

(i) The number of sources observed in a given range of flux density.

(ii) The average volume emissivity of different regions of space required to account for the observed background emission.

(iii) The observed isotropic distribution of sources situated at galactic latitudes $>20°$.

Using the earlier observations at a frequency of 81·5 Mc/s, it was shown that most of the sources must belong either to:

(i) a class of galactic object having $P \simeq 10^{14}$ watt (c/s)$^{-1}$ ster^{-1} (at 81·5 Mc/s) and an average space density throughout the galactic halo of $\rho \simeq 10^{-7}$ pc^{-3}; or

(ii) a class of powerful extragalactic emitters, having $P > 10^{23}$ watts (c/s)$^{-1}$ ster^{-1} and $\rho < 10^{-19}$ pc^{-3}.

This analysis will now be extended in the light of the new observations which are available. Since most of these observations were made at a frequency of 178 Mc/s it will be convenient to give the numerical values derived for source luminosity, volume emissivity etc. appropriate to this frequency; these quantities will differ by a factor of about two from the corresponding earlier figures. It will also be convenient, when considering extragalactic sources, to adopt the more recent figure of 100 km sec^{-1} Mpc^{-1} for Hubble's constant (Sandage 1958) instead of the value 180 km sec^{-1} Mpc^{-1}, previously used.

As before, a uniform but random distribution will be assumed for the region containing the more intense sources, with a dispersion of the luminosity of the form:

$$n(P) \propto \exp\left[-(\log_{10} P/P_0)^2/2\right]$$

where $n(P)$ represents the number of sources of luminosity P which occur in a sample producing flux densities within a given range. It may be rewritten to give the true space density $\rho(P)$ of sources of different P:

$$\rho(P) \propto P^{-3/2} \exp\left[-(\log_{10} P/P_0)^2/2\right].$$

By analogy with an undispersed luminosity function the constant of proportionality in the first relation may be written in the form $\rho_0 P_0^{3/2}$; ρ_0 is then seen to represent a weighted mean density of sources. In later considerations it will be convenient to work in terms of ρ_0 and P_0.

This dispersion covers a range of P similar to that used in the earlier analysis but its form is more probable. A smaller dispersion seems unlikely in view of the far larger values evident in optical stars and galaxies; the adopted dispersion is comparable with that found amongst identified ratio sources (Long and Marks 1961). If the actual dispersion were greater than that adopted it would impose more stringent restrictions than those derived below.

(*b*) *The number-flux density relation*

At distances corresponding to small red-shift the expected number of sources N per unit solid angle which have a flux density greater than S is given by:

$$N = \tfrac{1}{3}\rho_0 P_0^{3/2} S^{-3/2}.$$

As already indicated the observations are not consistent with a uniform spatial density, but an observational relationship between N and S can be established at a large value of N where the statistical errors are small and yet not near the limit of the observations. The value of $\rho_0 P_0^{3/2}$ derived in this way will be appropriate in the following analysis in which the source counts are related to the observations of the isotropy of the weak sources and to their contribution to the integrated emission.

Using the recent observations a value of $\rho_0 P_0^{3/2} = 1{\cdot}4 \times 10^{14}$ is found where ρ_0 is expressed in sources pc^{-3} and P_0 in watts (c/s)$^{-1}$ ster^{-1} at a frequency of 178 Mc/s. This result is shown in a plot of log P_0 against log ρ_0 in Fig. 1. Any class of source whose radio luminosity and space density are represented by a point on this line will satisfy the general observations of the number of sources falling in a given range of flux density, although not of course the non-uniformity in the observed relationship.

(c) Isotropy

The observations have shown that, except for low galactic latitudes and the area of the "spur" in the galactic emission at $l^{II} = 30°$, the sources are distributed isotropically. As has already been demonstrated (Ryle 1958) most of the sources must then either be extragalactic or they must be in the galactic halo. In order to establish closer limits on the spatial density of the sources in the latter case, some new observations have been made (Scott, Ryle and Hewish 1961) which were designed to detect any differences in the distribution of sources in two areas of sky chosen to represent a large and small extent of the galactic halo. It was shown previously that if the smaller extent is r_1 then, in the absence of dispersion in the luminosity, the source distribution will appear different in the two areas if the source density $\rho < 3N/r_1^3$, where N represents the number of sources per steradian which can be observed.

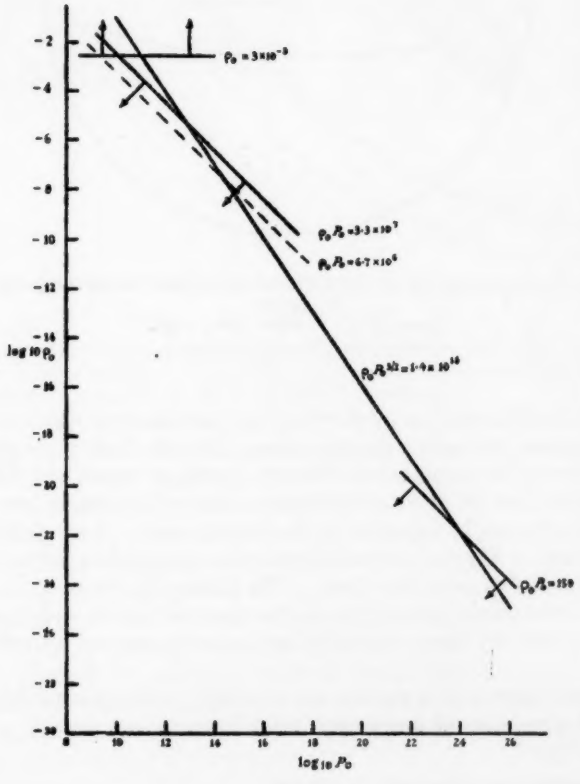

FIG. 1.—*Diagram relating the values of the effective radio luminosity P_0 and space density ρ_0 which are compatible with the counts of sources falling in a given range of flux density. The restrictions set by the observed isotropy of the sources, and the maximum contribution to the background emission, are also known.*

Observations were made of a strip of sky $02° < \delta < 08°$, and two regions $\alpha = 12^h$ to 16^h and $\alpha = 00^h$ to 04^h were analysed by the statistical method (Scheuer 1957). The positions of the two areas in relation to the emitting region associated with the galactic halo (Baldwin 1955) are shown in Fig. 2.

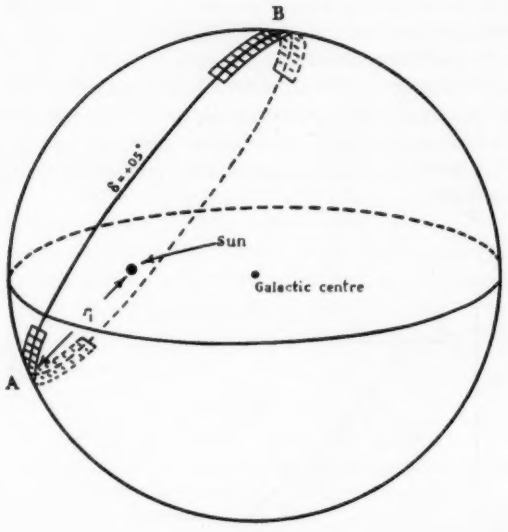

FIG. 2.—*The region of emission associated with the galactic halo, showing the two areas examined* ($r_1 \simeq 5$ *kpc*).
Centre of A: $l^{II} \simeq 160°$; $b^{II} \simeq -55°$.
Centre of B: $l^{II} \simeq 355°$; $b^{II} \simeq 45°$.

The results of this analysis are shown in Fig. 3 and show no signficant differences in the histograms derived for the two areas. Hewish (1961) has computed the theoretical curves for a number of different models of source distribution and in some of these a cut-off of sources below a certain flux-density was adopted to simulate the effect to be expected in the present case. Two of his theoretical curves are shown in Fig. 3; these correspond to similar models, but one of them has a cut-off at 2×10^4 sources/steradian. The differences between the theoretical curves are considerably greater than in the observed curves and it can therefore be concluded that the observations indicate no anisotropy at 2×10^4 sources per steradian.

This result shows that if the sources are mostly in the galactic halo, then with the adopted dispersion of luminosity, the effective space density ρ_0 must be at least 3×10^{-3} pc^{-3}.

(*d*) *The integrated emission from the sources*

Observations of the distribution of the background radiation have allowed the derivation of a model of the galactic emission, and hence the determination of the average emission per unit volume in different parts of the galaxy and also in extra-galactic space (Baldwin 1955). More recently, Costain (1960) has measured

the spectral distribution of some of the components and has thus been able to estimate the volume emissivity at different frequencies, both within the galactic halo and in extra-galactic space.

Without having to know the mechanism of the emission from either of these regions it is clear that the contribution made by the radio sources ($\Sigma\rho P$) cannot exceed, at any frequency, the volume emissivity determined in this way; this analysis then allows an upper limit for $\rho_0 P_0$ to be derived.

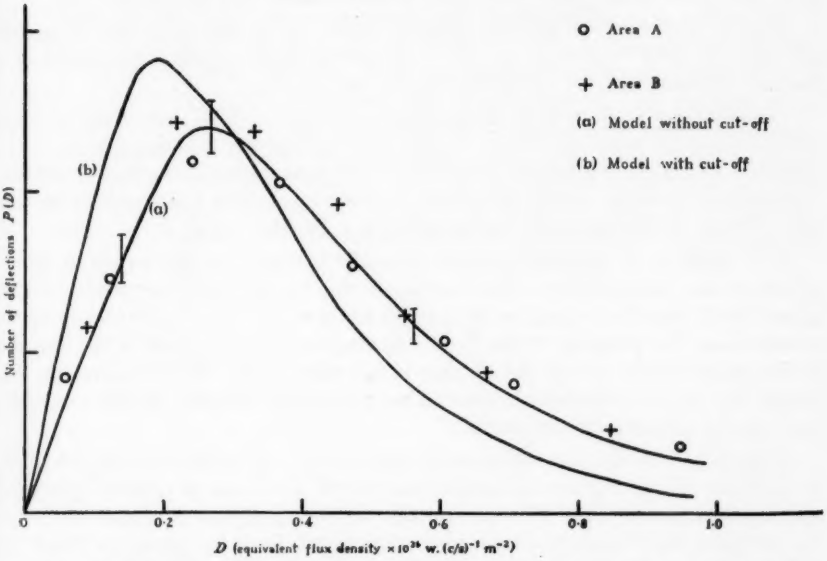

FIG. 3.—*Histograms of record deflections for the two areas A (anti-centre) and B (centre) shown in Fig. 2. The theoretical curves are also shown for two models, one of which has a cut-off at* $S=0{\cdot}15\times10^{-26}$ *watts* $(c/s)^{-1}\ m^{-2}$ $(2\times10^4$ *sources per steradian).*

Except for some of those at low galactic latitudes, most radio sources appear to have an emission which varies as $S\propto f^{-(0{\cdot}8\pm0{\cdot}2)}$ over the range of frequencies 38–960 Mc/s (Whitfield 1957; Harris and Roberts 1960). The radiation from the galactic halo, on the other hand, has been observed in the range 38–178 Mc/s to have a brightness temperature $T_b\propto f^{-(2{\cdot}37\pm0{\cdot}04)}$ a relation which corresponds to a volume emissivity proportional to $f^{-(0{\cdot}37\pm0{\cdot}04)}$. It is therefore clear that at the frequency of the present observations (178 Mc/s) only a fraction $(38/178)^{(0{\cdot}8-0{\cdot}37)}$ of the emission from the halo can be due to the sources.

With the adopted dispersion in source luminosity this leads to an upper limit for the volume emissivity of $\rho_0 P_0 < 3{\cdot}3\times10^7$ watts $(c/s)^{-1}\,pc^{-3}$; this limit is shown in Fig. 1 which shows to it be incompatible with the lower limit of ρ_0 derived from the observed isotropy of the sources.

This analysis may be extended in the light of recent observations of the galactic emission which have now been made over a range of frequencies of 100:1, and which can be fitted with a uniform spectral index of $-0{\cdot}37$ (Costain 1960; Chapman 1960: Seeger 1960). Without the adoption of a peculiar distribution of the spectrum of the sources outside the range 38–178 Mc/s, it is difficult to suppose

that they can make a significant contribution to the observed galactic radiation; the combination of the radiation from two types of source having different spectral indices can produce a uniform spectral index only if the spectra of the two components show opposite departures from linearity at approximately the same frequency. With the uncertainties in the present observations it seems unlikely that the sources could contribute more than 10 per cent of the emission from the galactic halo at a frequency of 178 Mc/s. The corresponding upper limit of $\rho_0 P_0 < 6{\cdot}7 \times 10^6$ watts $(c/s)^{-1}$ ster^{-1} pc^{-3} is shown dotted in Fig. 1.

The discrepancy between the derived limits of $\rho_0 P_0$, the lower limit of ρ_0 and the value of $\rho_0 P_0^{3/2}$ therefore makes it difficult to suppose that more than a few per cent of the sources are situated within the galactic halo.

A similar argument may now be applied to the case in which most of the sources are extra-galactic since their contribution to the total volume emissivity of extra-galactic space must not lead to a total sky brightness greater than that observed. The relation between volume emissivity and sky brightness now depends on the cosmological model adopted (Shakeshaft 1954; Priester 1954).

It is difficult to distinguish observationally between an extra-galactic component of the background emission and one due to the outermost shells of the galactic halo since both give rise to a distribution which is nearly isotropic when viewed from the position of the Sun. Owing to the differences in the spectra of the galactic halo and of the sources it is however, possible to determine the maximum contribution which sources having a given spectral distribution may make to the extragalactic emission.

Costain's observations (1960) can be used in this way to derive an upper limit of 25°K for the maximum sky brightness at 178 Mc/s due to sources having a spectral distribution $S \propto f^{-0{\cdot}8}$. In the case of the steady-state model and with the adopted dispersion in luminosity this result leads to an upper limit of $\rho_0 P_0 < 150$ watts $(c/s)^{-1}$ ster^{-1} pc^{-3}. The intercept of this line with the line $\rho_0 P_0^{3/2} = 1{\cdot}4 \times 10^{14}$ (Fig. 1) leads to a lower limit of $P_0 > 10^{24}$ watts $(c/s)^{-1}$ ster^{-1}.

In most evolutionary models the total sky brightness converges more slowly than for the steady-state model and a lower limit must be set to $\rho_0 P_0$; consequently the lower limit of the effective source luminosity P_0 must be increased for such models.

(*e*) *Discussion*

The extension of the previous analysis which has been carried out using the new observational material has effectively eliminated the possibility that a significant fraction of the observed sources are situated within the Galaxy. This possibility is in any case hard to accept in view of the observed non-uniform distribution in depth; if more than a small fraction of the sources were within the galactic halo it would be necessary to postulate a progressive change in luminosity or spatial density of the sources with distance from the Sun, up to several kiloparsec, if both the number-flux density counts and the isotropy were to be explained.

It may therefore be concluded that most of the sources are extra-galactic with an effective luminosity $P_0 > 10^{24}$ watts $(c/s)^{-1}$ ster^{-1}.

It is interesting to compare the limiting luminosity function derived in this way (Fig. 4(*a*)) with those derived by other arguments.

Measurements of the surface brightness of the sources (Allen, Palmer and Rowson 1960; Leslie 1961 a) allow a luminosity function to be derived if it is assumed that all sources are of galactic dimensions (Fig. 4 (*b*)). An analysis both of sources identified with optical objects, and of the limiting optical magnitudes of unidentified sources, has enabled Long and Marks (1961) to derive a luminosity function on the supposition that all sources have an absolute optical magnitude $M_{pg} = -20{\cdot}6 \pm 1{\cdot}0$, a range which includes all the identified sources whose distances have been measured. Two limiting cases of their distribution are shown in Fig. 4 (*c*). In connection with their results, it is interesting to note that sources of intermediate radio luminosity, such as NGC 1275 and M87, cannot represent a large fraction of those observed in a given range of flux-density; some authors have suggested that the presence of such sources would prevent the recognition of any cosmological effect due to more powerful sources.

Minkowski (1960), Bolton (1960) and Mills (1960) have also derived luminosity functions on the supposition that the sources which have been identified with optical objects represent a typical sample; their curves replotted to give the distribution in luminosity of the sources falling in a given range of flux density are shown in Fig. 4 (*d*).

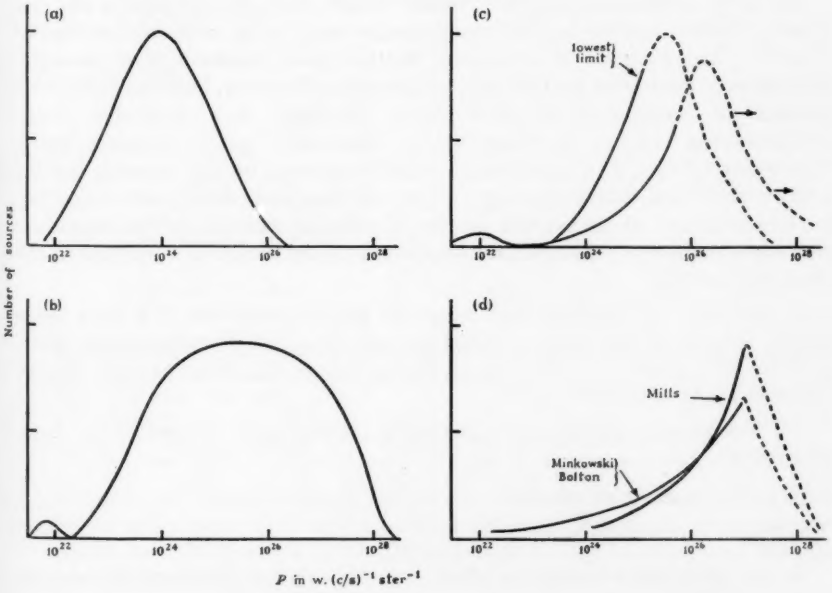

FIG. 4.—*The distribution in radio luminosity (P) of the sources falling in a given range of flux density.*

(*a*) *Lower limits derived from radio observations without assumptions concerning the nature of the sources.*

(*b*) *Model derived from consideration of the distribution of the surface brightness of the sources.*

(*c*) *Model derived from limits of* $(m_r - m_{pg})$ *for identified and unidentified sources* (*Long and Marks* 1961).

(*d*) *Models derived on basis of identified sources* (*Minkowski* 1960; *Bolton* 1960; *Mills* 1960).

All the available evidence therefore indicates that most of the sources observed in a given range of flux density have a luminosity P of 10^{24}–10^{27} watts $(c/s)^{-1}ster^{-1}$. Whilst arguments based on measurements of surface brightness and of optical luminosity are both dependent on assumptions concerning the nature of the unidentified sources, the results they provide agree with the lower limits which it has been possible to derive without such assumptions from the radio observations alone.

Even if this more conservative limit is adopted, the region investigated in the survey of individual sources with $S \geqslant 2 \times 10^{-26}$ watts $(c/s)^{-1}\,m^{-2}$ extends to distances of at least 10^9 pc. Any suggestion that the apparent non-uniformity in the distribution of the sources should be attributed to a local irregularity must now be discounted since the volume of space involved represents an appreciable fraction of the observable universe.

In the next section, an investigation is made into the effects of the red-shift on the counts of sources having luminosities of this order.

3. *The predicted number-flux density relationship.*—Several authors have examined the number-flux density ($N-S$) relationship expected for radio sources of given luminosity and have derived curves appropriate to a number of different cosmological models (McVittie 1957; Priester 1958; Davidson 1959).

In most of these models evolutionary effects have been neglected and the density of radio sources has been supposed to vary in the same way as that of galaxies. The problem of accounting for the radio emission from powerful extra-galactic sources of the type now envisaged has however, been examined by a number of authors (Greenstein 1955; Burbidge and Burbidge 1957; Ambartsumian 1958; Burbidge 1958; Shklovsky 1960; Tunmer 1960; Minkowski 1961). The conditions required to account for the emission involve a very considerable supply of energy and some of these authors have concluded that the kinetic energy of the gaseous content of colliding galaxies may represent the only adequate source—a conclusion supported by the nature of a number of the identified sources.

If the radio sources have their origin in galactic collisions then their space density is likely to show more marked changes than that of galaxies, and in the limit for field galaxies would vary as the square of the mean galactic density (Priester 1958; Davidson 1959).

In the present analysis two particular cosmological models have been considered.

(*a*) The steady-state model.

(*b*) The Einstein-de Sitter model.

In the latter case evolutionary effects and the variation of the total number of sources may both be important.

Curves have been plotted in Fig. 5 showing the variation with S of N/N_0, the ratio of the number of sources observed having a flux density greater than S, compared with the number which would be observed in a static Euclidean universe. In the Einstein-de Sitter model two limiting cases have been considered in which the density of sources is supposed to vary (i) as the density of galaxies and (ii) as the square of the galactic density.

The relations used in deriving these curves have been given by a number of authors (e.g. Bondi 1952; Davidson 1959). It is convenient to quote the formulae in terms of the red shift $(1+z)$ of the source and the associated distance r which is a function of the model adopted. ρ is the local density of sources and P the luminosity per steradian of the source which is assumed to obey a spectral law $P \propto f^{-x}$.

For all the models considered the flux density per unit bandwidth is

$$P/r^2(1+z)^{1+x}$$

where P has the value appropriate to the frequency of reception, not that of the original emission. In the steady-state model, which has a constant number of sources in a given proper volume, the number of sources in the range r to $(r+dr)$ is $4\pi\rho r^2 dr/(1+z)^3$ with $r=cz/H$ (where $H=$ Hubble's constant, $c=$ velocity of light). In relativistic models the number of galaxies per coordinate volume is constant and for the particular model chosen, the Einstein-de Sitter model, the corresponding relation is $4\pi\rho r^2 dr$ with $r=2c/H\ (1-(1+z)^{-1/2})$. The limiting case of an Einstein-de Sitter universe in which sources are produced by the collisions of galaxies leads to a number of sources which is proportional to the square of the proper density.

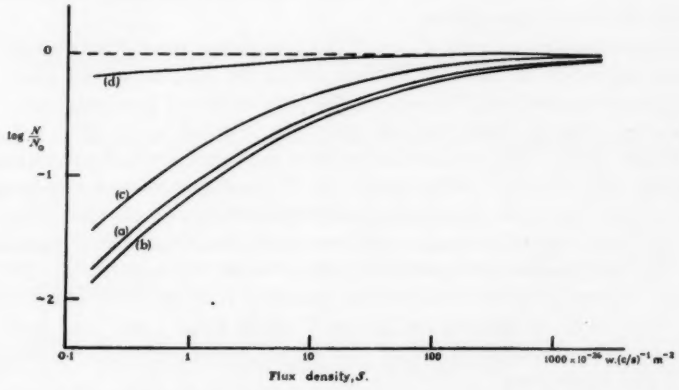

FIG. 5.—*Curves showing the variation of the number of sources (N) having a flux density greater than S, compared to the number (N_0) on a static Euclidean model.*

(*a*) *Steady-state* ($x=-0{\cdot}5$).
(*b*) *Steady-state* ($x=-1{\cdot}0$).
(*c*) *Einstein-de Sitter* (*number of sources proportional to mean galactic density*).
(*d*) *Einstein-de Sitter* (*number of sources proportional to square of galactic density*).

The method of presenting the results, in which the numbers of sources are compared with those in a corresponding static Euclidean universe, has the advantage that the predictions of different models may be compared without a knowledge of the absolute local density of sources.

The curves do not depend critically on the value of the spectral index x, as can be seen from Fig. 5, which shows two curves appropriate to the steady-state model with a non-dispersed luminosity $P=10^{26}$ watts $(c/s)^{-1}$ ster^{-1}, and $x=-0{\cdot}5$ and $-1{\cdot}0$. The curves for the Einstein-de Sitter models in which the number of sources is assumed to be proportional (i) to the density of galaxies and (ii) to the square of the density, are also shown in Fig. 5; a mean spectral index $x=-0{\cdot}8$ has been adopted and no evolutionary effects have been included.

The purpose of the present paper is not to determine a particular model which accounts for the observations, but to make a critical examination of the predictions of the steady-state model, which allows of no variations except those associated with the spectral index and the source luminosity function. In the next section the steady-state model will be compared with the observations.

4. *Comparison of the observed number-flux density relationship with that predicted on the steady-state model.*—The number-flux density relationship at galactic latitudes $>20°$ has been established directly for $S \geqslant 2 \times 10^{-26}$ watts $(c/s)^{-1}\,m^{-2}$ by combining the "whole-sky" observations of Miss Leslie (1961 a) with the high resolution observations of 0·6 steradians of sky (Scott and Ryle 1961). By using the statistical method of record analysis on the high resolution observations Hewish (1961) has been able to extend the analysis to cover sources having $5 \times 10^{-28} < S < 2 \times 10^{-26}$ watts $(c/s)^{-1}\,m^{-2}$.

All the observations are combined in Fig. 6 which shows for $S > 2 \times 10^{-26}$ watts $(c/s)^{-1}\,m^{-2}$ the values of N/N_0 derived from individual source counts together with the limits of error due to the statistical uncertainties, possible effects of extended sources, source clustering etc. Three models are shown for $S < 2 \times 10^{-26}$ watts $(c/s)^{-1}\,m^{-2}$, which represent limiting cases of models compatible with the observations.

The marked convergence shown by all three models at small S may be confirmed from a consideration of the contribution which the sources would make to the total background emission of the sky. As already indicated, the contribution to the extra-galactic radiation from sources having a spectral index of $-0·8$ cannot exceed about 25°K. The total emission from the sources which can be observed individually ($S \geqslant 2 \times 10^{-26}$ watts $(c/s)^{-1}\,m^{-2}$) corresponds to a sky brightness temperature of about 3°K, and the variation with S of N/N_0 found for $S > 2 \times 10^{-26}$ watts $(c/s)^{-1}\,m^{-2}$ cannot extend in the same way for $S < 2 \times 10^{-27}$ watts $(c/s)^{-1}\,m^{-2}$ or the permissible integrated emission would be exceeded. The three models (i), (ii) and (iii) derived from the statistical analysis of the interferometric records have been integrated for $S > 10^{-27}$ watts $(c/s)^{-1}\,m^{-2}$ and lead to sky brightness temperatures of 7·5, 8·5 and 11°K, all of which are compatible with the observed sky brightness.

The observed number-flux density relationship may now be compared with that predicted by the steady-state model, using the luminosity functions derived in Section 2. As can be seen from Fig. 5 the curves derived for the steady-state model do not depend critically on the spectral index, and a value of $-0·8$ has been adopted; a comparison of the intensities of a number of sources at frequencies of 159 and 960 Mc/s (Harris and Roberts 1960) has shown that most sources have over this range a spectral index of $0·8 \pm 0·2$ and errors in the predicted curve of N/N_0 are therefore likely to be small, at any rate for values of $z < 5$.

Two curves have been computed and are shown in Fig. 6: the first is based on the limiting luminosity derived from radio evidence alone; the second on the assumption that all sources have the same luminosity function as that derived for the identified sources. The point on each curve at which the median of the luminosity function corresponds to $z = 0·5$ is shown.

Both theoretical curves have been drawn to pass through the experimentally determined point at $S = 30 \times 10^{-26}$ watts $(c/s)^{-1}\,m^{-2}$. This is the largest value of S for which the statistical uncertainties are small enough to provide a useful value of N.

A comparison of the predicted and observed curves shows a marked discrepancy, even when the smallest permissible source luminosity is adopted; the observed number of sources in the range $0{\cdot}5 < S < 2 \times 10^{-26}$ watts $(c/s)^{-1}$ m^{-2} is $3 \pm 0{\cdot}5$ times that predicted by the steady-state model. If a luminosity function similar to that of the identified sources is assumed, the discrepancy is 11 ± 2.

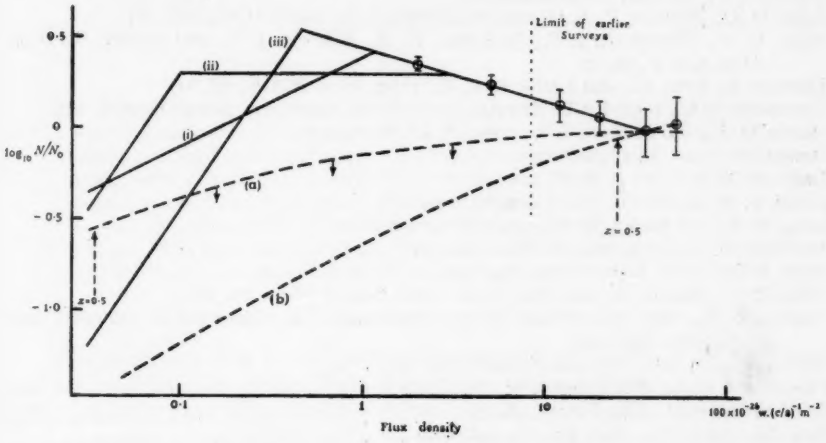

FIG. 6.—*Comparison of the observed N/N_0 relationship with that predicted by the steady-state model* ($x = -0{\cdot}8$).

(*a*) *Limiting luminosity function.*

(*b*) *Luminosity function similar to that of the identified sources.*

The flux density at which the median value of P corresponds to $z = 0{\cdot}5$ *for each of the models is indicated. The dotted line corresponds to the useful limit of observation in the earlier surveys (Bennett and Smith* 1961).

No attempt has been made here to provide an explanation for the observations in terms of an alternative model and it is evident that the introduction of the evolutionary changes which appear to be necessary will make the selection of a unique model difficult. These observations do, however, appear to provide conclusive evidence against the steady-state model.

We should like to express our thanks to Dr A. Hewish both for useful discussions and for allowing us to use the results of his analysis prior to publication. One of us (R. W. C.) is indebted to the D.S.I.R. for a maintenance allowance.

Mullard Radio Astronomy Observatory,
Cavendish Laboratory,
Cambridge:
1961 *January* 28.

References

Ambartsumian, V. A., 1958, *Izv. Akad. Nauk. Armyanski SSR*, **11**, 9.
Allen, L. R., Palmer, H. P., and Rowson, B., 1960, *Nature*, **188**, 731.
Baldwin, J. E., 1955, *M.N.*, **115**, 690.
Bennett, A. S., and Smith, F. G., 1961, *M.N.*, **122**, 71.
Boischot, A., 1960, 13th General Assembly U.R.S.I., London.
Bolton, J. G., 1960, 13th General Assembly U.R.S.I., London.
Bondi, H., 1952, *Cosmology*, C.U.P.

Burbidge, G. R., 1958, I.A.U./U.R.S.I. Symposium on Radio Astronomy, Paris, p. 541.
Burbidge, G. R., and Burbidge, E. M., 1957, *Ap. J.*, **125**, 1.
Chapman, J. H., 1960, 13th General Assembly U.R.S.I., London.
Costain, C. H., 1960, *M.N.*, **120**, 248.
Davidson, W., 1959, *M.N.*, **119**, 665.
Dewhirst, D. W., 1958, I.A.U./U.R.S.I. Symposium on Radio Astronomy, Paris, p. 507.
Dewhirst, D. W., 1961 (in preparation).
Edge, D. O., Scheuer, P. A. G., and Shakeshaft, J. R., 1958, *M.N.*, **118**, 183.
Edge, D. O., Shakeshaft, J. R., McAdam, W. B., Baldwin, J. E., and Archer, S., 1959, *Mem. R.A.S.*, **68**, 37.
Elsmore, B., Ryle, M., and Leslie, P. R. R., 1959, *Mem. R.A.S.*, **68**, 61.
Greenstein, J. L., 1955, I.A.U. Symposium on Radio Astronomy, Jodrell Bank, p, 179.
Harris, D. E., and Roberts, J. A., 1960, *P.A.S.P.*, **72**, 237.
Hewish, A., 1961 (in preparation).
Leslie, P. R. R., 1961 a, *M.N.*, **122**, 51.
Leslie, P. R. R., 1961 b, *M.N.*, **122** (in press).
Long, R. J., and Marks, D. R., 1961, *M.N.*, **122**, 61.
McVittie, G. C., 1957, *Aust. J. Phys.*, **10**, 331.
Mills, B. Y., 1960, *Aust. J. Phys.*, **13**, 550.
Mills, B. Y., Slee, O. B., and Hill, E. R., 1958, *Aust. J. Phys.*, **11**, 360.
Minkowski, R., 1960, Proceedings of 4th Symposium on Mathematical Statistics and Probability, Berkeley.
Minkowski, R., 1961, *Sky and Telescope*, **21**, 23.
Priester, W., 1954, *Zeit. f. Astr.*, **34**, 283.
Priester, W., 1958, *Zeit. f. Astr.*, **46**, 179.
Ryle, M., 1958, *Proc. Roy. Soc. A.*, **248**, 289.
Ryle, M., and Scheuer, P. A. G., 1955, *Proc. Roy. Soc. A.*, **230**, 448.
Sandage, A. R., 1958, *Ap. J.*, **127**, 513.
Scheuer, P. A. G., 1957, *Proc. Camb. Phil. Soc.*, **53**, 764.
Scott, P. F., and Ryle, M., 1961, *M.N.*, **122** (in press).
Scott, P. F., Ryle, M., and Hewish, A., 1961, *M.N.*, **122**, 95.
Seeger, C. L., 1960, 13th General Assembly U.R.S.I., London.
Shakeshaft, J. R., 1954, *Phil. Mag.*, **45**, 731.
Shakeshaft, J. R., Ryle, M., Baldwin, J. E., Elsmore, B., and Thomson, J. H., 1955, *Mem. R.A.S.*, **67**, 106.
Shklovsky, I. S., 1960, *A.J., USSR*, **37**, 945.
Tunmer, H. E. C., 1960, *M.N.*, **120**, 360.
Whitfield, G. R., 1957, *M.N.*, **117**, 680.
Williams, P. J., Dewhirst, D. W., and Leslie, P. R. R., 1961, *Observatory* (in press).

NGC 7492

James Cuffey

(Received 1961 March 10)*

Summary

Photometry of NGC 7492, a very faint, well resolved cluster, shows that it has a colour-magnitude relation similar in form to that of a typical globular cluster. A well defined but sparsely populated red giant branch is present, along with a horizontal branch, blue stars, and variables. The distance modulus, 17·17, and the distance, 27·2 kpc., are obtained. The colour excess appears to be negligible. The integrated photographic absolute magnitude is −4·84. The star density in the cluster is unusually low, being approximately 0·06 stars per cubic parsec for stars brighter than +2·5 absolute magnitude.

NGC 7492 is a very poorly populated cluster of unusually open appearance well removed from the Milky Way, in southern galactic latitude −65°. Intrinsically, it is one of the faintest of the globular clusters. Shapley (1930) describes its concentration class as XII, and its angular diameter as 3′·3. Nine variable stars are present according to Mrs Helen Sawyer Hogg (1947), although few details have been published. The cluster is unusually blue judging from the colour excess −0·20 obtained by Stebbins and Whitford (1936).

TABLE I

Photoelectric standards, NGC 7492

Star	*P*	*V*	*P*−*V*
A	13·60	13·04	+0·56
B	15·26	14·63	+0·63
G	15·75	14·27	+1·48
H	15·80	14·52	+1·28
I	16·82	16·75	+0·07
J	16·22	15·55	+0·67
N	16·71	15·88	+0·83
O	17·79	16·87	+0·92
P	17·93	18·26	−0·33
Q	16·43	15·73	+0·70
R	16·43	15·63	+0·80
S	16·11	15·54	+0·57
T	15·81	15·16	+0·65
U	16·77	15·78	+0·99
g	17·08	16·32	+0·76

The photometric measures of cluster stars reported here are based on photoelectric standard stars observed in 1951 with the 82-inch reflector at the McDonald Observatory (Table I), and on iris photometer measures of photographs taken with the 100-inch and the 200-inch reflectors of the

* Received in original form 1960 December 28.

Mt Wilson and Palomar Observatories (Table II). A dry ice refrigerated 1P21 photometer was employed in the photoelectric work, and the measures were later reduced to the *PV* system by measures with the 36-inch reflector of the Goethe Link Observatory to relate them to the *PV* (Eggen) and the *BV* (Johnson and Morgan) systems. These reductions appear in another publication (Cuffey and McCuskey 1956), and are very linear in nature. The values in Table I are reduced to the *PV* system (Eggen 1955).

TABLE II

NGC 7492, photographic observational material

Object	Plate no.	Exposure (min.)	Colour	Instrument	Aperture
NGC 7492	H 31 O	30	B	100	58
	PH 32 O	10	B	200	200
	H 109 C	60	B	100	58
	H 119 C	60	B	100	58
	H 134 C	30	B	100	58
NGC 7492	H 32 O	15	Y	100	58
	PH 33 O	20	Y	200	200
	H 110 C	60	Y	100	58
	H 120 C	60	Y	100	58
	H 133 C	30	Y	100	58

The photographic observations (Table II) made at the Mt Wilson and Palomar Observatories employed 103aO plates with a WG 2 filter, and 103aD plates with a GG 14 filter to cover the photographic and the yellow regions, respectively. Two of the plates, taken with the 200-inch reflector, and two of those taken with the 100-inch telescope were made by Dr Donald Osterbrock, who had begun a study of the cluster, and who very kindly presented them to me. The rest of the plates were taken by the author in 1955, as guest investigator at Mt Wilson Observatory. In addition to the plates listed, several photographs of Selected Areas 57 and 68 were made, and a number of similar plates were borrowed from Dr A. R. Sandage.

The photoelectric observations with the 82-inch reflector gave the zero point and scales of the *P* and *V* magnitudes in Table I in the range 12·0 to 18·4. However, in order to provide more numerous standard stars for the photographic reduction curves, supplementary stars were added, and their magnitudes determined by photographic interpolation and extrapolation. In order to perform this work, it was essential to determine accurately the form of the iris reading–magnitude relation, and the photographs of Selected Areas 57 and 68 were measured for this purpose. Photoelectric magnitudes and colours in the Selected Areas (Stebbins, Whitford and Johnson, 1950) were used, and also values by W. A. Baum, who kindly permitted me to use his photoelectric values in Selected Areas 57 and 68 in advance of publication. The Selected Area plates established the form of the iris photometer reduction curves, and showed them to be very smooth and free from bumps or wiggles. Therefore they could be used for accurate interpolation between the photoelectric standards. They also established the form of the reduction curves for the fainter stars so that extrapolation in the range 18·4 to 19·5 could be accomplished, although, it must be admitted, with considerably less confidence than the interpolation.

Table III summarizes the magnitudes and colours of all the standard stars, both those obtained photographically by interpolation and extrapolation of the photoelectric data, and also those re-derived for the stars in Table I. The zero point was derived from photoelectric comparisons with the North Polar Sequence, made with the 82-inch, and using the revised values of magnitudes which represent the *P* and *V* system, rather than with the older International Polar Sequence values. The scale is that of the photoelectric measures with the

TABLE III

NGC 7492, standard stars

Star	*P*	*V*	*P*−*V*	
A	13·77	13·13	0·64	
B	15·14	14·55	0·59	
C	16·90	16·71	0·19	
D	16·82	16·37	0·45	
E	16·99	16·30	0·69	
F	17·20	16·80	0·40	
G	15·78	14·18	1·60	
H	15·79	14·49	1·30	
I	...	...	...	D
J	16·37	15·57	0·80	
K	16·31	15·49	0·82	
L	16·58	15·82	0·76	
M	16·86	16·16	0·70	
N	16·85	16·07	0·78	
O	16·81	16·07	0·74	
P	17·18	17·00	0·18	V
Q	16·60	15·77	0·83	
R	16·25	15·31	0·94	
S	...	...	...	D
T	16·09:	15·24:	0·85:	D
U	16·59	15·81	0·78	
V	16·69	16·15	0·54	
W	17·05	16·72	0·33	
X	17·45	16·98	0·47	
Y	17·41	17·56	−0·15	
Z	17·17	16·79	0·38	
a	17·35	17·50	−0·15	
b	17·09	16·43	0·66	
c	17·43	16·74	0·69	
d	17·56	16·99	0·57	
e	16·82	16·24	0·58	
f	17·06	17·23	−0·17	
g	16·89	16·19	0·70	
h	17·22	16·65	0·57	
i	17·27	17·44	−0·17	

D = double star, V = variable.

82-inch reflector, and represents the photometric system of the present paper. The values could undoubtedly be improved by further measurements with a sensitive cell and a larger telescope, especially for the fainter stars, but they may be considered satisfactory for the present preliminary study of the cluster.

Magnitudes and colours for the resolved stars in NGC 7492 are given in Table IV, and the identifications are given by the chart in Fig. 1. Probable

TABLE IV

NGC 7492, catalogue of stars

No.	*P*	*V*	*P*−*V*
	S1R1		
1	17·63	17·06	+0·57
2	18·89	18·04	+0·85
3	17·99	17·41	+0·58
4	18·48	18·40	+0·08
5	18·13	17·67	+0·46
6	16·47	15·64	+0·83
7	16·94	17·02	−0·08
8	17·58	16·98	+0·60
9	17·28	17·43	−0·15
10	18·91	18·77	+0·14
11	18·88	18·50	+0·38
12	18·15	17·68	+0·47
13	19·65	18·81	+0·84
14	18·91	18·56	+0·35
	S1R2		
1	17·25	16·85	+0·40
2	17·05	17·23	−0·18
3	20·21	19·34	+0·87
4	19·92	18·94	+0·98
5	19·55	19·16	+0·39
6	19·29	18·59	+0·70
7	20·69	19·44	+1·25
8	17·50	17·74	−0·24
9	17·32	16·82	+0·50
10	20·09	18·91	+1·18
11	20·53	19·73	+0·80
12	20·68	19·57	+1·11
13	20·31	19·50	+0·81
14	19·25	18·83	+0·42
15	19·92	18·96	+0·96
16	20·05	19·20	+0·85
17	17·51	17·66	−0·15
18	17·38	17·55	−0·17
19	17·53	16·96	+0·57
20	17·09	17·22	−0·13
21	16·56	15·76	+0·80
22	19·04	18·20	+0·84
23	19·57	18·73	+0·84
24	17·47	16·85	+0·62
	S1R3		
1	19·84	18·92	+0·92
2	18·28	17·25	+1·03
3	19·26	17·78	+1·48
4	20·44	19·37	+1·07
5	18·01	17·45	+0·56
6	19·63	18·43	+1·20
	S2R1		
1	18·26	17·75	+0·51
2	17·13	17·27	−0·14
3	16·90	16·40	+0·50
4	18·95	18·21	+0·74
5	19·48	18·62	+0·86
6	17·20	17·37	−0·17
7	17·45	16·89	+0·56
8	18·28	17·80	+0·48
9	17·20	17·34	−0·14
10	18·97	18·47	+0·50
11	19·80	19·07	+0·73
12	17·43	16·90	+0·53
13	17·53	17·62	−0·09
14	18·24	17·71	+0·53
15	17·05	16·39	+0·66
16	16·72	16·15	+0·57
17	17·47	17·61	−0·14
18	19·06	18·52	+0·54
19	20·00	18·96	+1·04
20	20·03	19·13	+0·90
	S2R2		
1	19·10	18·32	+0·78
2	19·49	18·82	+0·67
3	19·14	18·53	+0·61
4	20·19	19·29	+0·90
5	18·81	18·10	+0·71
6	17·38	17·56	−0·18
7	19·11	18·38	+0·73
8	17·28	17·48	−0·20
9	18·86	18·17	+0·69
10	19·22	18·73	+0·49
11	19·45	18·63	+0·82
	S2R3		
1	18·80	18·16	+0·64
2	19·42	18·61	+0·81
3	15·10	14·53	+0·57
4	18·38	17·35	+1·03
5	20·01	19·22	+0·79
	S3R1		
1	17·07	17·27	−0·20
2	18·99	18·32	+0·67
3	18·62	18·00	+0·62
4	18·92	18·25	+0·67
5	18·40	17·82	+0·58
6	16·95	16·92	+0·03
7	17·38	16·77	+0·61
8	16·70	16·00	+0·70
9	17·11	17·25	−0·14
10	18·22	17·79	+0·43
11	18·95	18·33	+0·62
12	18·77	18·30	+0·47
13	19·00	18·27	+0·73
14	17·44	17·56	−0·12
15	17·46	17·58	−0·12
16	17·53	17·62	−0·09
17	19·25	18·54	+0·71
18	17·46	16·81	+0·65
19	17·94	17·31	+0·63
	S3R2		
1	20·52	19·45	+1·07
2	19·12	18·37	+0·75
3	19·01	18·31	+0·70
4	19·77	18·66	+1·11
5	20·18	18·92	+1·26
6	18·57	17·89	+0·68
7	17·25	16·60	+0·65
8	18·09	17·53	+0·56
9	17·34	17·45	−0·11
10	16·68	15·92	+0·76
11	16·80	15·99	+0·81
	S3R3		
1	19·25	18·34	+0·91
2	19·12	18·38	+0·74
3	19·43	18·63	+0·80
4	20·16	18·96	+1·20
5	20·30	19·00	+1·30
6	13·75	12·86	+0·89
7	18·83	18·07	+0·76
8	18·73	17·88	+0·85
	S4R1		
1	18·12	17·48	+0·64
2	19·36	17·68	+1·68
3	18·35	17·77	+0·58
4	18·18	17·63	+0·55
5	17·14	17·18	−0·04
6	16·82	16·21	+0·61
7	18·66	18·09	+0·57
8	19·28	18·38	+0·90
9	16·94	17·03	−0·09
9A	17·11	17·28	−0·17
10	17·17	17·28	−0·11
11	17·41	16·77	+0·64
12	16·96	16·23	+0·73
13	18·03	17·41	+0·62
	S4R2		
1	17·58	17·70	−0·12
2	18·89	18·19	+0·70
3	18·86	18·14	+0·72
4	18·65	17·99	+0·66
5	18·32	17·67	+0·65
6	18·51	17·99	+0·52
7	20·34	19·05	+1·29
8	17·23	17·32	−0·09
9	19·14	18·43	+0·71

TABLE IV (*cont.*)

No.	P	V	$P-V$	No.	P	V	$P-V$	No.	P	V	$P-V$
	S4R2			16	18·01	17·50	+0·51	3	16·30	14·83	+1·47
10	17·23	17·31	−0·08	17	18·90	18·14	+0·76	4	20·39	19·00	+1·39
11	18·23	17·68	+0·55	18	19·67	18·81	+0·86	5	20·39	18·94	+1·45
12	18·52	17·84	+0·68					6	17·70	17·10	+0·60
13	18·68	18·08	+0·60		S4R3			7	19·65	18·92	+0·73
14	18·81	18·24	+0·57	1	20·22	19·00	+1·22	8	20·47	19·21	+1·26
15	17·24	17·37	−0·13	2	18·15	17·60	+0·55	9	20·02	18·87	+1 15

errors, which reflect only the internal consistency of the data, are summarized as follows: brighter than $V=18{\cdot}5$, $\pm 0{\cdot}04$ in V, and $\pm 0{\cdot}06$ in $P-V$; fainter than $V=18{\cdot}5$, $\pm 0{\cdot}07$ in V and $\pm 0{\cdot}10$ in $P-V$. There are several factors which rendered the present photometry of NGC 7492 unusually difficult from the standpoint of obtaining the highest accuracy. The cluster's declination is 16° south, and the Mt Wilson plates, taken near the meridian, encountered somewhat higher fog than usual from the brightly illuminated sky over Pasadena. Improved photometry could result from observations made at a southern hemisphere observatory. The photoelectric observations, made at McDonald with the 82-inch reflector, however, were made under good observing conditions, and the magnitudes of Table IV are based on photoelectric standards to magnitude $V=18{\cdot}4$, so that they are probably unaffected by plate fog uncertainties to this limit. Fainter than $V=18{\cdot}0$, the present results should be regarded as provisional.

The colour–magnitude relation, Fig. 2, shows that in spite of its poverty in stars and its open structure, NGC 7492 is a globular cluster. The red giant branch is well defined, and stars as red as $P-V=1{\cdot}6$ lie on it. It is, however, poorly populated towards the red end, and this fact, along with the well populated horizontal branch, probably explains the negative colour excess obtained by Stebbins and Whitford (1936) who derived the colour excess by comparing NGC 7492 with other globular clusters. The horizontal branch reaches $P-V=-0{\cdot}24$, and this, combined with the cluster's high south galactic latitude ($-65°$), makes it probable that selective absorption is negligible. Fainter than $V=18{\cdot}0$, the observations have been plotted as open circles to indicate their tentative nature.

Nine variable stars are present, according to Mrs Helen Sawyer Hogg (1947). Much of the material, however, is unpublished, and insufficient data are now available on the variables to make them useful for distance determination in NGC 7492. Shapley (1920) listed one variable and four suspects. The variable, V1, is standard star P and it shows large residuals in the measures, thus confirming its variability. The suspects are, in the designation system of Table IV, S1R2 19, standard star f, and S4R2 1; Shapley suspect number 5 lies outside the area measured. None of the suspects investigated showed unusually large residuals in the present series of measures. Furthermore, only V1 lies at the expected location in the colour–magnitude relation; suspect V2 lies too far to the red to be on the horizontal branch, while V3 and V4 are too blue. Stars which should be further investigated for variability because of their location on the horizontal branch of the colour–magnitude relation are standard stars C, F, W, and Z, and stars S1R1 7, S1R2 1, S3R1 6, S4R1 5, and S4R1 9. The present series of plates is insufficient to give further information on the variables.

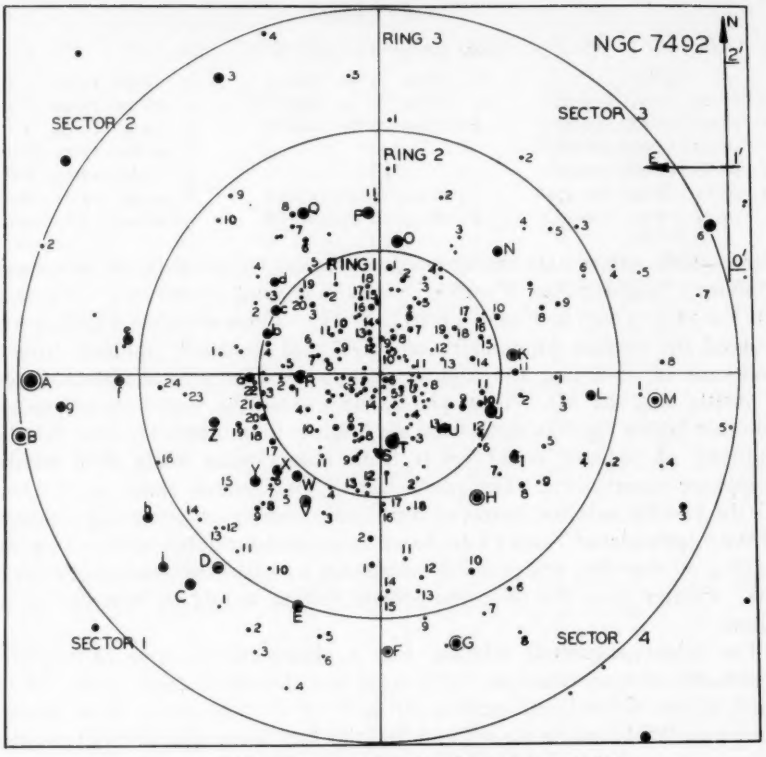

FIG. 1.—*NGC 7492 star chart. Standard stars are circled.*

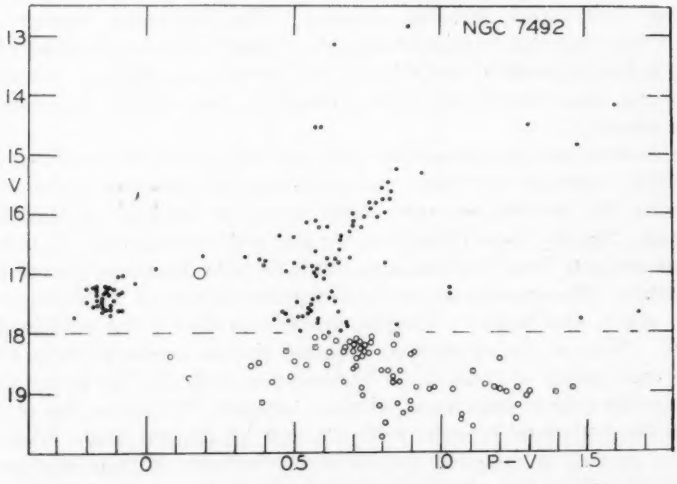

FIG. 2.—*NGC 7492, colour-magnitude relation. Variable star P is indicated as a circle. Fainter than V=18·0, the observations are plotted as open circles to indicate uncertainties in the photometry.*

The main sequence lies below the observational limits of Fig. 2. Fainter than $V = 18{\cdot}0$, the measures become uncertain because of interfering plate fog from the bright sky over Pasadena, and it is not possible to be sure that the sharp trend toward red stars at $V = 19{\cdot}0$ is real and not caused by systematic errors in the colours. Until a photoelectric check of the sequences at $V = 19{\cdot}0$ can be made, little attention should be paid to trends indicated in Fig. 2 fainter than $V = 18{\cdot}0$.

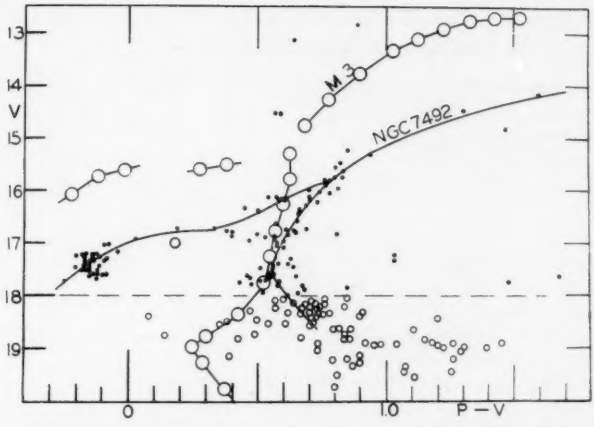

FIG. 3.—*Comparison of colour-magnitude relations in NGC 7492 and Messier 3.*

The distance for NGC 7492 was obtained by comparing its colour–magnitude relation with that of Messier 3 (Johnson and Sandage 1956). A zero-point shift of 0·17 magnitudes was used to allow for the difference between the $P-V$ and $B-V$ photometric systems. Since evidence for selective absorption is slight in both cases, no allowance was made for it. For Messier 3, the modulus 15·67 was used (Sandage 1953). From the blue stars the modulus for NGC 7492, 17·24, was obtained; the horizontal branch gives 16·91, and the red giant branch gives 17·37. We adopt the mean, or 17·17, as the best value, and the distance is 27·2 kpc. The integrated absolute photographic magnitude is then $-4{\cdot}84$, if the apparent magnitude 12·33 (Christie 1940) is used.

The cluster's diameter, estimated from the Palomar Atlas prints, is 3′·3 if the nucleus only is considered, and 4′·5 if the outlying stars are included. The nucleus is therefore 26·0 pc in diameter, and the whole cluster, 35·6 pc. The cluster's total population, brighter than $V = 19{\cdot}5$, was counted as 575 stars. Its mean density, for stars brighter than $+2{\cdot}5$, is 0·02 stars per cubic parsec; its central density, obtained from an analysis of star counts by Plummer's method, is 0·06 stars per cubic parsec.

The star counts showed that 8 per cent of the points in Fig. 2 can be attributed to field stars, so that the scatter in the colours of the fainter stars can be more probably blamed upon photometric uncertainties than interfering field stars.

NGC 7492 is located one full Milky Way diameter from the Milky Way plane, in fact, somewhat farther from it than the Magellanic Clouds. Two other clusters, NGC 5053, and 5466 resemble NGC 7492 in structure and in location well removed from the Milky Way plane. If they represent objects populating

intergalactic space, and are unrelated to the galactic system, it is tempting to speculate that they owe their common poverty in stars to the scarcity of star building material in intergalactic space at the time of the cluster's origin.

Acknowledgments are in order to Dr I. S. Bowen, Dr W. Baade, and others at the Mt Wilson Observatory, for their interest and cooperation; to Dr D. Osterbrok and Dr A. R. Sandage for the loan of plates; to Indiana University for travel funds and for student assistance; and to Mr M. Todd, of the Observatory machine shop, for completion of the iris photometer with which the measures of the photographs were made.

Astronomy Department,
Indiana University,
Bloomington,
Indiana, U.S.A.:
1961 *March.*

References

Christie, Wm. H., 1940, *Ap. J.*, **91**, 10.
Cuffey, J., and McCuskey, S. W., 1956, *Ap. J.*, **123**, 59.
Eggen, O. J., 1955, *A.J.*, **60**, 86.
Johnson, H. L., and Sandage, A. R., 1956, *Ap. J.*, **124**, 379.
Sandage, A. R., 1953, *Ap. J.*, **58**, 61.
Sawyer-Hogg, H., 1947, *Dunlap Obs. Pub.* 1, No. 20.
Shapley, H., 1920, *Ap. J.*, **52**, 73.
Shapley, H., 1930, *Star clusters*, p. 224 (Harvard Obs. Monographs, No. 2).
Stebbins, J., and Whitford, A. E., 1936, *Ap. J.*, **84**, 132.
Stebbins, J., Whitford, A. E., and Johnson, H. L., 1950, *Ap. J.*, **112**, 469.